Mercury Stabilization in Contaminated Sediment by Co-blending with Solid-Phase Reactive Media

by

Sara Christine Fellin

A thesis
presented to the University of Waterloo
in fulfilment of the
thesis requirement for the degree of
Master of Science
in
Earth Sciences

Waterloo, Ontario, Canada, 2016

Author's Declaration

I hereby declare that I am the sole author of this thesis.

This is a true copy of this thesis, including any final required revision, as accepted by my examiners.

I understand that this thesis may be made electronically available to the public.

Sara Fellin

Abstract

Mercury (Hg) is a toxic heavy metal and environmental contaminant that can accumulate in both terrestrial and aquatic environments. Pollutant Hg is derived primarily from anthropogenic sources such as mining, coal burning and other high-temperature incineration processes. Mercury tends to bioaccumulate in organisms via exposure to the highly neurotoxic organomercury compound methylmercury (MeHg). Remediation of Hg contamination in river systems is a complex process due to the persistence of Hg in the environment and the nature of Hg methylation, sorption to solids, transport and deposition. Elevated concentrations of Hg and MeHg are present throughout portions of the South River watershed in Virginia. Mercury was released to the river from 1929-1950 as a result of industrial processes and remains bound to riverbank sediments and floodplain soils. Erosion of riverbanks and floodplain runoff are now secondary sources of Hg to the South River, decades after the initial contamination.

Saturated column experiments were conducted to evaluate the effect of several inorganic soil amendments on Hg mobilization and transport. Contaminated sediment from the South River was blended with a 2 % amendment (dry weight) of limestone, attapulgite clay or sulfidized attapulgite clay and flushed with low-Hg water from the South River for 36 - 47 weeks representing 150 PV of flow. No appreciable stabilization or mobilization of Hg was observed in the sediment blended with limestone; Hg concentrations in the column effluent were similar in magnitude to the sediment control. Extensive Hg mobilization occurred in the sediment amended with attapulgite clay, with an increase in cumulative effluent 0.45 μm-filtered Hg of more than 200%. This result indicates that there is potential for both destabilization of Hg previously bound to the sediment and colloid-facilitated transport of Hg in the presence of a clay amendment.

Imparting S functional groups onto the surface of attapulgite clay greatly reduced Hg transport relative to both the unmodified clay and the sediment control. The cumulative release of Hg in the column effluent for the 0.45 μm-filtered fraction in the sediment amended with sulfidized clay was 24 % of the sediment control and 7.5 % of the unmodified clay. The strong interactions between Hg and S may have promoted binding of Hg to the surface of the modified clay and subsequent agglomeration and deposition of Hg-bearing clay particles. Elevated concentrations of MeHg were observed only in the sediment amended with unmodified clay, likely as a result of an increase in bioavailable Hg.

The use of biochar as an amendment to sequester Hg in contaminated sediment was evaluated in five saturated column experiments, including a sediment control, a 2 % (dry weight) amendment of unmodified biochar, a 2 % amendment of HNO_3-modified biochar, a 2 % amendment of sulfidized biochar and a 5 % amendment of sulfidized biochar. No suppression of Hg transport was observed in the sediment blended with unmodified biochar and HNO_3-modified biochar, while increased binding of Hg was observed in both the 2 % and 5 % amendments of sulfidized biochar. The cumulative release of 0.45 μm-filtered Hg in the effluent of the sediment blended with a 2 % amendment of sulfidized biochar was 29 % of that observed in the control, while the cumulative release for the 5% amendment of sulfidized biochar was 17 % of the control. In both columns, Hg was likely bound to the surface of the modified biochar through the formation of Hg-S complexes, rendering it less mobile. In all sediment amendment columns, effluent chemistry and net MeHg production were not appreciably impacted by the addition of biochar. The results of this study suggest that amendment of the Hg-bearing sediment with sulfidized biochar in saturated, dynamic conditions may lead to decreased Hg transport.

Acknowledgements

I would like to sincerely thank my supervisor Dr. Carol Ptacek for providing me the opportunity to work on this project and for her help and guidance over the past few years. I would also like to thank my committee members Dr. David Blowes and Dr. Doug Gould for their valuable input and advice. I extend my appreciation to Rich Landis, Jim Dyer and Erin Mack for their interest and support of this research project.

Huge thanks goes to Krista Paulson, who patiently fielded all of my question regardless of how many times I visited her office on a given day. Much appreciation goes to all members of the GGR group, especially Alana Wang and Peng Liu for always being willing to provide mercury know-how and Jing Ma for her analytical expertise.

I also have to extend many thanks to the friends I've made throughout this grad school adventure - Alysa, Matt, Jeff, Justin, Emily, the ever-changing Physics 110 gang and the entire BH/GH crew - thanks for all of the great times over the last few years.

Finally, special thanks and much appreciation goes to my family, who by now have heard more about "analysers", "columns" and "port sampling" than they probably ever thought possible. Your encouragement and support throughout this experience was invaluable and made completing this thesis possible. Thanks guys.

Table of Contents

List of Figures

List of Tables

List of Abbreviations

0.1-Hg	0.1 μm-filtered mercury
0.45-Hg	0.45 μm-filtered mercury
ACS	American Chemical Society
CaS_x	Calcium polysulfide
CVAFS	Cold vapor atomic fluorescence spectroscopy
DOC	Dissolved organic carbon
DOM	Dissolved organic matter
EXAFS	Extended X-ray absorption fine structure
HDPE	High-density polyethylene
IRB	Iron reducing bacteria
LCF	Linear combination fitting
MeHg	Methylmercury
PCR	Polymerase chain reaction
PV	Pore volume
RRM	Relative river mile
SRB	Sulfate reducing bacteria
SRW	South River water
THg	Total (unfiltered) mercury
U.S.-EPA	United States Environmental Protection Agency
XANES	X-ray absorption near edge structure

Chapter 1: Introduction

Mercury (Hg) is an environmental contaminant of global importance that can be derived from both natural and anthropogenic sources. Though it was once considered a "cure-all" for a variety of ailments, exposure to Hg is now known to be hazardous to human health and detrimental to natural ecosystems (Fitzgerald & Lamborg, 2013). The adverse health effects associated with Hg have been well documented and currently fish consumption and dental amalgams represent the primary routes of human exposure (Tchounwou et al., 2003; Clarkson & Magos, 2006; Karagas et al., 2012). Methylmercury (MeHg) is the organic form of Hg and is a particularly potent neurotoxin that accumulates in aquatic organisms. MeHg poisoning, sometimes referred to as Minamata disease, can cause neurological impairment, especially in infants, and visual and hearing impairment and chronic paresthesia (Ekino et al., 2007).

Mercury contamination derived from historic manufacturing processes has resulted in four rivers in the Shenandoah Valley, Virginia being defined by the state's Department of Environmental Quality as "impaired" waters. Elevated concentrations of Hg are present in the tissue of fish from the South River, South Fork Shenandoah River, North Fork Shenandoah River and the Shenandoah River, prompting fish consumption advisories by the Virginia Department of Health. Despite the more than 60-year period since the cessation of Hg discharge into the river system, Hg concentrations remain elevated due to continued leaching and erosion of Hg-bearing soils and sediments in and surrounding the rivers. Stabilization of Hg present in both the riverbank sediments and floodplain soils is considered vital to the remediation process and a field-scale bank-stabilization program is currently under way along sections of the South River (Flanders et al., 2010). The work presented in this thesis focuses on the evaluation of potential

strategies for *in situ* stabilization of Hg-bearing riverbank sediment from the South River, the site of the initial Hg release.

1.1 Distribution and Fate of Mercury in the Environment

Mercury occurs naturally in the environment as elemental mercury (Hg^0), the mineral cinnabar (HgS) and other phases. Major deposits of Hg are typically found near subduction zones and other tectonically active regions, where volcanism, erosion and volatilization from soils are the primary natural sources of Hg to the environment (Fitzgerald & Lamborg, 2013). Anthropogenic release of Hg is widespread and today is largely associated with the combustion of coal and municipal wastes (Fitzgerald & Lamborg, 2013). Historically, mining and industrial processes contributed significant amounts of Hg to the environment, heavily impacting aquatic environments (Wang et al., 2012). In many locations, this Hg persists in lake and river systems as "legacy" Hg, providing long-term sources of contamination. In Canada, numerous Hg-contaminated sites exist as a result of mining and industrial activities, including the English-Wabigoon river system in Ontario (Kinghorn et al., 2007), the Pinchi Hg Mine in central British Columbia (Weech et al., 2004), and the Murray Brook Mine in New Brunswick (Shaw et al., 2006). Internationally, the Idrija River in Slovenia (Hines et al., 2000), the Oak Ridge Reservation in Tennessee (Han et al., 2006), the Madeira River basin in Brazil (Lechler et al., 2000), the Carson River in Nevada (Wayne et al., 1996) and the New Almaden Hg Mine in California (Thomas et al., 2002) are examples of enduring anthropogenic Hg contamination.

Mercury released to aquatic environments can be found in three forms: elemental (Hg^0), inorganic (Hg^{2+}, Hg^{+}) and organic (MeHg). Inorganic Hg is highly reactive and can readily form

complexes with sulfides, chlorides, hydroxides and organic ligands. While Hg of all forms can be detrimental to human and wildlife health, it is the highly neurotoxic form MeHg that poses the most immediate concern due to its ability to bioaccumulate in organisms. Mercury methylation is a bacterially-mediated transformation typically attributed to sulfate-reducing bacteria (SRB), iron-reducing bacteria (IRB) and methanogens under anaerobic conditions (Kerin et al., 2006; Gilmour et al., 2013). The rate of MeHg formation is dependent on numerous factors, including the concentrations of electron donors (*e.g.*, organic substrates) and electron acceptors (*e.g.*, NO_3, Mn (III/IV), Fe (III), and SO_4) (Gilmour et al., 1992; Desrochers et al., 2015) and the nature of the microbial community (King et al., 2000). The speciation of inorganic Hg also plays a critical role in Hg methylation, as some forms of Hg and Hg-complexes are considered more bioavailable than others. In anoxic sediments, the presence of dissolved organic matter and sulfide are considered primary controls on Hg speciation and bioavailability (Graham et al., 2012). Biotic and abiotic demethylation are important controls on net MeHg production. Methylmercury has been shown to undergo photodegradation in surface water bodies (Sellers et al., 1996) and microbial demethylation by methanogens and SRB in soils and sediments (Marvin-Dipasquale & Oremland, 1998).

1.2 Site Background

The South River is located within the Shenandoah Valley in northwestern Virginia, USA and runs through the city of Waynesboro, VA (Fig. 1.1). Land use within the approximately 608 km^2 South River Watershed is primarily forested and agricultural (58 % and 31 % respectively) with most of the remaining land being developed (Eggleston, 2009). The bankfull width of the South

River surrounding the study area (relative river mile (RRM) 0.25) is approximately 26 m (Pizzuto, 2012) and the mean annual flow of the river near Waynesboro is 4.2 m^3/s (Eggleston, 2009). The South River joins the South Fork Shenandoah River downstream of Waynesboro near the town of Port Republic (Eggleston, 2009).

Sediment and flood plain soils at the South River contain elevated concentrations of Hg as a result of historical industrial practices in Waynesboro. Mercury sulfate was used as a catalyst at a textile manufacturing plant and was discharged to the river from 1929-1950. Due to transport and deposition processes, the river bottom and floodplain along a 39.6 km stretch of the South River downstream of the plant site now contain Hg-contaminated sediments and soils (Eggleston, 2009). Other sources of Hg to the river, including atmospheric deposition and agricultural fungicides have been documented but are considered insignificant relative to Hg from the textile manufacturing plant (Eggleston, 2009).

Mercury entrapped in soils and sediments surrounding river systems can act as a secondary source of Hg contamination, as seen at the River Nura in Kazakhstan where Hg entrapped in river bank sediments is mobilized following the annual spring flood (Ullrich et al., 2007). Studies at the South River have indicated that erosion of riverbank sediments and inundation of floodplain soils by floodwater provide a significant portion of dissolved and particulate Hg to the river water (Eggleston, 2009; Pizzuto, 2012).

1.3 Mercury Remediation

Selection of effective strategies for remediation of Hg at a given contaminated site greatly depends on the degree and scale of Hg distribution. Traditional *ex situ* techniques involving

direct removal of the contaminant, such as dredging and excavation, can be expensive and may result in sediment resuspension, promoting subsequent Hg release (Randall & Chattopadhyay, 2013). At the South River, Hg is present in varying concentrations over a large area, thus economics, mitigation of Hg remobilization and ease of implementation are important considerations in selection of remediation options. Given these criteria, one remediation technique currently being considered for use at the South River site involves sorption and partitioning of Hg onto sorbent amendments. This method does not directly remove Hg from the environment, but sequesters it, rendering it relatively immobile and less bioavailable (Ghosh et al., 2011). The selected material can be blended into contaminated soils (co-blending) (Kumpiene et al., 2008), used in a permeable reactive barrier (Blowes et al., 2000) or incorporated into engineered reactive caps or mats (Gidley et al., 2012), allowing for removal *in situ*. At the South River, a suitable *in situ* sorbent amendment could be utilised as a reactive mat to aid in riverbank stabilization or co-blended with floodplain soils to minimize Hg transport. Ideally, the amendment should be inexpensive, inert with respect to the surrounding environment, and efficiently limit Hg mobilization while not stimulating MeHg production.

1.4 Research Objectives

The primary objective of the research presented in this thesis is to evaluate the suitability of various solid-phase materials for the stabilization of Hg in contaminated soils and sediments by co-blending. While studies have been conducted to determine Hg uptake capacities of certain carbon-based and inorganic materials, few studies have blended these materials with sediment to control Hg in a dynamic, saturated system. This thesis focuses specifically on the impact of

modified and unmodified inorganic soil amendments on Hg mobilization; including the modification and enhancement of biochar, a material previously identified to effectively remove Hg from aqueous solution. These reactive materials will be assessed based on the following criteria:

- Minimization of Hg mobilisation and transport
- Limitation of the production of MeHg
- Reduction of the fraction of nanoparticulate and colloidal Hg

An amendment material considered suitable for use at the South River site should effectively sequester both dissolved and nanoparticulate/colloidal Hg and should not increase net MeHg production. Considering these factors, the overall goal of the studies is to reduce the mobility and bioavailability of Hg in the floodplain sediments of the South River watershed.

1.5 Thesis Organisation

This thesis includes two chapters structured as journal articles that each address an aspect of the above research objectives. In Chapter 2, the first article presents saturated column experiments to evaluate the effects of the inorganic soil amendments limestone and attapulgite clay on Hg-contaminated sediment. Sulfidization of the clay is employed in an attempt to increase the Hg uptake capacity of the clay. The second article is presented in Chapter 3 and describes the utility of co-blending biochar with the same contaminated sediment to sequester Hg. Modification of biochar with HNO_3 and sulfidization of the biochar are also evaluated as methods to increase Hg sequestration. In both chapters, emphasis is placed on Hg sequestration and suppression of MeHg production.

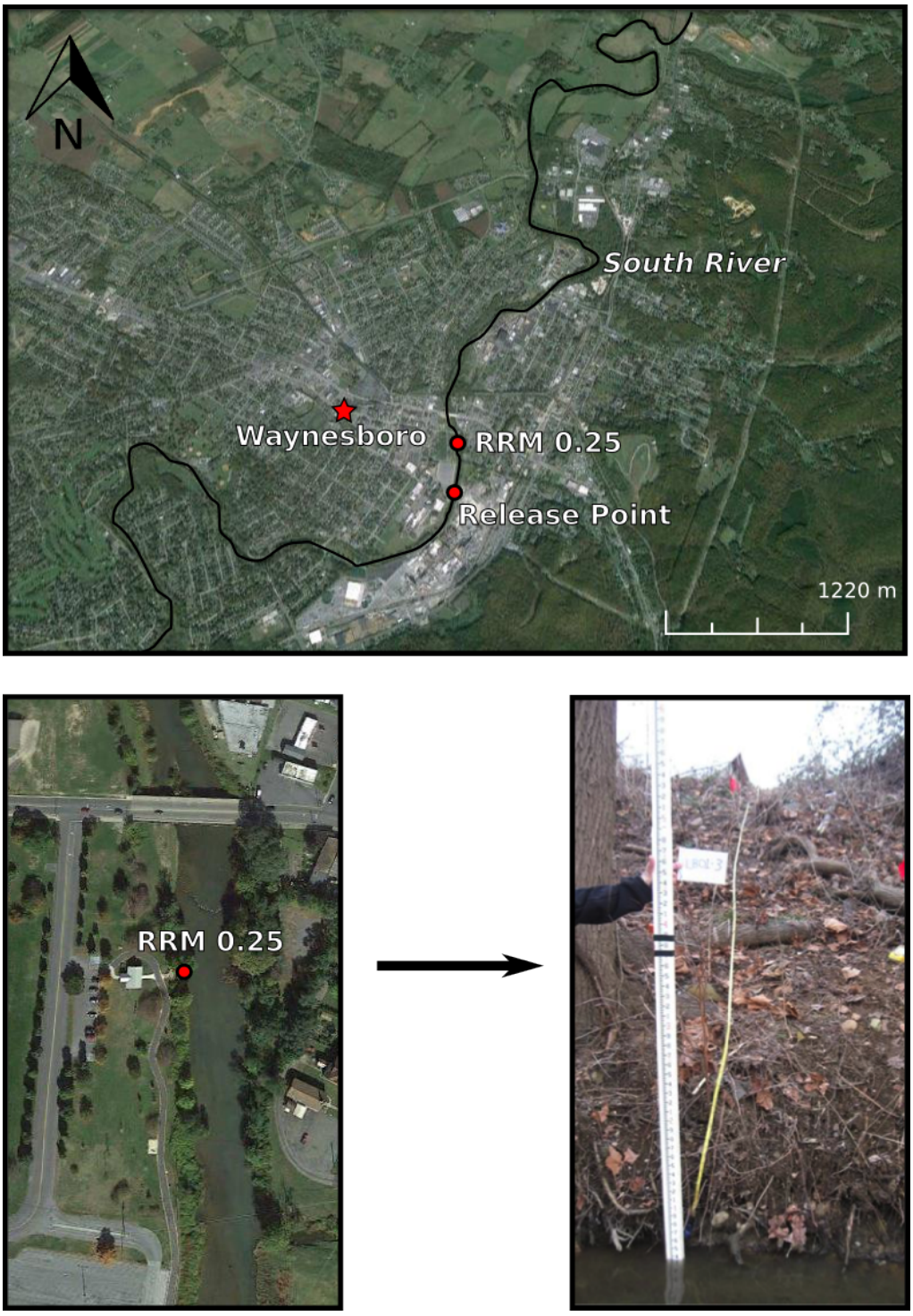

Figure 1.1: Map and photos showing locations of historical Hg release point and study area. Satellite images taken from Google Earth, riverbank picture (bottom right) courtesy of R. Landis.

Chapter 2: Inorganic Soil Amendments and their Effect on Mercury Contaminated Sediments from the South River, VA

2.1 Synopsis

Saturated column experiments were conducted to determine the effect of different inorganic soil amendments on mercury (Hg) transport in contaminated sediment. Riverbank sediment from the South River, VA was blended with either agricultural limestone, attapulgite clay or calcium polysulfide (CaS_x)-modified attapulgite clay in sealed acrylic columns that were continuously flushed with South River water containing low concentrations of Hg. Effluent concentrations of Hg, methylmercury (MeHg) and other parameters were monitored for a total of 41 - 46 weeks; equivalent to 150 PV of flow, before the experiments were terminated. Three times during the experiment, aqueous profile sampling was conducted using three ports distributed along the vertical length of the column. The water collected from this profile sampling was analysed to establish the mobility of Hg and evolution of porewater geochemistry within the columns. Effluent and profile samples indicate that the release of Hg from the limestone-amended sediment was similar to the release from the sediment control, indicating little stabilization of Hg. In contrast, results from the column containing unmodified attapulgite clay showed that Hg was extensively mobilized compared to the control. The cumulative percent of 0.45 μm filtered Hg leached into the effluent of the sediment co-blended with clay was more than 200% higher than that of the control. Methylmercury (MeHg) concentrations were also elevated in the effluent from the clay-amended sediment, likely as a result of the increase in bioavailability of the mobilized Hg. Treatment of attapulgite clay with a commercially available solution of CaS_x resulted in a

pronounced decrease in Hg release. Cumulative concentrations of 0.45 μm filtered Hg in the column effluent were 23 % of those in the control and 7.5 % of those in the unmodified clay. Effluent concentrations of MeHg in the sediment amended with CaS_x-modified clay were similar to the control, suggesting little effect of the S modification on net MeHg production. In addition, porewater chemistry in both the effluent and port samples taken from the sediment amended with CaS_x-modified clay were similar to the control; a trend observed in all sediment amendments. The decrease in Hg mobilization observed in the sediment blended with CaS_x-modified clay may be indicative of increased interaction between available Hg and the S groups present on the clay surface. These interactions may act to sequester Hg via the formation of Hg-S complexes, thus limiting its transport and bioavailability.

2.2 Introduction

Mercury is a highly toxic environmental contaminant that accumulates in watersheds and other terrestrial environments. Although it can be derived from natural sources, most Hg contamination is anthropogenic and is commonly associated with mining activities (Weech et al., 2004), chlor-alkali plants (Kinghorn et al., 2007), solid-waste incinerators (Chen et al., 2013), and other industrial and manufacturing processes. Soils and sediments can sequester Hg through interactions with clay minerals, fulvic and humic acids, amorphous metal hydroxides and oxyhydroxides and other soil constituents (Gabriel & Williamson, 2004). Mercury sequestration can result in sustained contamination long after active release of Hg has ceased. In watersheds, accumulated Hg can be leached from contaminated soils and sediments and deposited in surface water bodies through erosion, floodwater inundation, precipitation, surface runoff and

groundwater discharge (Balogh et al., 1998; Mason & Sullivan, 1998; Miller et al., 1998). After Hg is discharged to a river system, Hg can be readily bound to natural suspended colloids, rendering it highly mobile (Babiarz et al., 2001; Lowry et al., 2004; Slowey et al., 2005). Colloid-facilitated transport and subsequent deposition of Hg can result in the spread of Hg contamination far from the initial source. Riverbank soils and sediments are ideal environments for the formation of the organomercury species methylmercury (MeHg), which is produced primarily by sulfate-reducing and iron-reducing bacteria under anaerobic conditions (Gilmour & Henry, 1991; Graham et al., 2012). Methylmercury is a potent neurotoxin that can biomagnify within a food chain, resulting in elevated MeHg concentrations in the tissue of fish and other organisms (Fitzgerald and Lamborg, 2013). The complex nature of Hg transport and deposition and the potential for Hg methylation and demethylation processes necessitates but greatly complicates the remediation of Hg-contaminated sites.

Elevated concentrations of Hg are present in the surface water, groundwater and sediments surrounding the South River (Eggleston, 2009; Flanders et al., 2012). Between 1929 – 1950, a textile plant in Waynesboro, VA discharged Hg to the river in the form of a $HgSO_4$ catalyst (Carter, 1977). Since this initial release, Hg in the South River spread approximately 40 km downstream of the historical release point and is present in soils throughout the 100-year floodplain (E.I. du Pont de Nemours and Company, 2013). Mercury concentrations in the South River have not decreased significantly since first measured in the 1970s and elevated concentrations of Hg are still present in soils and groundwater at the plant site (Eggleston, 2009). Flanders et al. (2012) have established that Hg derived from contaminated floodplain soils and

riverbank sediments is the largest current source of Hg to the river, thus stabilization and sequestration of Hg in these areas is critical to remediation of the site.

Traditional remediation techniques for Hg-contaminated soils and sediments generally consist of excavation and dredging. These methods can be effective for localized areas of relatively high contamination, but are often expensive and logistically challenging for large expanses of polluted soils and sediments. The application of *in situ* amendments to contaminated sites has received attention as an effective and potentially lower cost method of contaminant immobilisation that can be applied on a large scale (Blowes et al., 2000; O'Day & Vlassopoulos, 2010; Ghosh et al., 2011). Some materials that have been utilised for Hg stabilization include activated carbon (Gilmour et al., 2013), biochar (Desrochers, 2013), natural zeolites (Campbell et al., 2006) and clay minerals (Green-Ruiz, 2005).

In this study, saturated column experiments were conducted to evaluate the effectiveness of three different inorganic minerals as co-blending amendments for decreasing Hg transport and mobilization from sediment from the South River. The mobility of Hg in sediments amended with limestone, attapulgite clay or sulfidized attapulgite clay was monitored to determine their capacity for Hg sequestration at the South River site. Limestone has long been used in agriculture to increase the pH of soils and supply calcium for plant nutrition (O'Day & Vlassopoulos, 2010). Dissolution of limestone in saturated sediments can increase the ionic strength of the surrounding pore waters via the release of Ca^{2+} ions. In classical colloid filtration theory, this increase in ionic strength can promote aggregation and deposition of colloidal material in an aqueous medium, limiting its transport (Yao et al., 1971; Ryan & Elimelech, 1996). Limestone has also been shown to moderately reduce the mobility of heavy metals in contaminated soils (Basta & McGowen,

2004; Lee et al., 2009). In this study, it is postulated that the addition of limestone to South River sediment will lead to a decrease in the mobility of Hg-bearing colloids and nanoparticles by promoting coagulation reactions. Attapulgite clay is a hydrated magnesium aluminum silicate that is non-swelling and bears a needle-like structure. As a result of this structure it has a surface area and sorptivity that is higher than most industrial clays (bentonite, kaolin) (Haden & Schwint, 1967). Clay minerals are often used in metal remediation for their sorptive qualities and attapulgite clay amendments have been shown to reduce heavy metal leaching from soils (Álvarez-Ayuso & García-Sánchez, 2003; Liang et al., 2014). Modification of clay minerals can be employed to increase metal retention capacity (Stathi et al., 2007; Bhattacharyya & Gupta, 2008). In Hg remediation, the use of S-containing modifiers is of particular interest due to the strong interaction between Hg and S (Wang et al., 2012). Gibson et al. (2011) has shown that S-modified clay can remove nearly all available Hg from solution in static "batch" experiments. In this study, attapulgite clay treated with a S solution (calcium polysulfide, CaS_x) was used to provide improved stabilization of Hg through enhanced binding reactions. Calcium polysulfide has been approved by the U.S.-EPA for use in the environment and is most often employed in agriculture and horticulture as a fungicide (U.S.-EPA, 2005). The overall goal of this study was to identify potential materials for sequestration of Hg in floodplain soils at the South River site, while considering their effect on net MeHg production and pore water chemistry.

2.3 Materials and Methods

2.3.1 Sediment and Water Collection

Sediment used in all column experiments was collected from a riverbank along the South River 0.4 km (relative river mile (RRM) 0.25) downstream from the textile manufacturing plant, the point source of Hg release. The sampling location is found on the west side of the South River. At the sampling location, the banks of the South River are relatively steep and the river width is approximately 30 m. The sediment was collected October 2010, at an elevation just above the base-flow level of the river, 3-3.7 m (10-12 ft) below the top of the bank. The sediment was shipped to the University of Waterloo where it was homogenized and stored at 4 °C and protected from light. South River water (SRW) was used as the column influent solution. This water was collected on a bimonthly basis from a location approximately 5 km upstream of the initial Hg release point, and was shipped on ice to the University of Waterloo where it was stored in the dark at 4 °C.

2.3.2 Soil Amendments

Attapulgite clay (Zemex Industrial Minerals Inc., Attapulgus, GA) utilised in this experiment was obtained as a fine powder. Modification of the attapulgite clay was performed using a commercially available solution of calcium polysulfide (CaS_x, lime sulfur) (Sure-gro Inc., Brantford, ON). A mixture containing 20 g of attapulgite, 1.7 mL of CaS_x and 200 mL of ultrapure water (Milli-Q purification system) was shaken and left to react for seven days under anaerobic conditions. The resulting material was rinsed with ultrapure water and dried at room

temperature in a laboratory fume hood. The agricultural limestone utilised was ground and sieved to 0.5 mm – 1.0 mm in diameter. Prior to column packing, South River sediment was mixed with a 2 % (dry weight) addition of attapulgite clay, sulfidized attapulgite clay or limestone. The mixing was done in small batches to ensure equal distribution of the amendment material throughout the sediment.

2.3.3 Experimental Set-up

Four column experiments (Table 2.1) were conducted using acrylic columns that were 15 cm long with an inner diameter of 4 cm, and a volume of 171.9 cm^3 ± 2.7 cm^3. The columns were packed with unamended sediment (Column 1; Control), limestone-amended sediment (Column 2; Limestone), attapulgite clay-amended sediment (Column 3; Clay) and CaS_x-modified clay-amended sediment (Column 4; CaS_x-clay). Each column included three 0.75 cm diameter ports installed at 3.5 cm, 7.5 cm and 11.5 cm from the bottom of the column to allow for profile sampling. Coarse and fine NITEX screens were placed at the bottom of each column and topped with a 1 cm layer of silica sand to prevent sediment loss. Columns were then packed by slowly pumping SRW upwards through the column while adding small amounts of the sediment mixture. This procedure was used to ensure saturation and lessen the formation of preferential flow paths. When the packed sediment was ~1 cm from the top of the column, an additional layer of silica sand, and coarse and fine NITEX screens were added prior to the column being sealed. A multi-channel peristaltic pump (Ismatec, Switzerland) was used to pump SRW through the columns at a constant rate of flow (Table 1).

2.3.4 Aqueous Sample Collection and Analysis

Column effluent was collected in 125 mL sealed amber bottles that were purged with $N_{2(g)}$ prior to each sample collection to minimize sample oxidation. Effluent samples were drawn from the collection bottles using 30 mL sterile polypropylene/polyethylene luer-lock syringes (Norm-Ject). Samples were collected from the ports in 30 mL glass syringes (BD Multi-Fit) at the unaltered flow-rate of the column. This profile sampling was completed three times over the course of each column experiment: once at the beginning (3-7 PV), once near the middle (45-89 PV) and once just before the end (143-183 PV) of the experiment. Samples were filtered using 32 mm diameter syringe filters containing 0.1 μm or 0.45 μm Supor Membranes (Acrodisc®). Samples collected for total mercury (THg), MeHg, dissolved organic carbon (DOC) and nutrient (NH_3-N, PO_4-P) analysis were stored in 15 mL vacuum and ionized amber borosilicate bottles (Qorpak). Samples for cation and anion analyses were collected in 15 mL polypropylene bottles (Nalgene™). Effluent collected for THg and cation analysis was acidified to pH<2 using ultrapure HNO_3; for MeHg analysis to pH < 2 using analytical grade HCl; and for DOC and nutrient analyses to pH<2 with OmniTrace Ultra High Purity H_2SO_4. Anion samples were left unacidified. All samples were stored at 4 °C with the exception of those intended for MeHg and anion analysis, which were frozen at -20 °C immediately after collection.

Analysis of all parameters was performed on samples that were passed through 0.45 μm filters. In addition, unfiltered and 0.1 μm filtered samples for THg analysis were collected on a monthly basis. Total Hg was analysed using cold vapour atomic fluorescence spectroscopy (CVAFS) (Tekran®) following U.S-EPA method 1631 (U.S-EPA, 2002). A summary of the quality assurance/quality control (QA/QC) measures taken during Hg analysis can be found in

Appendix C. Methylmercury (0.45 μm filtered) was quantified using the distillation, aqueous ethylation, purge and trap and CVAFS technique (Tekran®) as per U.S-EPA method 1630 (U.S-EPA, 2001). Determinations of the concentrations of major cations were obtained using inductively coupled plasma optical emission spectroscopy (iCAP 6000; ThermoFisher Scientific) and for trace elements using inductively coupled plasma mass spectroscopy (X-Series 2; ThermoFisher Scientific). Anion samples were analysed using ion chromatography (Dionex ICS-5000) with a KOH eluent and an IonPac™ AS18 2 × 250 mm column. When organic acids (acetate, formate, lactate, propionate) were analysed in addition to inorganic anions, an IonPac™ AS11 0.4 × 250 mm column was utilised. Standards for both anions and organic acids were prepared on the day of analysis. DOC concentrations were measured using a wet oxidation total organic carbon analyser (Aurora 1030W). The nutrients ammonia-nitrogen (NH_3-N) and phosphorus as orthophosphate were analysed with a spectrophotometer (HACH DR 2800). Ammonia-nitrogen was quantified using the salicylate method with a spectrophotometer (HACH DR 2800, Method 8155 from the DR 2800 manual) and PO_4-P analysis was adapted from the ascorbic acid spectrophotometric method 4500-P from the Standard Methods for Examination of Water and Waste Water (HACH DR 2800).

2.3.5 Solid-Phase Sample Collection

The column experiments were terminated after 150 PV of flow, after which the sediment mixture was extracted under anaerobic conditions in 2 cm intervals along the length of the column. Solid samples for total Hg, MeHg and sequential extraction were collected at the 1-3 cm, 5-7 cm and 9-11 cm intervals relative to column influent using 70% ethanol-washed tools. The remaining

sediment was stored in glass vials and all samples were frozen immediately and stored at -20 °C until analysis.

2.4 Results and Discussion

2.4.1 Mercury Mobilization

Release of Hg from the sediment control column (Control) was greatest within the first seven weeks of sampling (0 – 25 PV) (Fig. 2.1). The maximum concentration of 0.45 μm-filtered Hg (0.45-Hg) observed in the control column effluent was 1500 ng L^{-1} at 21 PV. Maximum concentrations of both unfiltered (THg) and 0.1 μm-filtered (0.1-Hg) Hg (2830 ng L^{-1} and 1000 ng L^{-1} respectively) were observed at 9.5 PV. By 30 pore volumes of flow, 0.45-Hg declined to 180 ng L^{-1} and by approximately 48 PV all fractions of Hg decreased to 40 ng L^{-1} – 160 ng L^{-1}, remaining within this range until termination of the experiment. At early times, the majority of effluent Hg was associated with the >0.45 μm size fraction, indicating an initial rapid release of particulate-bound Hg. After 48 PV the distribution among fractions switched to Hg predominantly associated with the nanoparticulate/dissolved fraction (<0.1 μm). Concentrations of 0.45-Hg in the pore water extracted from ports along the length of the column were the highest at early times (4 PV), reaching a maximum of 194 ng L^{-1} in the samples obtained from the top port (Fig. 2.2). By the second sampling session at 49 PV concentrations of 0.45-Hg were less than 65 ng L^{-1} at all distances along the column and by the final sampling (183 PV) 0.45-Hg was less than 30 ng L^{-1}. Mercury in the column pore waters typically increased from the bottom to the top of the column, likely as the influent SRW was allowed to interact for longer times with the contaminated sediment and transporting leached Hg upwards through the column.

In comparison to the Control, release of Hg in the effluent from the Limestone column occurred more rapidly, reaching a maximum 0.45-Hg concentration of 1380 ng L^{-1} and subsequently declining to 470 ng L^{-1} by 14 PV. The highest concentrations of THg and 0.1-Hg also were observed at early times (by 8 PV) and were similar in magnitude to the control. Concentrations of filter passing Hg (both 0.45-Hg and 0.1-Hg) decreased to concentrations <200 ng L^{-1} and THg to levels <350 ng L^{-1} by 44 PV and by termination of the experiment concentrations of 0.45-Hg had declined to approximately 100 ng L^{-1}. Concentrations of 0.45-Hg measured in aqueous profile samples from the Limestone column were higher than the Control at the first sampling session (3 PV), with a peak in concentration of 231 ng L^{-1} observed at the middle distance. Mercury concentrations then declined at the next sampling session of 45 PV, and declined further to <10 ng L^{-1} in all ports by 152 PV. In contrast to the Control, the proportion of Hg associated with the particulate (>0.45 μm) fraction did not decline considerably with time in the effluent of the Limestone column. This finding suggests that particulate-bound Hg was transported through the limestone-amended sediment at a consistent rate, rather than the rapid leaching of particulate Hg observed in the effluent of the Control column.

The greatest observed release of effluent Hg occurred in the sediment amended with unmodified clay. By 6.5 PV, concentrations of 0.45-Hg reached a maximum of 4500 ng L^{-1}, a value approximately three times higher than the Control. Concentrations of both 0.1-Hg and THg were similarly elevated, with maximum concentrations of 3300 ng L^{-1} and 6300 ng L^{-1} respectively. As observed for all columns, the release of Hg from the unmodified clay-amended sediment was highest at early times before all Hg filter fractions declined to <1500 ng L^{-1} by 33

PV. Mercury concentrations further declined in all filter fractions to concentrations <300 ng L^{-1} by 90 PV and by the end of the experiment ranged between 18 ng L^{-1} and 30 ng L^{-1}.

As observed with the effluent Hg concentrations, concentrations of 0.45-Hg in pore waters collected along the length of the Clay column were elevated in comparison to the other columns at early times. At the first profile sampling session (7 PV), the concentration of 0.45-Hg in porewater collected from the top port of the Clay column was 7860 ng L^{-1}. This concentration was more elevated than the maximum THg concentration in the Clay column effluent collected at 11 PV of flow. As with the measured effluent Hg, concentrations of 0.45-Hg in the port samples declined over time and by 150 PV were <12 ng L^{-1} along the length of the column. Both the effluent and port sampling results suggest that the addition of clay promoted an increase in Hg mobility in South River sediment compared to the unamended sediment. Work by both Álvarez-Ayuso & García-Sánchez (2003) and Liang et al. (2014) demonstrated decreased heavy metal mobility in contaminated soils with the addition of attapulgite clay. Álvarez-Ayuso & García-Sánchez suggest that reaction with silanol groups present on the surface of attapulgite is the primary mechanisms of metal sorption and retention. Analysis of the distribution of Hg among filter fractions indicates that throughout the course of the column experiment, an average of 50% of all measured Hg was in the nanoparticulate/dissolved phase (<0.1 μm). This distribution is slightly higher than the 40% average seen in the Control and indicates that while Hg sorption to clay particles and subsequent mobilization through the column may have occurred, it does not account for the significant portion of Hg present in the sub-100 nm category. One hypothesis may be that the electrostatic interaction between clay particles and Hg, which can occur in soils (Gabriel and Williamson, 2004), was strong enough to scavenge some Hg from the sediment but

not enough to cause sorption, thereby destabilising Hg and causing it to be transported through the column in the dissolved phase.

Effluent Hg concentrations from the CaS_x-clay column reached maximum values in all filter fractions by the first sampling event at 1.5 PV. At this time, the peak 0.45-Hg concentration in the column effluent was 280 ng L^{-1} while 0.1-Hg and THg were 287 ng L^{-1} and 298 ng L^{-1} respectively. The concentration of Hg in all filter fractions was consistently below 50 ng L^{-1} by 35 PV and at the termination of the experiment all were approximately 10 ng L^{-1}. Similar concentrations of Hg were observed in the port samples collected along the length of the CaS_x-clay column.. By the first port sampling session at 6 PV of flow, a maximum 0.45-Hg concentration of 162 ng L^{-1} was observed in effluent from the top port. Measured 0.45-Hg in the second and third port sampling sessions (89 PV and 143 PV) did not vary significantly along the vertical profile and were consistently lower than concentrations in the Control column. Comparison of effluent filter fraction distribution highlights the discrepancies between the CaS_x-clay and the unmodified version. On average, 82 % of measured Hg in the CaS_x-clay column effluent was in the <0.1 μm fraction, a value double the control and approximately 60 % higher than the unmodified clay. This suggests that like the unmodified clay, Hg is not simply attaching to clay particles and being mobilized through the column. Research conducted by Gibson et al. (2011) utilised extended X-ray absorption fine structure (EXAFS) analysis to measure Hg bond lengths on two thiadiazole-modified attapulgite clays and suggested the formation of Hg-S bonds. In the CaS_x-modified attapulgite amendment, Hg-bearing particles may form similar aggregates with available clay particles enhanced by the strong interaction between Hg and S present on the modified clay. These aggregates likely settle out of aqueous suspension, resulting in free

dissolved Hg not in contact with clay particles being readily transported and constituting the majority of Hg present in the column effluent.

2.4.2 Cumulative Hg Release

Aqueous Hg concentrations can provide insight into Hg transport within a column but do not account for variability in the amount of Hg-bearing sediment present in each column. To accurately compare the effects of sediment amendments on Hg release, the cumulative percent Hg released from all column experiments was calculated using both 0.45-Hg and THg concentrations. These calculations were used to normalize the Hg concentrations measured in column effluent to the total mass of Hg in each column as determined by the total mass of contaminated sediment in each column and allows for direct comparisons of Hg transport. By the completion of the experiment, 0.19 % of the total 0.45-Hg and 0.41 % of the THg was leached from the Control (Fig. 2.3). In comparison nearly 0.6 % of available 0.45-Hg was observed in the effluent of the Clay column, illustrating the pronounced increase in Hg mobilization associated with the clay amendment. Zhu et al. (2012) also observed increased Hg mobilization in a sand column when it was flushed with slurry of clay (kaolinite), attributed to the ability of kaolinite to strip Hg from the sand particles, resulting in colloid-facilitated Hg transport.

The cumulative release of both aqueous 0.45-Hg and aqueous THg from the Limestone column was higher than the Control, reaching 0.26 % and 0.51 % respectively by the end of the experiment. Geochemical speciation modelling (PHREEQC) performed on aqueous effluent samples indicates that there was no appreciable change in ionic strength induced by the addition of limestone to the sediment (Appendix A). Furthermore, the saturation indices for calcite

($CaCO_3$), aragonite ($CaCO_3$) and dolomite ($CaMg(CO_3)_2$) as determined using PHREEQC were similar in effluent samples from both the Control and the Limestone columns, suggesting there was likely little dissolution of the agricultural limestone during the experiment. The similarity in transport of Hg between the Control and Limestone columns is likely due to the lack of change in chemistry in the presence of the amendment.

Leached 0.45-Hg in the CaS_x-clay column effluent was 0.05 % of the total available solid-phase Hg, representing a 76 % decrease compared to the control and a 92 % decrease relative to the unmodified material. Similar results were observed for the cumulative release of total Hg from each column, indicating that the CaS_x treatment was effective at treating both particulate and filter-passing Hg. The presence of S has frequently been cited as contributing to Hg sequestration (Zhu et al., 2009; Kim et al., 2011). Research by Blue et al. (2010) found that a synthetic thiol compound (1,3-benzenediamidoethanethiol) added to a solution containing Hg will immediately form a Hg-S precipitate. More recently, Crockett et al. (2016) synthesized a sulfur-limonene polysulfide that sequesters aqueous Hg^{2+} as an insoluble Hg deposit. In this study with modified clay, the attapulgite clay was likely just a carrier for the CaS_x solution rather than acting as a sorbent material itself. It is possible that the same CaS_x treatment could be applied to a number of other sorbents to increase the S content and enhance Hg uptake.

2.4.3 Aqueous Porewater Chemistry

The addition of each of the amendment materials to the contaminated sediment led to minimal changes in porewater chemistry for all of the columns. Measurements of pH in the effluent of all columns were initially 7.8 and gradually declined over the course of the experiments to between

7.2 and 7, indicating that soil amendments did not appreciably influence porewater pH. Profile sampling for pH indicated very consistent values for all columns at each port sampling session, with values close to 7.5 in each of the three ports along the vertical length of the columns (Appendix A). Eh values in the effluent of both the Control and Limestone columns decreased sharply at early time, with a value of 112 mV observed in the Control column effluent and a value of -18 mV observed in the Limestone column effluent by 10 PV. This decrease in effluent Eh was also reflected in aqueous profile sampling results from the Limestone column at three PV of flow, though not in the Control. Both columns stabilized at Eh levels above the SRW input (~340 mV) by 24-30 PV in the effluent and by 45-49 PV along the vertical profile In contrast, Eh measurements in the effluent of both the Clay column and the CaS_x-clay column started at 400 mV – 470 mV and declined with time to values of 56 mV and -41 mV. Measurements of Eh from the profile sampling of both columns also followed a similar pattern, beginning at 400 mV– 450 mV at the first port sampling and declining to 150 mV – 300 mV by 150 PV.

The addition of limestone did not significantly alter effluent alkalinity, as demonstrated by a peak concentration of ~300 mg L^{-1} alkalinity as $CaCO_3$ being observed in both the Control and Limestone columns. Both clay-containing columns reached a maximum effluent alkalinity concentration of 200 mg L^{-1} as $CaCO_3$ by 10 PV. Upon 150 pore volumes of flow, alkalinity in all columns had decreased to at or just below the SRW input concentration of 110 mg L^{-1} as $CaCO_3$. Alkalinity was similar in samples extracted from the ports of all columns and typically increased with distance along the length of the columns, likely as a result of the increased dissolution of $CaCO_3$ as the porewater migrated upwards through the sediment. The concentration of major ions, with emphasis on those associated with clay mineral transport (*e.g.*

Al, Mg, Ca, Si, K), was monitored in both column effluent and ports to track trends in colloidal transport (Appendix A). Generally, these parameters did not vary significantly among the columns. Concentrations of Mg, Ca, Si and K were typically highest at early times, corresponding to the onset of reducing conditions that have been shown to influence colloid release (Tadanier et al., 2005; Thompson et al., 2006), before declining to approximately SRW concentrations by experiment termination. Release of Al was an exception to this trend, with elevated concentrations measured in the effluent of the Clay column and from samples taken from the uppermost port of the CaS_x-clay column. The increase in Al concentrations at 103 PV for the Clay column corresponded with small spikes in effluent Si and may be indicative of a sudden release of colloidal material.

2.4.4 Net MeHg Production

In the context of contaminated site remediation, a sorbent amendment that controlled Hg transport but stimulated Hg methylation would not be suitable due to the harmful effects of MeHg accumulation in the environment. As such, effluent MeHg concentrations were tracked in all columns in this study to monitor the effect of amendment materials on net MeHg production. The net production of MeHg in the effluent of the Control and Limestone columns followed a similar trend with time (Fig. 2.5). Concentrations of effluent MeHg were <1 ng L^{-1} for both columns at early time, but increased to a peak of approximately 7 ng L^{-1} by 28 PV. In the Control column, MeHg concentrations declined quickly and returned to <1 ng L^{-1} by 60 PV, remaining in this range for the duration of the experiment. This decline to low effluent MeHg concentrations was also observed in the Limestone column but was followed by a secondary increase in MeHg

concentrations at 86 PV. Of all the experiments, the most elevated concentrations of MeHg were measured in the effluent of the Clay column. Like the Control and Limestone columns, MeHg concentrations in the Clay column effluent were <1 ng L^{-1} at early time. After approximately 20 PV flushes the concentration of effluent MeHg began to rapidly increase and by 29 PV had peaked at 29 ng L^{-1}. Methylmercury concentrations in the effluent of the Clay column then declined to 2 ng L^{-1} by 48 PV, remaining between 1 ng L^{-1} – 3 ng L^{-1} until 123 PV before returning to <1 ng L^{-1}. The elevated concentrations of MeHg observed in the Clay column effluent may have resulted from enhanced transport of MeHg by sorption to clay particles (Babiarz et al., 2012) or by the destabilization and subsequent methylation of sediment-bound Hg induced by the attapulgite clay amendment. In contrast to the addition of unmodified attapulgite clay, effluent MeHg concentrations were not significantly altered by the CaS_x-clay amendment when compared to the control. Effluent MeHg in the CaS_x-clay column reached a peak concentration of 6.8 ng L^{-1} by 17 PV. Though slower to decline than the Control column, MeHg concentrations in sediment amended with CaS_x-clay decreased with time and were <1 ng L^{-1} by 103 PV. The MeHg results observed in the CaS_x-clay column are consistent with work done by Jay et al. (2002) who found methylation rates by certain SRB did not increase in the presence of polysulfides; a finding attributed to the charged nature and large size of Hg-polysulfide complexes.

Changing reduction-oxidation (redox) conditions can greatly affect Hg behaviour in aqueous systems by influencing mineral precipitation and dissolution, complexation and speciation (Ullrich et al., 2001; Gabriel & Williamson, 2004). Bacteria present within saturated, O_2-limited sediments can oxidize available organic carbon within sediments coupled to terminal

electron acceptors such as NO_3, SO_4, Mn^{4+} and Fe^{3+}. In particular, the production of MeHg occurs primarily under sulfate-reducing or iron-reducing conditions by SRB and IRB present in anoxic sediments (Hsu-Kim et al., 2013). In this study, the concentrations of electron donors (DOC), products of organic carbon degradation (NH_3-N, PO_4-P) and concentrations of electron acceptors (NO_3, Mn, Fe, SO_4) were measured to monitor changes in biogeochemical conditions caused by the addition of soil amendments (Fig. 2.4). Release of effluent DOC was similar for all columns, regardless of amendment material. DOC concentrations were most elevated at early time, ranging between 12 mg L^{-1} – 16 mg L^{-1} within the first 20 PV. In the Control and Limestone columns, these elevated concentrations of effluent DOC observed within the first PV flushes were typically associated with high effluent concentrations of acetate (Appendix A). Acetate can be produced by the microbially-mediated oxidation of other organic compounds (*e.g.* lactate, propionate) and therefore the observed elevated concentrations of acetate and hence DOC may be indicative of SRB activity within the columns (Widdel & Pfennig, 1982; Oyekola et al., 2009). With increasing PV flushes, effluent DOC declined in all columns to at or just above SRW input concentrations (~1 mg L^{-1}) as available DOC was likely consumed or flushed out of the column.

The oxidation and subsequent degradation of organic carbon can lead to the release of NH_3-N and PO_4-P (Waybrant et al., 2002). In all columns, effluent NH_3-N concentrations peaked between 6-13 PV before declining to below SRW input levels (0.5 mg L^{-1}) by approximately 50 PV. Release of effluent PO_4-P was delayed in comparison to NH_3-N, with peak PO_4-P concentrations measured in the effluent of the columns by 25-48 PV of flow. This attenuation may have resulted from interactions between PO_4-P and Fe(III) oxyhydroxides, for which

potential PO_4-P sorption sites are increased under Fe-reducing conditions (Reddy et al., 1999). Concentrations of both NH_3-N and PO_4-P were typically aligned with effluent alkalinity in all columns, another product of organic carbon oxidation.

Nitrate concentrations in the effluent of all columns were highest by the first PV of flow. In both the Control and Clay column effluent, maximum NO_3 concentrations of 420 mg L^{-1} – 470 mg L^{-1} were measured, while maximum effluent NO_3 concentrations in the Limestone and CaS_x-clay columns ranged from 230 mg L^{-1} – 270 mg L^{-1}. Effluent NO_3 concentrations rapidly declined to below the method detection limit (MDL) of 0.03 mg L^{-1} by 4-7 PV for both the Clay and CaS_x-clay columns and by 18-21 PV for the Control and Limestone columns. Effluent concentrations of SO_4 were similarly at the most elevated value in each column by the first PV flushing of input SRW. The highest concentration of SO_4 measured in the effluent of a column experiment was 39 mg L^{-1} in the Control. In contrast, SO_4 in the Clay column reached a maximum concentration of 21 mg L^{-1}. After 10 PV, effluent SO_4 concentrations in all columns had declined to <7 mg L^{-1} (SRW input), remaining between input concentrations and the MDL (0.1 mg L^{-1}) for the duration of the experiments. The decline of effluent NO_3 and SO_4 to below SRW input concentrations was likely indicative of denitrification (Eq. 1) and SO_4 reduction (Eq. 2) corresponding with the onset of reducing conditions within the columns.

$$CH_2O + \frac{4}{5}NO_3^- \rightarrow \frac{2}{5}N_2 + HCO_3^- + \frac{1}{5}H^+ + \frac{2}{5}H_2O \qquad \text{Eq. 1}$$

$$CH_2O + \frac{1}{2}SO_4^{2-} \rightarrow HCO_3^- + \frac{1}{2}HS^- + \frac{1}{2}H^+ \qquad \text{Eq. 2}$$

Analysis of aqueous profile samples from the columns indicates that NO_3-reducing conditions were established soon after the start of the experiments. Nitrate concentrations measured in

samples extracted from the ports were <2 mg L^{-1} along the vertical transect of the Control and Limestone columns and below the MDL in the Clay and CaS_x-clay columns by the first port sampling session (Appendix A). Sulfate was not initially depleted in aqueous samples extracted from the ports, but did decline to concentrations equal to or less than the SRW input by the second and third port sampling sessions.

Release of effluent dissolved Mn was greatest in the Clay column with a peak concentration of 3500 µg L^{-1} measured at 80 PV. Manganese concentrations in all columns were initially elevated, ranging from 1350 µg L^{-1} – 2300 µg L^{-1} by approximately 30 PV and remaining above input levels for the duration of the experiments. Dissolved Fe was most elevated in the Control column effluent, with a maximum concentration of 314 µg L^{-1} measured at 26 PV. Effluent Fe was elevated in the Clay column by the first PV of flow and reached a maximum concentration of 280 µg L^{-1} by 103 PV. In contrast, effluent Fe was highest in both the limestone and CaS_x-clay columns by approximately 30 PV with concentrations of 170 µg L^{-1} and 125 µg L^{-1} respectively. Bacteria are capable of oxidizing organic carbon present in sediment by pairing with Mn(IV) oxides and Fe(III) oxyhydroxides as terminal electron acceptors (Lovley & Phillips, 1988). This process can result in elevated concentrations of dissolved Mn and Fe through reduction of the mineral phases (Eq. 3 and Eq. 4).

$$CH_2O + 2MnO_2 + 3H^+ \rightarrow 2Mn^{2+} + HCO_3^- + 2H_2O \quad \text{Eq. 3}$$

$$CH_2O + 8FeOOH + 15H^+ \rightarrow 8Fe^{2+} + 2HCO_3^- + 12H_2O \quad \text{Eq. 4}$$

Instances of elevated MeHg concentrations in the effluent of all columns were typically associated with peaks in dissolved Mn, Fe and organic carbon and occurred after the depletion of

NO_3 and SO_4. The correlation between dissolved Fe and aqueous MeHg has also been observed in several studies (Paulson, 2014; Hellal et al., 2015; Desrochers et al., 2015) and is attributed to microbially mediated Fe(III) reduction by IRB. At the South River, Both IRB and SRB contribute to MeHg production, with SRB being dominant in the upper layers of sediment and IRB contributing to net methylation at depth (Yu et al., 2012).

2.4.5 Conclusions

These saturated column studies demonstrate that limestone and attapulgite clay were ineffective at minimizing Hg transport when blended with contaminated sediment. While the addition of limestone did not result in an appreciable change in Hg mobilization relative to the control, attapulgite clay caused rapid and extensive Hg transport likely through the de-stabilization of sediment-bound Hg. Net production of MeHg was similarly elevated in sediment blended with attapulgite clay, likely as a result of colloid-facilitated transport and the increase in destabilized and subsequently more bioavailable Hg observed with this amendment. Experiments did show that modification of attapulgite clay with a CaS_x solution greatly decreased Hg mobilization with respect to the unmodified material and the control without significantly altering MeHg production or porewater geochemistry. Increased interactions between the S groups on the clay and Hg appear to have countered the destabilization effects seen with the unmodified clay and promoted aggregation and deposition of clay-bound Hg.

The results of this study lend promise to the use of CaS_x-modified sorbent amendments for *in situ* remediation of Hg-contaminated sediments. Treatment with CaS_x is relatively simple and inexpensive, utilises a reagent approved for environmental use by the U.S.-EPA and could

likely be applied to variety of different materials, including those that demonstrate limited Hg uptake capacity.

Table 2.1 – Summary of amendments and flow parameters for column experiments.

Column ID	Control	Limestone	Clay	CaS_x-Clay
Amendment Type	N/A	Agricultural Limestone	Attapulgite Clay	CaS_x-modified Attapulgite Clay
Amendment Percentage (dry weight)	N/A	2%		
Mass of Dry Sediment in Column (g)	211	192	172	172
Average Pore Volumes Flushed per Week	3.9	3.3	3.5	3.5
Total Pore Volumes Flushed	187	154	153	145

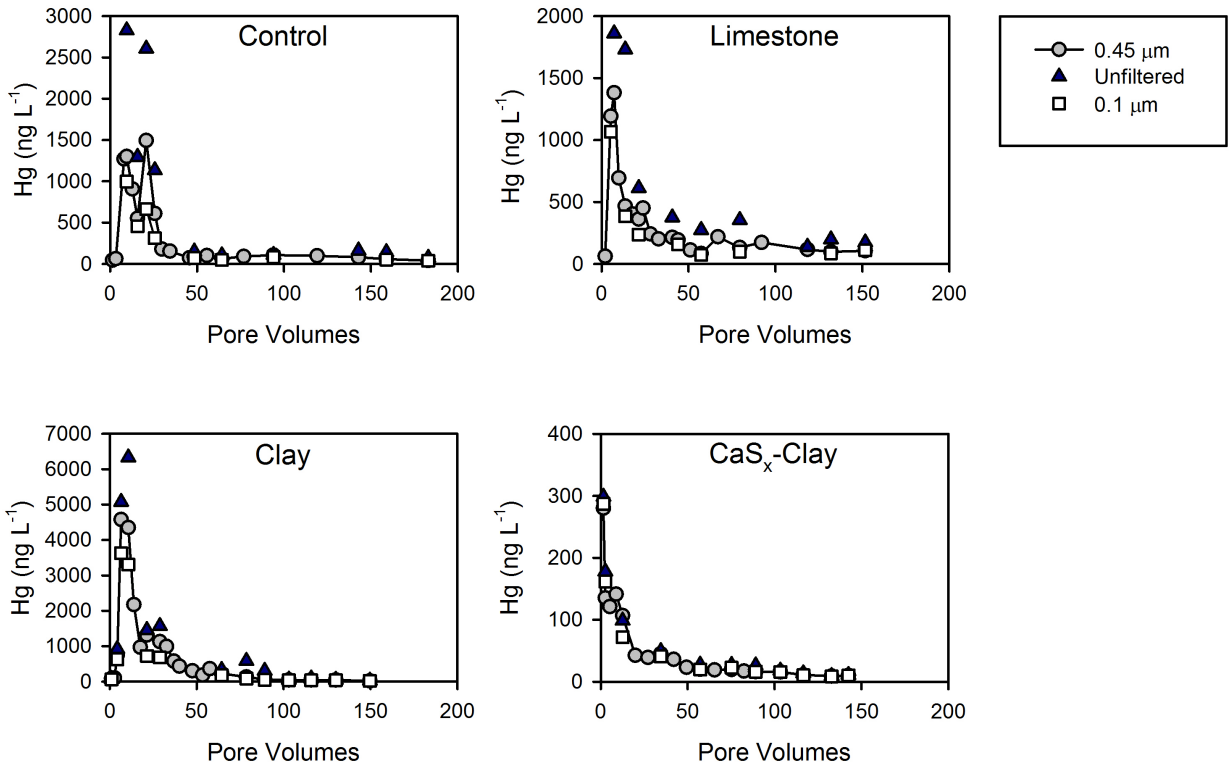

Figure 2.1 – Concentrations of THg, 0.45-Hg and 0.1-Hg in the effluent of the column containing Hg-contaminated sediment (Control), sediment amended with agricultural limestone (Limestone), sediment amended with attapulgite clay (Clay) and sediment amended with CaS_x-modified attapulgite clay (CaS_x-Clay). Note the changes in scale found on the Hg axis.

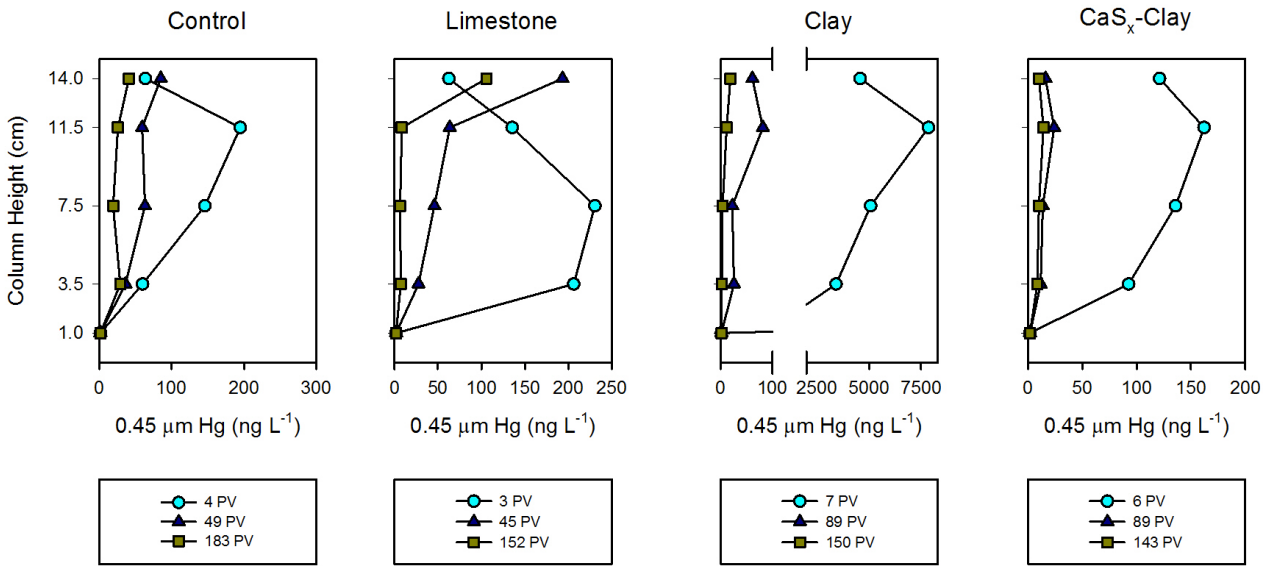

Figure 2.2 - 0.45 um-filtered Hg measured samples extracted from the ports of the column containing Hg-contaminated sediment (Control), sediment amended with agricultural limestone (Limestone), sediment amended with attapulgite clay (Clay) and sediment amended with CaS_x-modified attapulgite clay (CaS_x-Clay). Note the change in scale found in the Hg axis.

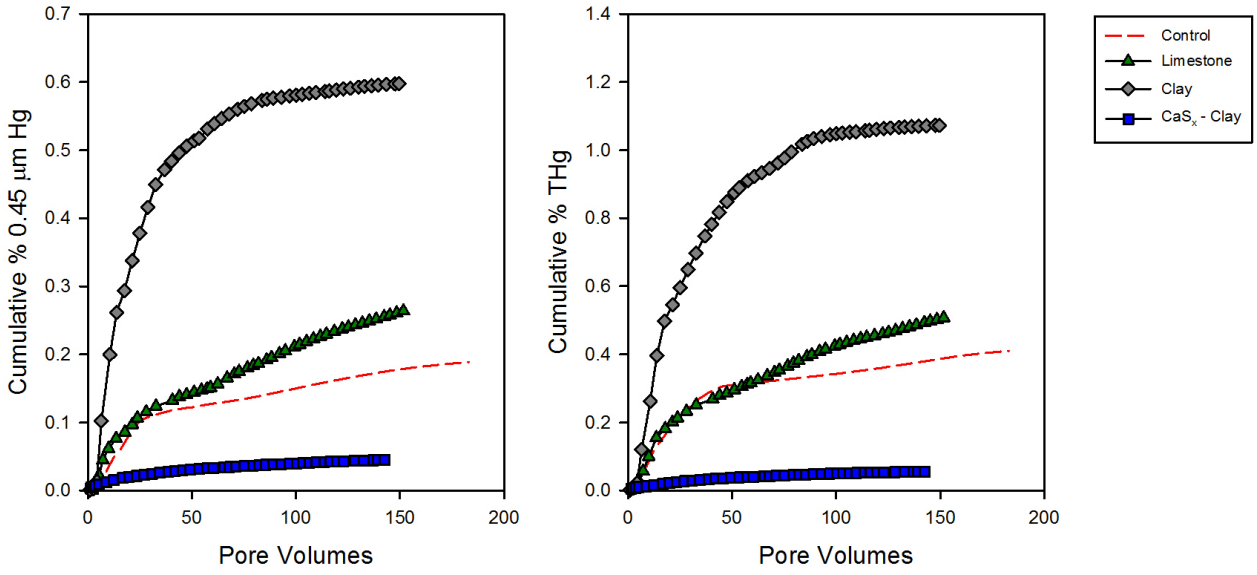

Figure 2.3 - Cumulative 0.45 µm filtered Hg (left) and cumulative unfiltered total Hg (right) measured in the effluent of the column containing Hg-contaminated sediment (Control), sediment amended with agricultural limestone (Limestone), sediment amended with attapulgite clay (Clay) and sediment amended with CaS_x-modified attapulgite clay (CaS_x-Clay). Cumulative Hg is expressed as a percent of the total solid-phase Hg present within each column. Note that the y-axis scale for the subplot on the right is double that of the subplot on the left.

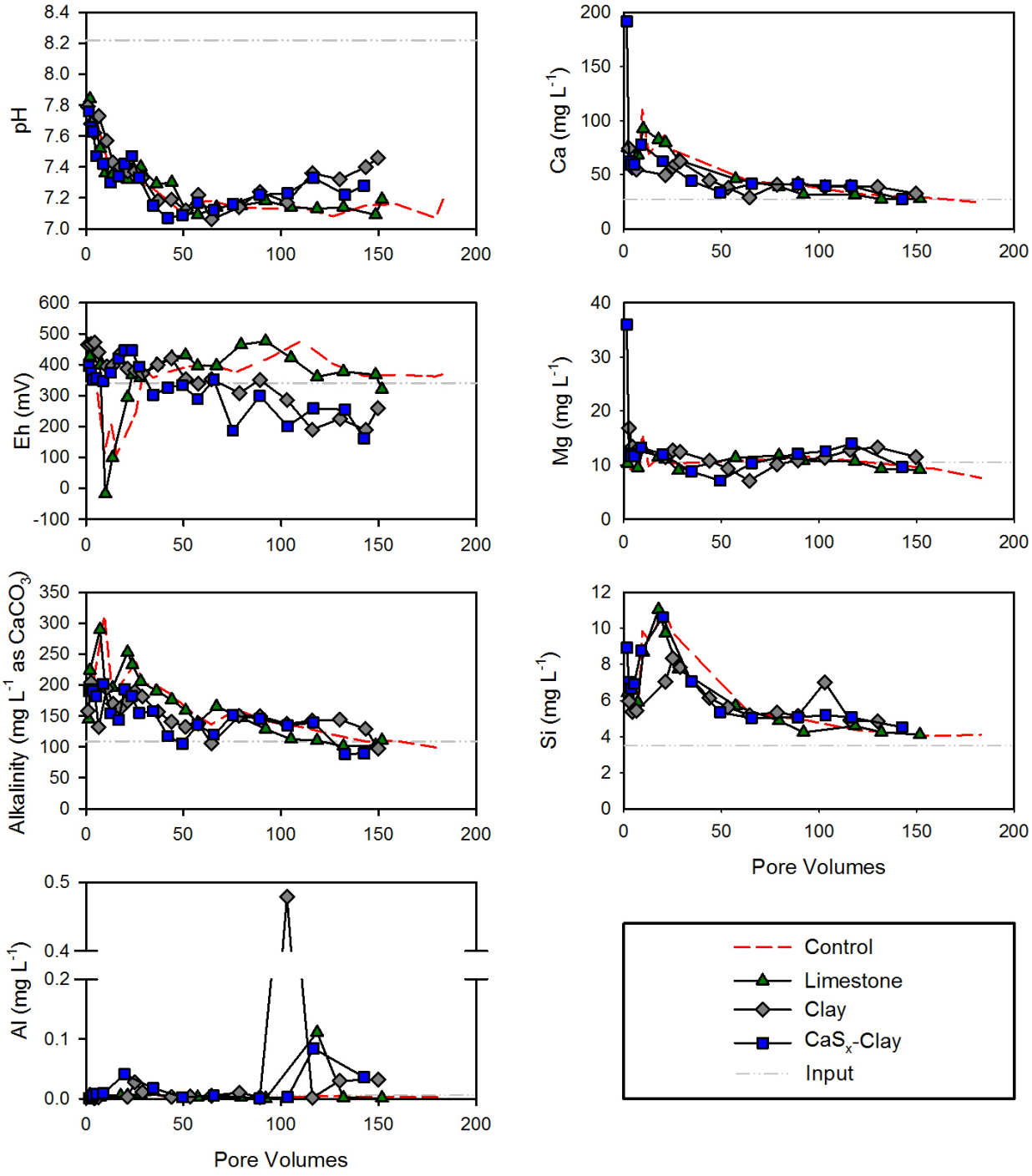

Figure 2.4 - Aqueous composition of the effluent from of the column containing Hg-contaminated sediment (Control), sediment amended with agricultural limestone (Limestone), sediment amended with attapulgite clay (Clay) and sediment amended with CaS_x-modified attapulgite clay (CaS_x-Clay).

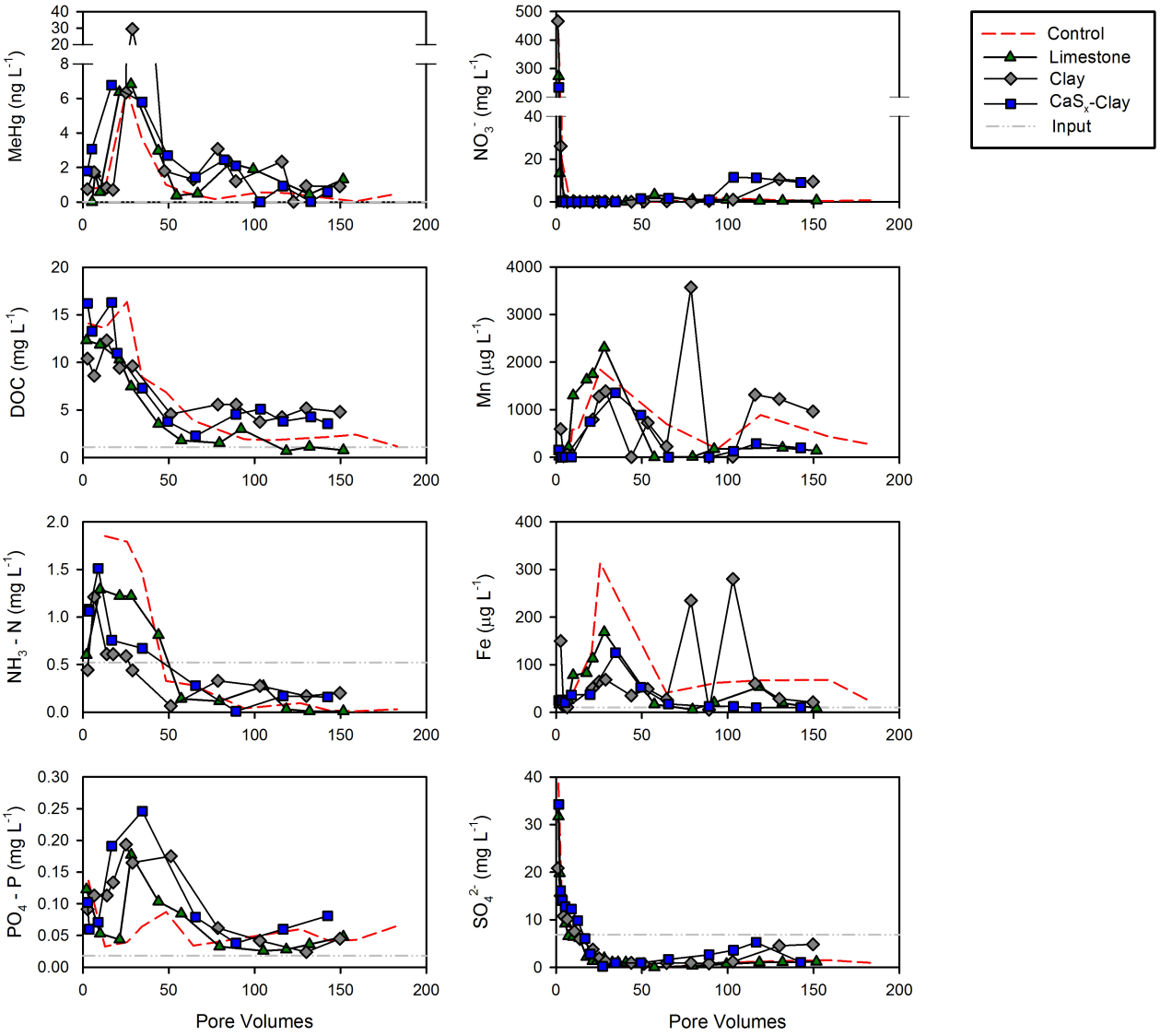

Figure 2.5 - Concentrations of MeHg and select redox indicators in the effluent of the column containing Hg-contaminated sediment (Control), sediment amended with agricultural limestone (Limestone), sediment amended with attapulgite clay (Clay) and sediment amended with CaS_x-modified attapulgite clay (CaS_x-Clay).

Chapter 3 – Co-blending of Biochars to Stabilize Mercury in Contaminated Riverbank Sediment from the South River, VA

3.1 Synopsis

In riverine environments, mercury (Hg) contamination derived from mining or industrial processes can persist long after direct Hg inputs have ceased. In many instances, complete removal of Hg-contaminated soils and sediments from affected riverbanks and floodplains is not feasible due to the wide spread occurrence of Hg downstream of the initial source; instead, *in situ* remediation techniques can be employed to immobilize Hg and render it less bioavailable. Flow-through, saturated column experiments were conducted to evaluate the effectiveness of different biochar materials to sequester and stabilize Hg when blended with contaminated sediment. Modification of biochar with either HNO_3 or with a solution of calcium polysulfide (CaS_x) was employed to alter the physiochemical properties of the material and render it more effective for Hg remediation. Five column experiments were conducted by mixing biochar with Hg-contaminated riverbank sediment from the South River, VA, including a) unamended sediment control, b) 2 % amendment of unmodified biochar, c) 2 % amendment of HNO_3-modified biochar, d) 2 % amendment of CaS_x-modified biochar, and e) 5 % amendment of CaS_x-modified biochar. All columns were continuously flushed with low-Hg river water collected from the South River while effluent and profile samples were collected at regular intervals and analysed for Hg, methylmercury (MeHg) and other aqueous chemistry parameters. Release of Hg from the sediment amended with unmodified and HNO_3-modified biochar was similar to the unamended sediment, suggesting little control of Hg transport by those materials. In contrast, concentrations of Hg measured in effluent and profile samples for the experiments containing

CaS_x-modified biochar were significantly lower. Mercury leaching (0.45 µm-filtered) from the sediment amended with 2 % CaS_x-modified biochar decreased by 71 % relative to the control. When the percentage of CaS_x-modified biochar was increased to 5 %, an 83 % reduction in Hg release was observed relative to the sediment control. These results suggest that the presence of CaS_x-modified biochar may be an effective amendment for limiting the release of Hg from contaminated sediment. This control is likely a result of favourable interactions between available Hg and S groups present on the biochar surface. Net production of MeHg was not appreciably altered by the biochar amendments, although increased leaching of dissolved organic carbon, Mn and PO_4-P was observed from the sediment amended with 5 % CaS_x-modified biochar. Sulfur X-Ray absorption near edge structure spectroscopy (XANES) on both the unmodified and CaS-modified biochars indicate that a greater proportion of reduced S was present on the surface of the CaS_x-biochar than on the unmodified material. This investigation provides critical information regarding the suitability of CaS_x-modified biochar for stabilization of Hg contamination and the feasibility of co-blending as a Hg-remediation strategy.

3.2 Introduction

Mercury (Hg) is a highly toxic heavy metal that is released to the environment primarily from anthropogenic activities. Globally, the majority of contaminant Hg is released into the atmosphere as a result of fuel (coal) combustion and waste incineration (Driscoll et al., 2013). Once airborne, atmospheric Hg can be transported long distances and ultimately deposited in aquatic and terrestrial environments (Lindqvist et al., 1991; Schroeder & Munthe, 1998; Fitzgerald & Lamborg, 2013). Currently, atmospheric transport and subsequent deposition of Hg

is considered the largest source of Hg to most watersheds (Fitzgerald et al., 1998). On a local scale, Hg can be introduced to watersheds and riverine systems by direct inputs from industrial processes, mining and chlor-alkali plants (Driscoll et al., 2013). Numerous river systems have been affected by anthropogenic Hg contamination, including the Carson River in Nevada (Wayne et al., 1996), the English-Wabigoon river system in Ontario (Kinghorn et al., 2007) and the Idrija River in Slovenia (Bonzongo et al., 2002). Due to the strong interactions between Hg and natural organic matter present in soils, Hg can remain sequestered in riverbank sediments and floodplain soils for many years after contaminant release has ceased. Sequestered Hg can be re-mobilized by riverbank erosion, surface runoff and de-gassing from soils, thus providing a secondary source of Hg contamination (Miller et al., 1998; Amos et al., 2013).

The processes controlling the re-mobilization of Hg in riverbank sediments and floodplain soils are complex (Hellal et al., 2015; Poulin et al., 2016). Mercury is bound to sediments and soils through sorption to clays, other inorganic materials (hydroxides, oxyhydroxides) and organic matter constituents (thiol compounds, OH^-, Cl^-, S^{2-}) (Gabriel & Williamson, 2004). Erosion, precipitation and flooding processes can perturb these soils and sediments, releasing Hg-bearing particles that are highly mobile and can be redistributed downstream of the initial site of contamination. Anoxic soils and sediments associated with riverine systems are also ideal environments for the production of the organomercury species methylmercury (MeHg) (Gilmour & Henry, 1991). Methlymercury is a powerful neurotoxin that can pass through the blood-brain barrier and accumulate in the tissue of organisms (Ceccatelli et al., 2010). Bioaccumulation can result in MeHg concentrations in fish that are many times higher than the surrounding water (Fitzgerald and Lamborg, 2013). Formation of MeHg is a bacterially-mediated process attributed

primarily to sulfate-reducing and iron-reducing bacteria (SRB and IRB) present in anoxic sediments (Gilmour et al., 1992; Kerin et al., 2006; Yu et al., 2012). The availability of electron donors (organic substrates) and acceptors (NO_3, Mn(III/IV), Fe(III) and SO_4) utilized by methylating bacteria are important controls on the rate of MeHg production. In addition production of MeHg is dependent on the speciation of Hg with neutrally-charged Hg-ligand complexes and more recently, HgS nanoparticles considered most bioavailable to methylating bacteria under anoxic conditions (Graham et al., 2012; Pham et al., 2014).

In contaminated watersheds where Hg has been transported downstream of the initial point source, site remediation will require strategies for stabilization of Hg in potentially large expanses of floodplain soils and river sediments. One option for remediation that can be used for treatment of Hg *in situ* is the application of sorptive and/or reactive amendments to contaminated soils and sediment. These amendments can be blended into soil or sediment and serve to sequester Hg, rendering it less mobile and less bioavailable. Amendment materials that can be effective for Hg remediation include activated carbons and biochars (Gomez-Eyles et al., 2013), cements (Serrano et al., 2016), and S-functionalized amendments (Chaves et el., 2011).

Biochar is widely defined as a carbon-rich material produced by thermal decomposition of biomass at low temperatures (<700 °C) and under low oxygen conditions (Johannes Lehmann & Joseph, 2009). It is similar to the commonly used activated carbon, but does not undergo an additional post-production activation step and thus is widely considered to be less expensive (Beesley et al., 2011). As a soil amendment, biochar has been used for remediation of heavy metal contamination due in part to its large surface area, presence of surface functional groups and longevity in soils (Beesley et al., 2010; Jiang et al., 2012). Several studies have demonstrated

the effectiveness of Hg removal from solution by biochar (Desrochers, 2013; Paulson, 2014; Xu et al., 2016) but few have focused on the sequestration of Hg by biochar when mixed directly into contaminated soils or sediments.

Modification of carbon-based soil amendments (activated carbon, biochar) can be useful in enhancing properties such as surface area, surface charge and the presence of functional groups. In heavy metal remediation, modification of biochars is employed to increase the presence of oxygen-containing functional groups (carboxyl, hydroxyl, phenolic) considered key to metal-binding ability (Uchimiya et al., 2011, 2012). Impregnation of activated carbon with S has been shown to increase the uptake capacity of both aqueous and volatile Hg from industrial processes, due to the strong interaction between S and Hg (Liu et al., 2000; Krishnan & Anirudhan, 2002).

Co-blending biochar with contaminated sediment provides an option for *in situ* treatment of floodplain soils and river sediments with elevated Hg concentrations. In this study, a series of laboratory column experiments was conducted under saturated flow conditions to evaluate the effectiveness of co-blending biochars to stabilize mercury and prevent its release from contaminated sediment. The sediment utilised in this experiment was collected from the South River, VA, USA. Historical release of Hg from a textile plant in Waynesboro, VA resulted in widespread contamination of riverbank sediments and floodplain soils within the South River watershed. Mercury released from these sediments and soils provides the largest current source of Hg contamination to the river (Eggleston, 2009; Flanders et al., 2010).

Several biochar materials were evaluated in this experiment, including an unmodified biochar and two modified biochars. One biochar was modifed with HNO_3 to increase oxygen-containing functional groups and promote Hg-chelation and a second biochar sample was

modified with calcium polysulfide (CaS_x) to impart S-bearing groups and promote formation of Hg-S complexes. Calcium polysulfide is a commercially available fungicide that is approved by the U.S.-EPA for environmental use (U.S.-EPA, 2005). It is typically employed as a chemical reductant and was used for *in situ* remediation of chromium at the Coast Wood Preserving Superfund site located in California (U.S.-EPA, 2011). Samples of biochar were collected at the termination of the experiments and analysed using synchrotron-based X-ray absorption near-edge structure (XANES) spectroscopy to evaluate the influence of CaS_x on S groups present on biochar and to investigate changes in those S groups with time in a flowing, water-saturated environment. The results of these experiments provide insight into the utility of biochar as material for Hg sequestration, with implications for the South River and other Hg-contaminated sites.

3.3 Materials and Methods

3.3.1 Sediment and Water Collection

Sediment used in the experiments was collected from a riverbank located ~0.4 km downstream (relative river mile (RRM) 0.25) of the point of historical Hg release. At RRM 0.25, the South River is approximately 30 m wide with steep banks. The sediment collection site was located on the western bank of the river, 3-3.7 m (10-12 feet) below the top of the riverbank close to the base-flow level of the river. After collection, the sediment was shipped to the University of Waterloo where it was later homogenized, separated into 1L Nalgene bottles, wrapped in aluminum foil and stored at 4°C. Sediment from RRM 0.25 was classified as containing a relatively low concentration of Hg when compared to other sediments from the South River, with

a solid-phase Hg concentration of 5.2 μg g^{-1}. South River Water (SRW) used in the experiments was collected on an approximately bimonthly basis upstream of the mercury release point and shipped to the University of Waterloo on ice where it was subsequently stored at 4°C away from light.

3.3.2 Reactive Material

Biochar used in all experiments (Cowboy Charcoal, Albany, KY) was produced from oak and maple hardwoods that were charred at approximately 700 °C under low-O_2 conditions. Prior to use, the biochar was crushed and subsequently sieved to remove fines, with the 0.5 mm – 2.36 mm diameter fraction retained for the column experiments. Nitric acid-modified biochar was produced by soaking 90 g of biochar in 1.5 L of 0.5M HNO_3 for 24 hours under aerobic conditions. The resulting material was rinsed with de-ionized water until a constant pH was observed in the supernatant and dried at room temperature. Enhancement of biochar with additional S groups was achieved using a solution of CaS_x. Production of CaS_x-modified biochar involved combining 20 g of biochar with 2.17 mL CaS_x solution (Sure-gro Inc., Brantford, ON) and 400 mL ultrapure water (Milli-Q purification system). The mixture was left to react for four days under anaerobic conditions, rinsed with ultrapure water and dried at room temperature.

3.3.3 Experimental Set-Up

Five column experiments (Table 3.1) were conducted using acrylic columns that were 15 cm long with an inner diameter of 4 cm and a volume of 171.9 cm^3 ± 2.7 cm^3: Control (unamended sediment), CC (sediment + unmodified biochar), CC+HNO_3 (sediment + HNO_3-modified biochar), CC+2%CaS_x (sediment + 2 % amendment of CaS_x-modified biochar) and CC+5%CaS_x

(sediment + 5 % amendment of CaS_x-modified biochar). Sediment was amended with 2 % or 5 % biochar (dry weight) prior to being packed into columns. The required mass of biochar was blended with sediment in small batches to ensure an even distribution of the material. All columns were then packed by first placing coarse and fine NITEX screens on the bottom of the column followed by a 1 cm layer of silica sand to ensure sediment was adequately contained. SRW was then continuously pumped upwards through the column while sediment was added in small increments to ensure saturation. When the sediment was approximately 1 cm from the top of the column, another layer of silica sand as well as both coarse and fine NITEX screens were placed on top of the sediment and the column was sealed. The input solution for all columns consisted solely of SRW, stored at laboratory temperature with minimal exposure to light. South River water was pumped upwards through the columns at a constant rate (Table 3.1) using a multi-channel peristaltic pump (Ismatec, Switzerland). All column experiments were conducted for a duration of 36 – 47 weeks, representing approximately 150 pore volumes (PV) of flow.

3.3.4 Aqueous Sample Collection and Analysis

Column effluent was collected in 125 mL narrow-mouth amber bottles that were purged with N_2 gas prior to sample collection to minimise exposure to atmospheric O_2. Samples were drawn from the collection bottle using 30 mL sterile polypropylene/polyethylene luer-lock syringes (Norm-Ject). Columns were outfitted with three 0.75 cm diameter ports that were evenly distributed along the length of the columns and allowed for collection of pore water along the length of the column. Samples from the ports were collected in 30 mL glass syringes (BD Multi-Fit) at the unaltered column flow rate. Profile sampling was conducted three times over the length

of all experiments: once at early time (2-9 PV), once in the middle of the experiment (17-107 PV) and once at the end of the experiment (148-183 PV). Sample filtration was performed using 32 mm diameter syringe filters with 0.1 µm or 0.45 µm Supor Membranes (Acrodisc®). All samples were stored in 15 mL amber borosilicate bottles that were pre-cleaned using a vacuum and ionization process (Qorpak) with the exception of samples for cation and anion analysis, which were stored in 15mL polypropylene bottles (Nalgene).

Samples for Hg analysis were acidified to pH<2 using ultrapure HNO_3 and kept at 4 °C until analysis by cold vapour atomic fluorescence spectroscopy (CVAFS) (Tekran®) following U.S.-EPA Method 1631 (U.S. EPA, 2002). A summary of quality assurance/quality control (QA/QC) measures taken during Hg analysis can be found in Appendix C. Analysis of MeHg was performed on 0.45 µm filtered samples that were acidified using analytical grade HCl and kept frozen at -20 °C until use. MeHg concentrations were determined by the U.S.-EPA method 1630 (U.S. EPA, 2001) using the distillation, aqueous ethylation, purge and trap and CVAFS technique (Tekran®).

Anion samples were filtered (0.45 um), left unacidified and frozen at -20 °C immediately after collection. After thawing, anion concentrations were determined by ion chromatography (Dionex ICS-5000) with an IonPac™ AS18 2 × 250 mm column and a KOH eluent. Concentrations of organic acids (formate, lactate propionate, acetate) were determined using an IonPac™ AS11 0.4 × 250 mm column. Standards for both anions and organic acids were prepared on the day of analysis. Samples for cation analysis were acidified with ultrapure HNO_3 and stored at 4 °C until analysis using inductively coupled plasma optical emission spectroscopy (iCAP 6000) for major cations and inductively coupled plasma mass spectroscopy (X-Series 2)

for trace elements. Geochemical speciation modelling was performed on effluent samples from the Control, CC, CC+HNO_3, CC+2%CaS_x and CC+5%CaS_x columns using PHREEQC. A summary of ionic strength, charge balance error and saturation indices for select minerals can be found for each column in Appendix B.

Ammonia, phosphorus and dissolved organic carbon (DOC) analyses were completed on samples that were passed through 0.45 µm filters and acidified using OmniTrace Ultra High Purity H_2SO_4. Ammonia-nitrogen (HN_3-N) was analysed with a spectrophotometer (HACH DR 2800) using the salicylate method (Method 8155 from the DR 2800 manual). Phosphorus as orthophosphate (PO_4-P) was quantified using the ascorbic acid spectrophotometric method derived from method 4500-P from the Standard Methods for Examination of Water and Waste Water (HACH DR 2800). DOC was measured using a wet oxidation total organic carbon analyser (Aurora 1030W).

3.3.5 Solid-Phase Sample Collection

Samples for solid-phase analysis were extracted from all columns upon termination of the experiments at 150 PV. The sediment and biochar mixture was removed from the columns in 2 cm intervals under anaerobic conditions. Samples for THg digestion, total MeHg determination and Hg sequential extraction were collected from the 1-3 cm, 5-7 cm and 9-11 cm intervals relative to the column influent and stored in glass vials. The sediment mixture for DNA extraction was collected from the 1-3 cm, 5-7 cm and 9-11 cm intervals using 70 % ethanol-washed tools and stored in autoclaved 50 mL polypropylene vials. All solid-phase samples were frozen immediately after collection at -20 °C.

3.3.6 Polymerase Chain Reaction Analysis

Extraction of DNA for polymerase chain reaction (PCR) analysis was performed on solid-phase samples collected from the Control, CC and CC+HNO_3 columns within 9 weeks of termination of the column experiments. DNA extractions were performed using an UltraClean® Soil DNA Isolation Kit (MoBio Laboratories) within an AC600 Series Combination PCR Workstation (AirClean®, Raleigh, NC). Isolated DNA was shipped frozen from the University of Waterloo and PCR analysis was performed with an average of 3k reads (MR DNA, Shallowater, TX). A single-step 30-cycle PCR analysis using a HotStarTaq Plus Master Mix Kit (Qiagen, Valencia, CA) was performed with the 16S primer pair 515F/806R. Amplicon products from the PCR analysis were purified using Agencourt Ampure beads (Agencourt Bioscience Corporation, MA) and pyrosequencing was performed using a Roche 454 FLX titanium instrument and reagents as per the manufacturer's instructions. The resulting Q25 sequence data was processed using a proprietary analysis pipeline (MR DNA, Shallowater, TX). Sequences were depleted of barcodes and primers, with sequences containing <200 base pairs, ambiguous base calls and sequences with homopolymer runs exceeding six base pairs being removed. Remaining sequences were then denoised and operational taxonomic units (OTUs) were defined by clustering at 3 % divergence. Singleton sequences and chimeras were removed (Dowd et al., 2008a; Dowd et al., 2008b; Edgar, 2010) and OTUs were taxonomically classified using BLASTn against a database derived from GreenGenes (DeSantis et al., 2006).

3.3.7 Synchrotron Analysis

Synchrotron-based X-ray absorption near edge structure (XANES) spectroscopy was performed at the SXRMB beamline at the Canadian Light Source in Saskatoon, SK. Biochar and sediment samples extracted from column experiments were freeze-dried and ground to a fine powder. Prior to being ground, biochar samples were rinsed with nanopure water to remove sediment particles. At the beamline, samples were mounted on double-sided, conducting carbon tape and loaded into a vacuum chamber. The S K-edge XANES spectra were collected using fluorescence mode and data was processed with the program ATHENA (Ravel & Newville, 2005).

3.4 Results and Discussion

3.4.1 Mercury Immobilization by Biochar

Mercury release from the Control column sediment was characterized by a short period of active Hg leaching resulting in initially elevated effluent Hg concentrations, followed by a decline to stable, relatively low effluent Hg concentrations at later times. The concentration of 0.45-μm filtered Hg (0.45-Hg) measured in the Control column effluent reached a maximum concentration of 1500 ng L^{-1} by 21 PV (Fig. 3.1). Maximum effluent concentrations of both unfiltered Hg (THg) and dissolved/nanoparticulate Hg (0.1 μm-filtered, 0.1-Hg) were observed at 9.5 PV, with concentrations of 2830 ng L^{-1} and 1000 ng L^{-1} respectively. By approximately 48 PV, concentrations of effluent Hg observed in all filter fractions (<0.1 μm, 0.1 μm – 0.45 μm, >0.45 μm) had stabilized to within 40 ng L^{-1} – 160 ng L^{-1}, remaining in this range until the end of the experiment. Analysis of filter fraction distribution indicates that at early times (10 PV – 16 PV),

the majority of Hg in the Control column effluent was found in the >0.45 μm fraction, representing elution of particulate-bound Hg during the first two weeks of column flow. After 21 PV of flow, the percentage of Hg associated with the <0.45 μm fraction began to increase and by 48 PV the distribution of Hg switched to Hg found predominantly in the <0.1 μm fraction. These results suggest an initial flushing of particulate/colloidal-bound Hg followed by prolonged leaching of Hg in the dissolved/nanoparticulate form.

Concentrations of 0.45-Hg measured in aqueous samples extracted from the ports of the Control column are consistent with the trend in Hg leaching observed in the column effluent. Profile Hg samples were most elevated at early times, with the maximum 0.45-Hg concentration of 194 ng L^{-1} observed in sample extracted from the top port at 4 PV (Fig. 3.2). With time, concentrations of Hg in profile samples declined and by the second sampling session at 49 PV, 0.45-Hg measured in samples extracted from all ports was < 65 ng L^{-1}. By experiment completion at 183 PV, concentrations of 0.45-Hg measured in profile samples had declined to <30 ng L^{-1}.

Release of Hg from the sediment amended with unmodified biochar (CC column) occurred in a similar fashion to the Control. Concentrations of 0.45-Hg observed in the CC column effluent reached a maximum value of 1900 ng L^{-1} by 22 PV. At this time concentrations of both THg and 0.1-Hg were also most elevated, with maximum effluent concentrations of 2400 ng L^{-1} and 990 ng L^{-1} respectively. After the initial release of Hg, effluent Hg concentrations from the CC column quickly declined, with all filter fractions stabilizing at Hg concentrations <300 ng L^{-1} by 40 PV of flow. Throughout the duration of the CC column experiment, Hg was evenly distributed between the dissolved/nanoparticulate (<0.1 μm) and particulate (>0.45 μm)

fractions. When compared to the Control, particulate Hg comprised a smaller fraction of the total Hg present in the CC column effluent, but there was little effect on the fate of 0.45-Hg and 0.1-Hg. These results suggest that in a dynamic setting, biochar may act as a filter for Hg-bearing particles, mitigating their transport through the sediment, but does little to increase the Hg sorption capacity of the sediment and sequester Hg in the <0.45 μm fraction.

The addition of HNO_3-modified biochar to the contaminated sediment did not greatly affect Hg sequestration when compared to the Control. Effluent Hg concentrations measured in the CC+HNO_3 column peaked at 22 PV with a 0.45-Hg concentration of 1120 ng L^{-1}. At this time the concentration of 0.1-Hg measured 435 ng L^{-1} and THg measured 1700 ng L^{-1}, representing the most elevated effluent concentrations of Hg in the dissolved/nanoparticulate and particulate fractions. After 42 PV flushings, Hg concentrations in all filter fractions were <250 ng L^{-1} and by the end of the column experiment had declined to <50 ng L^{-1}. Similar to the CC column, a relatively even distribution of Hg among the different filter fractions was observed over the course of the CC+HNO_3 experiment.

Throughout the duration of the CC+HNO_3 column experiment, the highest Hg concentrations were observed in aqueous samples extracted from the ports. Although 0.45-Hg was <100 ng L^{-1} at both the first (3 PV) and last (150 PV) profile sampling sessions, by the middle session at 18 PV, 0.45-Hg measured 2700 ng L^{-1} in the sample from the bottom port and 1500 ng L^{-1} in the sample from the top port. These measurements were made just before the maximum release of effluent Hg at 22 PV and may represent accumulations of Hg in the sediment at the top and bottom of column.

Concentrations of Hg were substantially lower in the effluent of both columns containing CaS_x-modified biochar (CC+2%CaS_x, CC+5%CaS_x) relative to the Control and CC columns. Effluent 0.45-Hg concentrations in the CC+2%CaS_x column reached a peak of 220 ng L^{-1} by 6.6 PV, representing a nearly 7-fold reduction in Hg release compared to effluent from the Control column. Concentrations of 0.1-Hg and THg also peaked at 6.6 PV, measuring 191 ng L^{-1} and 222 ng L^{-1} respectively. By 17 PV, Hg concentrations in all filter fractions were <100 ng L^{-1} and subsequently decreased to <20 ng L^{-1} by 50 PV. At the termination of the experiment, concentrations of Hg in all filter fractions were <10 ng L^{-1}.

Release of aqueous effluent 0.45-Hg in the CC+5%CaS_x column was defined by an immediate peak in Hg concentrations followed by a rapid decline to stable levels. By 3 PV of flow, effluent 0.45-Hg was measured at a maximum concentration of 590 ng L^{-1}. Effluent concentrations of both 0.1-Hg and THg were also most elevated at 3 PV, with concentrations of 560 ng L^{-1} and 690 ng L^{-1} respectively. These effluent concentrations rapidly declined and by 6 PV effluent Hg concentrations in all filter fractions were <100 ng L^{-1}, representing the fastest decrease in Hg concentrations observed in all of the column experiments. By 30 PV, Hg concentrations were consistently below 25 ng L^{-1}, remaining in this range for the duration of the experiment.

In both columns containing sediment amended with CaS_x-modified biochar, approximately 80 % of measured Hg was present in the <0.1 μm fraction. This distribution of Hg indicates that the majority of mobilized Hg was in the nanoparticulate/dissolved fraction while particulate Hg was effectively sequestered within the sediment. This mobile fraction may

represent Hg strongly bound to dissolved organic matter (DOM) that cannot interact with reduced S on the biochar surface and is flushed from the column upon the ingress of SRW.

Mercury concentrations measured in profile samples collected from the CC+2%CaS_x column were significantly lower than Hg measured in profile samples from the CC column and of a similar magnitude to those measured in the Control. A maximum 0.45-Hg concentration of 170 ng L^{-1} was observed in samples from the top port of the CC+2%CaS_x column at the first profile sampling session (10 PV). By the second profile sampling session at 76 PV, Hg concentrations in samples from all ports were <30 ng L^{-1} and by the final profile sampling session at 149 PV Hg concentrations were <5 ng L^{-1}. Mercury concentrations were lower in samples extracted from the ports than in the effluent of the CC+5%CaS_x column, with the most elevated concentration of 102 ng L^{-1} measured in a sample from the top port during the first profile sampling session (6 PV).

Comparison of effluent Hg concentrations from all columns suggests a common trend, where Hg is readily flushed from the column sediment at early times followed by prolonged leaching of lower concentrations of Hg after 30 – 40 PV. Similar behaviour has been observed in other column experiments (Daugherty, 2010; Desrochers, 2013; Poulin et al., 2016) and can be attributed to the nature of Hg sorption. Dissolved Hg-DOM complexes residing in sediment pore water are likely first to elute from the column upon the input of influent SRW, followed by Hg bound to weak sediment binding sites such as carboxyl and phenol groups (Drexel et al., 2002; Xiong et al., 2009). Mercury associated with strong binding sites, such as thiol groups present in the sediment, may be leached more slowly thus producing the plateau in Hg concentrations observed at later times (Xiong et al., 2009).

3.4.2 Cumulative Hg Release

The concentrations of both 0.45-Hg and THg collected in the effluent of a given column were normalized at each sampling point to the total mass of solid-phase Hg in that column (Equation 3.1) (Fig. 3.3). This approach was used to directly compare the effectiveness of each treatment material by accounting for variability in the mass of Hg-bearing sediment present in each column experiment.

$$\frac{\sum [volume\ of\ sample\ (L) \times aqueous\ Hg\ concentration\ of\ sample\ (ng\ L^{-1})]}{mass\ of\ sediment\ in\ column\ (ng) \times Hg\ concentration\ of\ sediment\ (ng\ g^{-1})} \times 100 \qquad \text{Eq. 3.1}$$

As illustrated in Figure 3.3, the cumulative release of 0.45-Hg from the Control column sediment was 0.19 %. The same percent cumulative release of 0.45-Hg released in the effluent of the CC column was higher than the Control at 0.21 %, indicating that Hg was not effectively immobilized in the CC column. Studies conducted by Gomez-Eyles et al. (2013) found that biochar had a much lower capacity for inorganic Hg sorption than activated carbon in a static system spiked with a Hg solution. They also noted that in a modelled simulation of Hg-contaminated sediment, biochar was relatively ineffective at reducing porewater Hg concentrations. In this experiment, the percent Hg released from the CC column was slightly lower than the Control when considering THg concentrations rather than 0.45-Hg (Fig. 3.3), supporting the hypothesis that unmodified biochar acts primarily as a filter for particulate-bound Hg rather than as a sorbent material. Similar results were observed in the HNO_3-modified biochar column, where there was no appreciable control of Hg consistent with both the Control and CC columns.

Cumulative Hg leaching of both the 0.45-Hg and THg fractions was greatly reduced in both columns containing CaS_x-modified biochar. The cumulative percent of 0.45-Hg observed in the effluent of the CC+2%CaS_x column was 0.05 %, while in the CC+5%CaS_x column the cumulative 0.45-Hg percent release was 0.03 %. The release of total, unfiltered Hg also decreased in sediment amended with CaS_x-modified biochar, with cumulative THg measured in the CC+2%CaS_x column effluent being 15 % of that released from the Control and cumulative THg released in the effluent of the CC+5%CaS_x column being 11 % of the Control. These results suggest that the addition of S-containing groups onto the biochar surface increased the Hg treatment capacity of the material under co-blended conditions.

Gomez-Serrano et al. (1998) and Asasian and Kaghazchi (2015) both observed increases in Hg adsorption from aqueous solution on sulfurized activated carbons, which they attributed to the surface reactions between Hg and S present on the activated carbons. Liu et al. (2016) postulate that Hg binding to reduced S is more energetically favourable than to carboxyl and hydroxyl functional groups typically found on biochar and suggest the following mechanism for Hg binding to polysulfude:

$$-S-S-+Hg^{2+} \rightarrow -S(Hg)S- \qquad \text{Eq. 3.2}$$

The presence of excess S introduced to the system by the modified biochar may have led to stronger interactions between Hg derived from sediment and biochar, promoting formation of Hg-S complexes and reducing Hg mobility. Kim et al. (2011) found that increasing S loading on polysulfide-rubber polymer-coated activated carbon resulted in greater removal of $HgCl_2$ from water and suggest that polysulfide groups control Hg binding.

Comparison of the CC+2%CaS_x and CC+5%CaS_x columns illustrates the effect of amendment percentage on Hg removal from sediment porewater. Whereas both 2 % and 5 % amendments by dry weight are considered typical amendment ratios for field applications (Ghosh et al., 2011), a greater reduction in Hg leaching was observed in the sediment with a 5 % amendment of CaS_x-biochar, compared to the 2 % amendment of the same material. The cumulative percentage of 0.45-Hg released from the CC+5%CaS_x column was 60 % of that released from the 2 % amendment, while the cumulative percentage of THg released from the CC+5%CaS_x column was 70 % of that released from the 2 % amendment. This reduction in Hg observed with the 5 % amendment of CaS_x-biochar was likely a result of more effective interactions between Hg and biochar associated with the increased amendment dosage.

3.4.3 Aqueous Porewater Chemistry

Porewater chemistry was monitored in all columns to evaluate changes in geochemical conditions induced by biochar amendments (Fig. 3.4). The chemical composition of the pore water was similar for both the effluent and profile sampling among the columns containing biochar-amended sediment and the results did not differ greatly from the sediment control. Effluent pH ranged from 7.0 – 7.8 in all columns over the course of the experiments. Measurements of pH were typically highest at early times before stabilizing to values between 7.0 – 7.4 by approximately 50 PV. Values of pH in samples taken from the column ports did not fluctuate greatly, remaining between 7.5 – 7.8 at each profile sampling session. Effluent Eh in the Control column measured between 100 mV – 250 mV at early times before increasing to above SRW input (340 mV) by 30 PV. Eh in the CC column effluent ranged between 350 mV – 550 mV

throughout the duration of the experiment, while values of Eh in the CC+HNO_3 column effluent reached a minimum of 0 mV by 2.5 PV before increasing to above the SRW input. Measurements of Eh in the CC+2%CaS_x column effluent were initially similar to the CC column but decreased steadily with time to 130 mV by the end of the experiment. Effluent Eh values in the CC+5%CaS_x column were close to the SRW input at early times before sharply declining at 55 PV and continuing at <300 mV. Measurements of Eh made on samples extracted from the ports of both the CC and CC+HNO_3 columns were lowest (<300 mV) at the first profile sampling session before increasing to at or above input levels by the second profile sampling. This finding is in contrast to both columns containing amendments of CaS_x-modified biochar, where Eh measurements on profile samples were highest at early times and declined to below SRW input values for the second and third profile sampling sessions. Alkalinity in the Control column effluent peaked at 310 mg L^{-1} as $CaCO_3$ by 10 PV before gradually declining to SRW input concentrations (100 mg L^{-1}) by the end of the experiment. Effluent alkalinity in both the CC and CC+HNO_3 columns peaked at 230 mg L^{-1} – 240 mg L^{-1} as $CaCO_3$ by approximately 25 PV followed by a decline similar to the Control. Alkalinity in the columns containing sediment amended with CaS_x-modified biochar peaked at 2-3 pore volumes of flow, with the maximum alkalinity concentration of 590 mg L^{-1} as $CaCO_3$ in the CC+5%CaS_x column more than double that of the unmodified biochar and 2% CaS_x-biochar amendment. In all columns, alkalinity measured in sample extracted from the ports typically increased from top to bottom as the influent SRW moved upwards through the column and like the effluent results, alkalinity decreased with time (Appendix B).

Concentrations of major cations (Al, Ca, Mg, Si) followed similar trends in the effluent of all columns. The highest observed Al concentration of 490 μg L^{-1} was measured in the effluent of the CC+2%CaS_x column at 114 PV. Effluent Al concentrations peaked at a similar PV in both the CC and CC+HNO_3 columns, but lower Al concentrations of approximately 100 μg L^{-1} were observed. Concentrations of effluent Mg in all columns remained close to the SRW input concentration of 10 mg L^{-1} throughout the experiments, with the exception of the CC+5%CaS_x column from which a peak effluent Mg concentration of 32 mg L^{-1} was observed at 3 PV. The most elevated Ca concentration of 230 mg L^{-1} was also observed in the CC+5%CaS_x column effluent at 3 PV of flow. Calcium in the remaining columns peaked between 80 mg L^{-1} – 110 mg L^{-1} by 10 – 20 PV before declining to SRW input concentrations. Effluent Si concentrations in all columns were most elevated at early times, declining to input concentrations by experiment completion.

3.4.4 Net Methylmercury Production and Aqueous Redox Parameters

Measurements of aqueous MeHg concentrations in the effluent of all column experiments were made to determine the suitability of both unmodified and enhanced biochars for use in *in situ* Hg remediation. A significant increase in net MeHg production linked to the addition of biochar to sediment would likely render the material unfavourable for field application. In addition to effluent MeHg, the concentration of electron acceptors (NO_3, Mn, Fe, SO_4), electron donors (dissolved organic carbon (DOC)) and products of organic matter degradation (NH_3-N, PO_4-P) were monitored over the duration of the column experiments to observe changes in porewater redox conditions that potentially affect Hg speciation and MeHg production (Fig. 3.5).

Effluent concentrations of MeHg were similar for the Control and each of the columns containing an amendment. Aqueous effluent MeHg concentrations in both the Control and CC columns were <1 ng L^{-1} at early times before peaking at 6 ng L^{-1} – 7 ng L^{-1} by approximately 27 PV. Concentrations of MeHg then returned to <1 ng L^{-1} by 50 – 60 PV, remaining at this concentration for the duration of the experiments. Similarly, effluent MeHg measured from CC+HNO_3 column was initially low before reaching a maximum concentration of 7.4 ng L^{-1} by 35 PV and returning to low (<1 ng L^{-1}) concentrations by the termination of the experiment. Concentrations of MeHg were slightly lower in the column containing a 2% amendment of CaS_x-modified biochar than in the Control. The most elevated aqueous MeHg measured in the CC+2%CaS_x column effluent was 5.5 ng L^{-1} at 33 PV of flow. Following this peak, MeHg production rapidly declined and excluding a small secondary peak observed at 127 PV, effluent MeHg concentrations in the CC+2%CaS_x column were <1 ng L^{-1} for the majority of the experiment. Concentrations of MeHg measured in the CC+5%CaS_x column effluent deviated from the pattern of results observed in all other columns. Aqueous MeHg concentrations peaked rapidly at 10 ng L^{-1} by 6 PV of flow. The concentrations of effluent MeHg then remained slightly elevated, reaching a secondary peak of 3.4 ng L^{-1} by 29 PV; the same approximate time at which MeHg concentrations were most elevated in all other columns. Net production of MeHg in the CC+5%CaS_x column then proceeded to decline with time and by 77 PV flushings effluent MeHg concentrations were <1 ng L^{-1}.

The similarity between aqueous MeHg concentrations measured in the effluent of the Control and all biochar-amended sediment columns suggests that the rates of Hg methylation were controlled by the sediment properties and were independent of the added biochar. Elevated

MeHg concentrations were observed in the effluent of all columns at similar times (25 PV – 35 PV), suggesting a common control on MeHg production and/or transport across all columns. The delay in maximum MeHg concentrations observed in the effluent of the columns relative to elevated inorganic Hg concentrations may is attributed to a lag in establishment of Fe(III)-reducing and SO_4-reducing conditions within the columns. Hellal et al. (2015) observed MeHg release from columns containing sand and iron oxides spiked with increases in Hg(II) concentrations during periods of Fe(III) and SO_4 reduction, corresponding to increased IRB and SRB activity. Yu et al. (2012) linked net rates of Hg methylation production in South River sediment to both SRB and IRB activities, highlighting the importance of the microbial community in production of MeHg. In this study, comparison of the classes of bacteria identified by PCR analysis on sediment extracted from the Control, CC and CC+HNO_3 columns indicates that considerable change in the bacterial community was not induced by the addition of both unmodified and HNO_3-modified biochar amendments (Appendix B). A comparison of PCR results to a library of predicted methylating bacteria (ORNL, 2016), the percentage of sequence counts in classes containing known methylators was similar in sediment collected from the Control, CC and CC+HNO_3 columns, with an average of 37 % ± 3 %. The percentage of sequence counts in classes containing methylating bacteria typically increased along the length of the columns, away from the SRW input. These results suggest that Hg methylation occurred primarily within the top 7 cm – 13 cm of column sediment, where reducing conditions could develop at greater distances from the influx of O_2-rich SRW.

The peak concentrations of MeHg in the effluent of the Control and all biochar-amended sediment columns were observed after the depletion of both NO_3 and SO_4, indicating the onset of

reducing conditions and bacterial activity necessary for MeHg production. Effluent NO_3 concentrations rapidly declined to below the method detection limit (0.03 mg L^{-1}) by 7 PV in the biochar-amended sediment columns and by 20 PV in the Control, likely as a result of microbially facilitated denitrification reactions. Effluent SO_4 concentrations measured 30 mg L^{-1} – 55 mg L^{-1} in all columns within the first few PV of flow, representing an initial flushing of soluble SO_4. These SO_4 concentrations then declined to below the SRW input concentration of 6.8 mg L^{-1} by approximately 20 PV, corresponding to increases in net MeHg production and suggesting bacterial SO_4 reduction was linked to methylation reactions. Profile sampling results corroborated this rapid onset of NO_3-reducing conditions followed by the transition into SO_4-reducing conditions observed in the effluent of the columns. Nitrate was typically depleted by the first profile sampling session in all columns, while SO_4 was often most elevated at the first profile sampling before declining to below SRW input by the second and third profile sampling sessions. The CC+5%CaS_x column was an exception to this trend, as effluent SO_4 concentrations were below the SRW input by 3 PV and SO_4 measured in the samples extracted from the ports was lowest (~2 mg L^{-1}) at the first sampling session, indicating that SO_4-reducing conditions were established soon after the influx of SRW. Nitrate concentrations measured in samples extracted from the ports increased in all columns to above the SRW input by the second or third profile sampling session, suggesting production of NO_3 within the column sediment occurred at later times. Some studies have established a link between anaerobic nitrification and reduction of metal oxides in marine sediments (Luther III et al., 1997; Anschutz et al., 2000; Fernandes et al., 2015). In particular, manganese oxides are thought to act as the terminal electron acceptor in the

oxidation of ammonia, thus producing NO_3 outside of the typical oxic nitrification process (Equation 3.3) (Hulth et al., 1999; Bartlett et al., 2008).

$$4MnO_2 + NH_4^+ + 6H^+ \rightarrow 4Mn^{2+} + NO_3^- + 5H_2O \quad \text{Eq. 3.3}$$

Release of dissolved Mn and Fe was greatest in the column containing sediment blended with a 5 % amendment of CaS_x-modified biochar. The concentration of Mn in the CC+5%CaS_x column effluent peaked at 4200 μg L^{-1} by 3 PV of flow, representing a 128 % increase relative to Mn observed in the Control. Iron was most elevated in the sample from the top port of the CC+5%CaS_x column, measuring 2200 μg L^{-1} at the first profile sampling session (6 pore volumes). In anaerobic sediments, Mn and Fe can be released into the surrounding pore water via the bacterially mediated reductive dissolution of Mn(IV) oxides and Fe(III) oxyhydroxides (Equations 3.4 and 3.5) (Lovley & Phillips, 1988; Myers & Nealson, 1988).

$$CH_2O + 2MnO_2 + 3H^+ \rightarrow 2Mn^{2+} + HCO_3^- + 2H_2O \quad \text{Eq. 3.4}$$

$$CH_2O + 8FeOOH + 15H^+ \rightarrow 8Fe^{2+} + 2HCO_3^- + 12H_2O \quad \text{Eq. 3.5}$$

In this study on biochar-amended systems, peaks in effluent Mn and Fe concentrations were observed close together and were often aligned with declines in effluent SO_4 and elevated concentrations of MeHg. In particular, the rapid release of large quantities of dissolved Mn observed in the CC+5%CaS_x column effluent occurred at the same time as the decline in SO_4 concentrations to below input levels, the highest concentrations of effluent Hg and MeHg observed in the column and the peak release of several major ions (Al, Ca, Mg). These results suggest that reductive dissolution of Fe and Mn oxides and oxyhydroxides and thus the release of previously bound Hg and Al/Ca/Mg colloids in the CC+5%CaS_x column may have been promoted by the addition of CaS_x, a known reducing agent.

Dissolved organic carbon in the Control column effluent was most elevated at early times, peaking at 16 mg L^{-1} by 25 PV before gradually declining to SRW input concentrations (1 mg L^{-1}) by the end of the experiment. Release of DOC was of a similar magnitude in the effluent of the CC and CC+HNO_3 columns, although a secondary peak of DOC was observed in both columns at 120 – 130 PV. This delayed release of DOC may be attributed to the gradual breakdown of biochar present in the sediment. Liu et al., (2015) found that hard-wood based biochar released more DOC in a short-term continuous leaching test than activated carbon. Biochar, although considered relatively recalcitrant in soils, can also be vulnerable to microbial degradation, resulting in the release of excess DOC when bacterial colonies are active (Lehmann et al., 2009).

Concentrations of DOC were elevated in the effluent of both columns containing CaS_x-modified biochar when compared to the sediment control and to sediment blended with unmodified or HNO_3-modified biochar. Although release of effluent DOC from the CC+2%CaS_x column began similar to the Control, CC and CC+HNO_3 columns, by 76 PV DOC was observed at a maximum concentration of 58 mg L^{-1}. In contrast to this delayed occurrence of DOC in the CC+2%CaS_x column effluent, release of DOC from the CC+5%CaS_x column was rapid, with the peak concentration of 264 mg L^{-1} observed at 3 PV of flow. This elevated concentration of DOC was correlated to the peak effluent concentration of Mn and occurred just before the maximum release of effluent Fe. The association between DOC, Fe and Mn in anaerobic sediments has been well documented and is attributed to both the bacterially mediated oxidation of organic carbon using Mn and Fe oxides as the terminal electron acceptor and to the release of DOC previously bound to these minerals via reductive dissolution (Hamilton-Taylor et al., 1996; Chadwick et al., 2006). Alkalinity, a product of organic matter oxidation under anaerobic conditions, was

observed at peak effluent concentrations in the CC+5%CaS_x column when Mn and DOC were most elevated.

The oxidation and degradation of organic carbon can also produce NH_3-N and PO_4-P (Waybrant et al., 2002). The most elevated concentration of PO_4-P measured in all column experiments was observed in the effluent of the CC+5%CaS_x column, approximately 15 PV after the maximum release of DOC. The increase in concentrations of Mn, DOC, alkalinity and PO_4-P seen in the CC+5%CaS_x column effluent relative to the Control and all other biochar-amended sediment columns seem to suggest either an increase in microbially-mediated oxidation of organic carbon or the onset of more strongly reducing conditions brought about by the addition of CaS_x to the system. Chrysochoou et al. (2012) observed increased leaching of both Fe and Mn from sediment treated with a pulse of CaS_x solution in a flow-through column experiment. An earlier study also found that the addition of CaS_x solution to soil induced the rapid onset of reducing conditions in bench-top batch experiments (Chrysochoou et al., 2010). If a portion of the CaS_x sorbed to the surface of the modified biochar was labile, it is possible that some previously sorbed CaS_x was released from the treated biochar upon the influx of SRW, prompting more reducing conditions in the sediment porewater. This phenomenon was likely more pronounced in the 5 % amendment of CaS_x-biochar than the 2 % amendment as a result of the increased mass of CaS_x-biochar and thus of CaS_x present in the column. Despite the indications of changes to the pore water redox conditions and the introduction of excess S to sediment in the CC+5%CaS_x column relative to all other column experiments, no significant increase in MeHg production was observed and release of Hg from the contaminated sediment was effectively mitigated by the 5 % amendment of CaS_x-biochar.

3.4.5 Amendment Characterization – S XANES

Sulfur XANES spectra were collected to characterize the S species present on the surface of biochar treated with CaS_x. A number of S reference materials were analysed in addition to biochar extracted from terminated column experiments and fresh biochar that had not been blended with sediment (Fig. 3.6). The resulting S XANES spectra are consistent with the increased presence of reduced S on CaS_x-modified biochar (CaS_x-CC) compared to the unmodified material (Fig. 3.6). The most intense peak on the S XANES spectra for CaS_x-CC corresponds with the peak energy for reduced S (2472.7 eV, S^0). The peak with the greatest intensity observed on the S XANES spectra for unmodified CC is positioned at a higher peak energy, corresponding with oxidized S (2482.5 eV, SO_4). These results suggest that reduced S is imparted to the surface of the biochar after reaction with the CaS_x solution. This finding also demonstrates that the CaS_x treatment can withstand multiple water rinsings and exposure to an aerobic environment despite treatment of the biochar with CaS_x solution for a relatively short period of 4 days.

Comparison of the S XANES spectra for the fresh CaS_x-CC with biochar extracted from the CC+2%CaS_x and CC+5%CaS_x columns illustrates changing intensities of reduced S and oxidized S (SO_4) with time (Fig. 3.6). The most intense peak corresponding to the energy of reduced S was observed for the fresh CaS_x-CC. This material was not run in a column experiment and therefore was not exposed to continuous rinsing with the SRW input. A decrease in the intensity of the reduced S peak and simultaneous increase in the oxidized S peak intensity was seen in biochar removed from the CC+5%CaS_x column at 53 days of column run time. This

decrease in the reduced S peak and increase in the oxidized S peak was more pronounced in biochar removed from the CC+2%CaS_x column at 174 days of run time.

Linear combination fitting (LCF) was conducted to determine the similarity between S XANES spectra for biochar samples and S reference materials (Table 3.2; Fig. 3.7). A combination of dibenzothiophene and $CaSO_4$ provided the best fit for fresh unmodified biochar. The addition of elemental S was required to provide the best fit for biochar extracted from the CC, CC+2%CaS_x and CC+5%CaS_x columns. The percentage of elemental S utilized in the LCF varied among the different biochar materials. A fit that included the lowest percentage of elemental S (21 %) provided the closest match for spectra obtained for biochar extracted from the CC column. The best fit for biochar from the CC+2%CaS_x column required 53 % elemental S while the best fit for biochar from the CC+5%CaS_x column required 74 % elemental S. The differences in the percentage of reduced S required to provide the best LCF result for the different biochar materials is consistent with the differences in intensity of the reduced S peak observed in the S XANES spectra for all biochar samples.

The results of both the S XANES spectra and LCF indicate that although reduced S is imparted to biochar treated with CaS_x, the treatment is not stable. When the CaS_x-modified biochar is exposed to continuous flushing with oxygenated water, as would be expected in a field setting, the proportion of reduced S present on the modified biochar decreases. Despite these findings, there was no perceivable impact on the Hg-treatment capacity of the S-modified biochars. Concentrations of Hg in both the effluent of the 2% and 5% amendment columns were consistently lower than the control and unmodified biochar. It may be possible that the majority of available Hg was already associated with recalcitrant Hg-S complexes (cinnabar) therefore the

loss of reduced S was excess and did not affect Hg treatment. In addition, an increase in aqueous SO_4 concentrations as a result of this shift from reduced to oxidized S was not observed. This result indicates that S imparted to the surface of the biochar, independent of speciation, is strongly bound and not likely to accumulate in sediment pore water. This finding has implications for MeHg production in sediments amended with CaS_x-biochar, as there was no evidence for substantial stimulation of methylation reactions induced by the presence of oxidized S (SO_4) on CaS_x-biochar observed in the effluent of the CC+2%CaS_x and CC+5%CaS_x columns.

3.4.6 Implications for Hg Contaminated Sites

The results of this study indicate that co-blending with unmodified biochar at a low amendment percentage does little to mitigate Hg release from contaminated sediments. Although biochar has been shown to be effective at removing Hg from aqueous solutions in static batch tests (Desrochers, 2013; Liu et al., 2016), the Hg sequestration capacity of the material when co-blended with sediment appears to be less effective under dynamic flow conditions. Less effective stabilization may arise from the strong binding of Hg to sediment constituents and the short interaction time between Hg and biochar particles when biochar is applied at a 2 % amendment ratio These finding suggest that unmodified biochar may be most effective in a flow-through remediation technique such as permeable reactive barriers or reactive mats, where contact between Hg and biochar is increased.

The addition of biochar to contaminated sediment had little effect on MeHg production and transport. While no reduction in MeHg concentrations was observed in the CC column

effluent, production of MeHg was not stimulated by the amendment, suggesting that it may be suitable for anaerobic applications where methylation may be a concern.

The use of HNO_3 to oxidize the surface of biochar did not provide any improvement to Hg uptake capacity or suppression of MeHg production under co-blended conditions. It is likely any additional O_2-bearing functional groups imparted to the biochar surface via HNO_3 oxidation were unable to strip Hg already strongly sorbed to sediments or complexed with DOM. In contrast, the use of a commercially available CaS_x solution to impart S functional groups onto the surface of biochar greatly enhanced the Hg uptake capacity relative to the unmodified material. An increase in the proportion of reduced S groups on the biochar, as seen in S XANES spectra, may have resulted in stronger interactions between biochar and available Hg and promoted the precipitation of Hg as solid HgS. Similar effects have been observed with CaS_x-modified clay, where the modified material added as a soil amendment significantly reduced Hg transport when compared to unmodified clay (Chapter 2). The CaS_x-modified biochar was most effective when applied as a 5% amendment to contaminated sediment, although the 2% amendment of the same material also mitigated Hg release. When considering future applications, the addition of CaS_x to biochar did not result in pronounced changes to net MeHg production, despite altering the redox conditions present within the sediment porewater. Although synchrotron characterization revealed that the proportion of reduced S present on the CaS_x-modified biochar decreases with time under saturated conditions, this result did not seem to impact the Hg removal or pore water chemistry of sediment containing CaS_x-modified biochar.

For the South River and other Hg contaminated sites, the use of modified biochar can be a low-cost option for remediation of large areas. While other studies have explored inorganic

materials for Hg stabilization, including limestone and attapulgite clay, CaS_x-modified biochar yielded the most significant reduction in Hg mobilization under co-blended conditions (Chapter 2). Treatment of biochar with a CaS_x solution is a simple process that renders the charcoal many times more effective at Hg removal than its unmodified counterpart. In addition to the ease of production, blending CaS_x-modified biochar into contaminated soils and sediments can eliminate the potential for hazardous waste disposal, the destruction of surrounding ecosystems and minimizes engineering challenges faced with other remediation techniques such as dredging and sediment capping.

Table 3.1- Overview of contents, operating conditions and duration of experiment for the Biochar-amended sediment columns.

Column I.D	**Control**	**CC**	**CC+HNO_3**	**CC+2%CaS_x**	**CC+5%CaS_x**
Amendment Material Type	N/A	Biochar	HNO_3-modified biochar	CaS_x-modified biochar	
Amendment Percentage (dry weight)	N/A	2%			5%
Mass of Dry Sediment in Column (g)	211	173	182	166	173
Average Pore Volumes Flushed Per Week	3.9	3.5	3.4	3.2	4.4
Final Pore Volumes Flushed	187	155	154	152	155

Table 3.2 – Percentage (%) of different S forms and reduced chi squared for the fresh unmodified biochar, biochar from the CC column, biochar from the CC+2%CaS_x column and biochar from the CC+5%CaS_x column as determined by LCF.

Standard	Fresh Unmodified Biochar	Biochar from CC	Biochar from CC+2%CaS_x	Biochar from CC+5%CaS_x
Dibenzothiophene	57	34	10	8
$CaSO_4$ (Gypsum)	43	45	37	18
S^0 (Elemental S)	--	21	53	74
Reduced chi squared	0.03	0.1	0.03	0.02

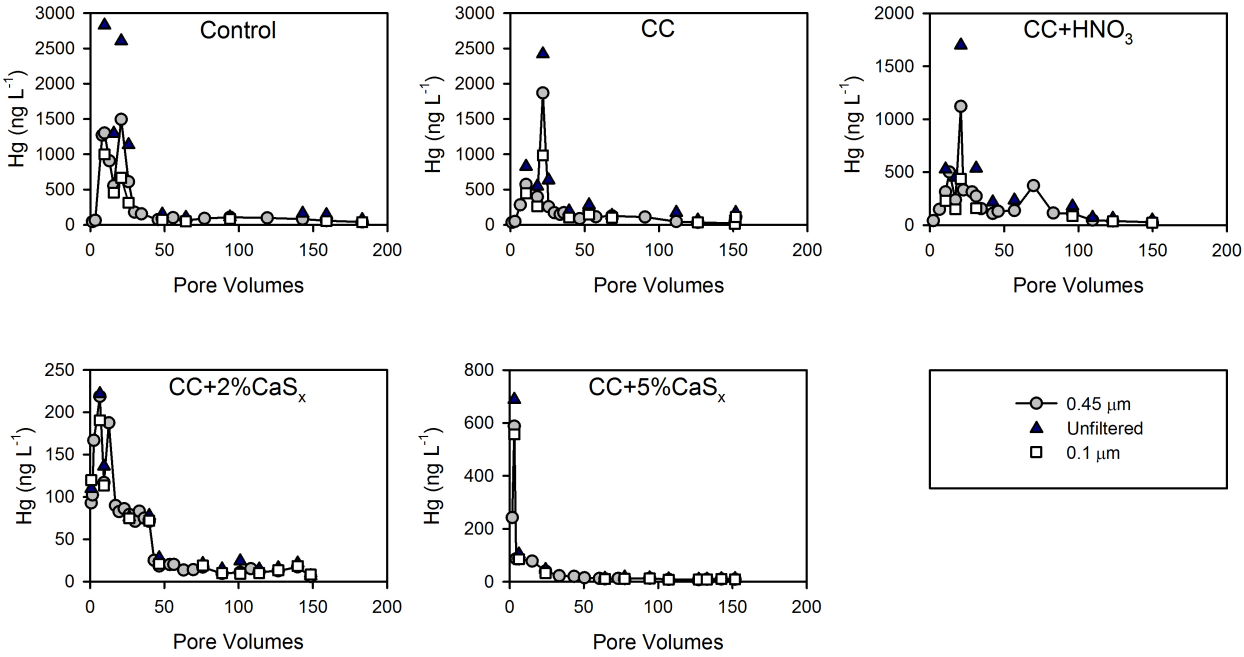

Figure 3.1 – Aqueous concentrations of 0.1-Hg, 0.45-Hg and THg measured in the effluent of column containing Hg-contaminated sediment (Control) and columns with amendments, including hard-wood biochar (CC), HNO_3-modified biochar (CC+HNO_3), a 2 % amendment of CaS_x-modified biochar (CC+2%CaS_x) and a 5 % amendment of CaS_x-modified biochar (CC+5%CaS_x). Note the change in scale along the Y-axis of all plots.

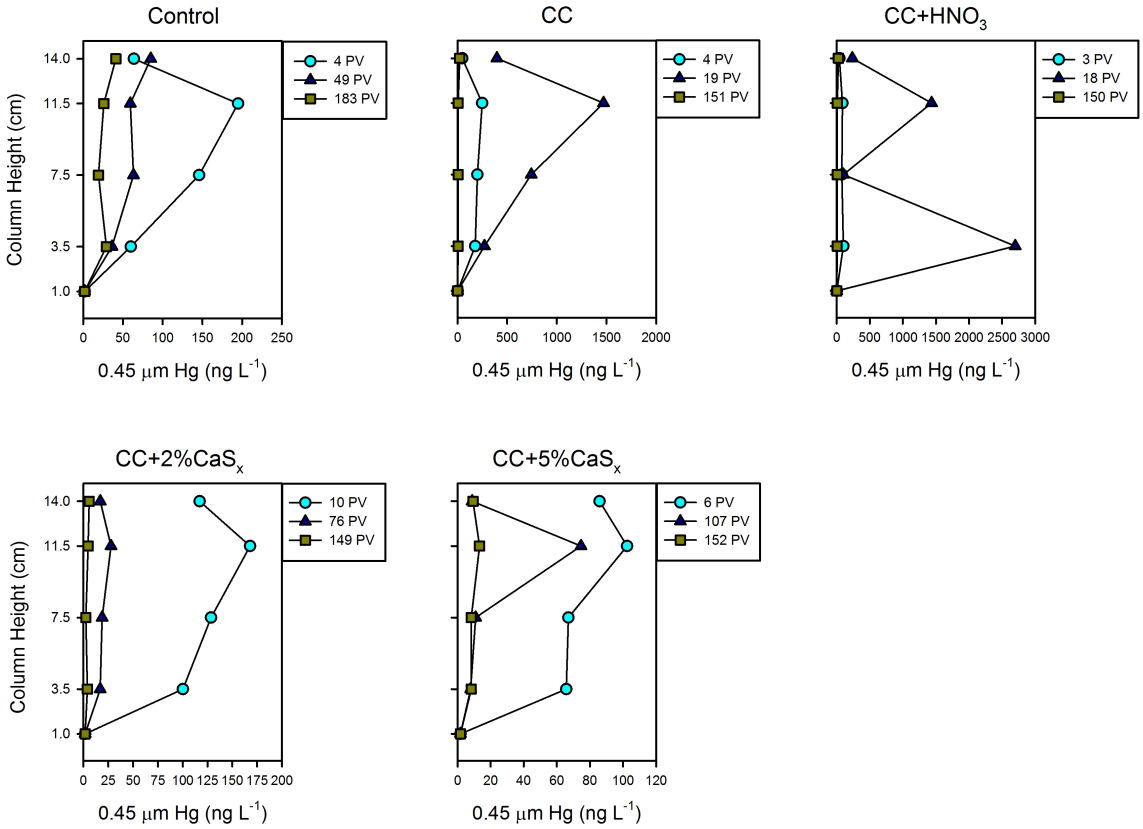

Figure 3.2 – Aqueous concentrations of 0.45-Hg measured in samples extracted from the ports of the column containing Hg-contaminated sediment (Control) and columns with amendments, including hard-wood biochar (CC), HNO_3-modified biochar (CC+HNO_3), a 2 % amendment of CaS_x-modified biochar (CC+2%CaS_x) and a 5 % amendment of CaS_x-modified biochar (CC+5%CaS_x). Hg concentrations measured in the SRW input (column height = 1.0 cm) and in the effluent of each column at the given pore volume (column height = 14.0 cm) are included on the plots. Note the change in scale along the x-axis for the different plots.

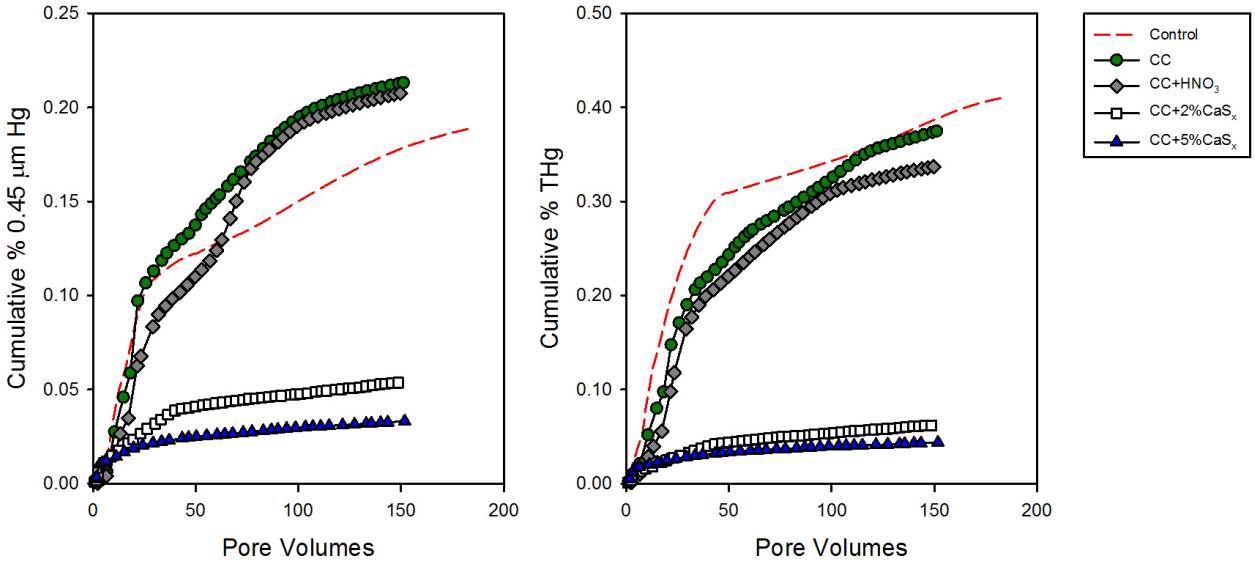

Figure 3.3 – Cumulative concentrations of 0.45-Hg (left) and THg (right) measured in the effluent of the column containing Hg-contaminated sediment (Control) and columns with amendments, including hard-wood biochar (CC), HNO_3-modified biochar (CC+HNO_3), a 2 % amendment of CaS_x-modified biochar (CC+2%CaS_x) and a 5 % amendment of CaS_x-modified biochar (CC+5%CaS_x). Cumulative Hg released is expressed as a % of total solid-phase Hg present in each column.

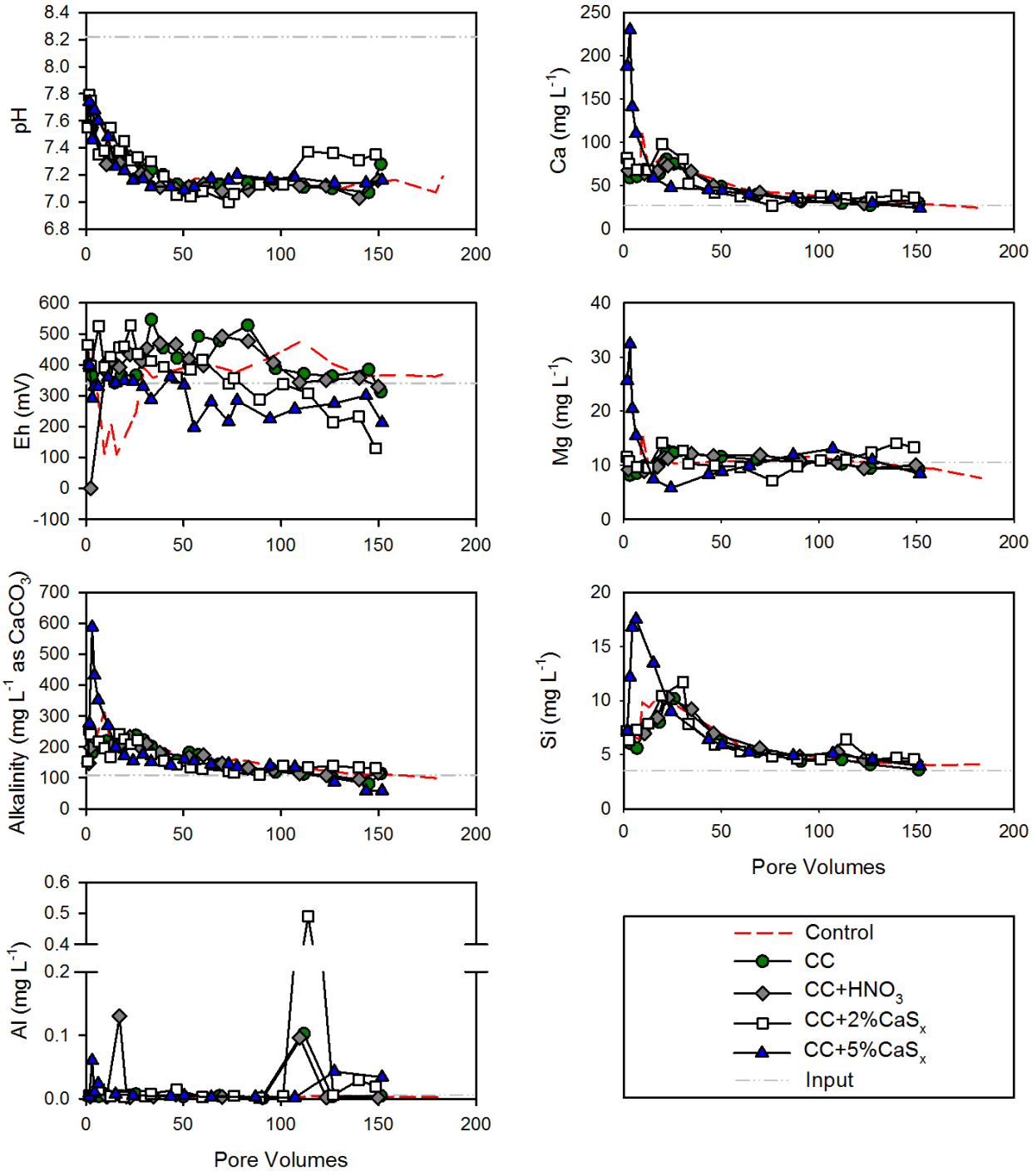

Figure 3.4 – Aqueous chemistry measured in the effluent of the column containing Hg-contaminated sediment (Control) and columns with amendments, including hard-wood biochar (CC), HNO_3-modified biochar (CC+HNO_3), a 2 % amendment of CaS_x-modified biochar (CC+2%CaS_x) and a 5 % amendment of CaS_x-modified biochar (CC+5%CaS_x).

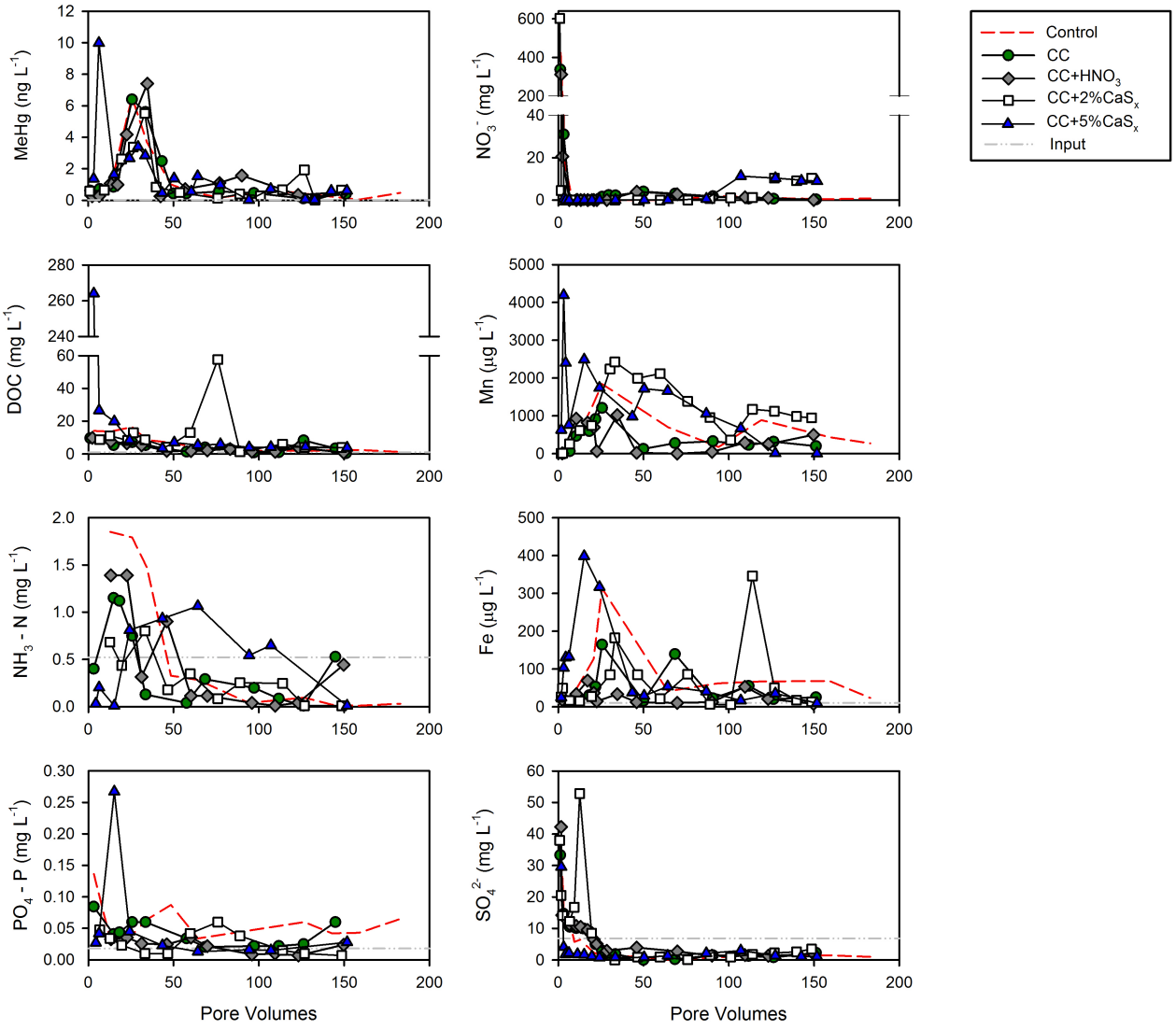

Figure 3.5 - Aqueous concentrations of MeHg and redox parameters measured in the effluent of the column containing Hg-contaminated sediment (Control) and columns with amendments, including hard-wood biochar (CC), HNO_3-modified biochar (CC+HNO_3), a 2 % amendment of CaS_x-modified biochar (CC+2%CaS_x) and a 5 % amendment of CaS_x-modified biochar (CC+5%CaS_x).

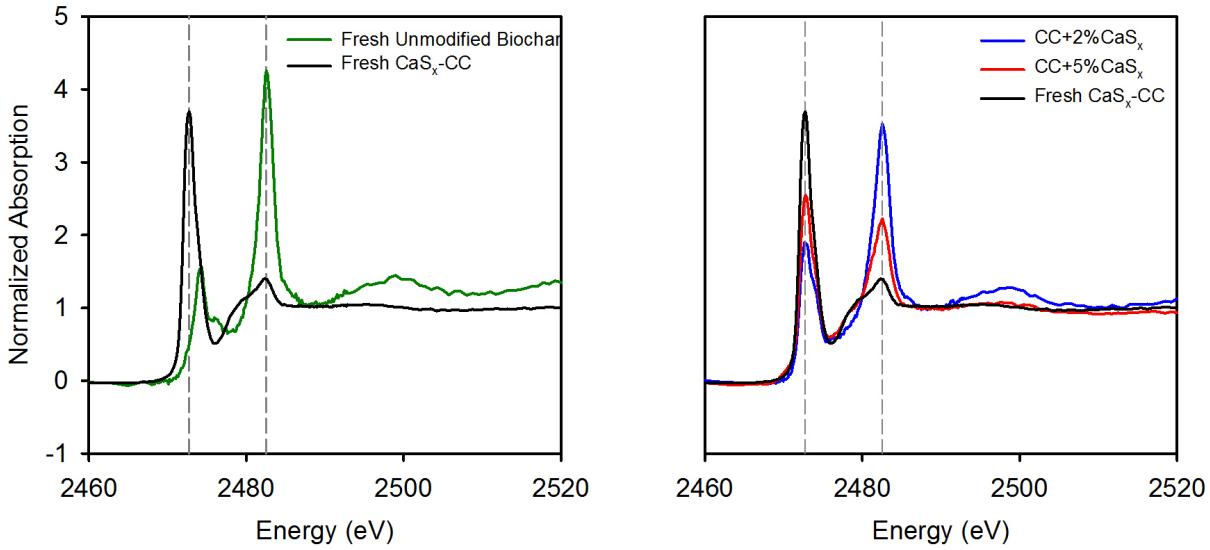

Figure 3.6 – S K-edge XANES for fresh unmodified and CaS_x-modified biochar (left). Comparison of S K-edge XANES for fresh CaS_x-modified biochar, CaS_x-CC from the 2% amendment column and CaS_x-CC from the 5% amendment column. The grey dashed lines represent the peak energies of reduced S (2472.7 eV) and sulfate (2482.5 eV).

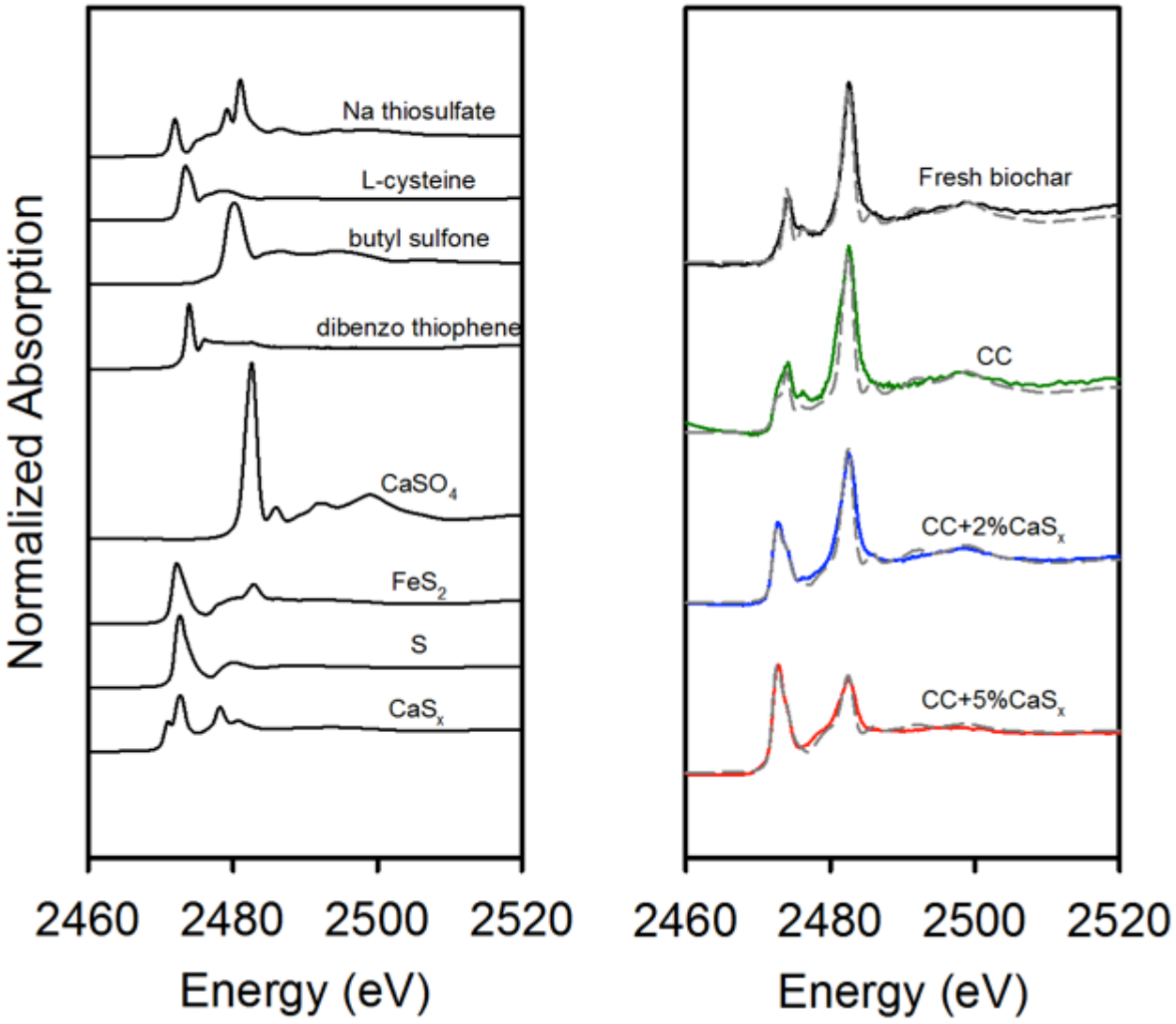

Figure 3.7 – Sulfur K-edge XANES for eight S reference materials (left). Sulfur K-edge XANES for fresh unmodified biochar, unmodified biochar from the CC column, CaS_x-CC from the CC+2%CaS_x column and CaS_x-CC from the CC+5%CaS_x column (right). The dashed grey line represents the fitted curve for each sample using LCF.

Chapter 4 - Conclusions and Recommendations

Remediation of Hg-contaminated sites presents many challenges due to the recalcitrant nature of Hg in the environment and the tendency for bacterial conversion of Hg to the highly toxic MeHg. Atmospheric transport and deposition coupled with Hg transport in riverine environments can result in large areas of Hg-contamination, further complicating the identification of successful remediation strategies. The column studies presented in Chapter 2 and Chapter 3 of this thesis demonstrated the effects of various inorganic and carbon-based amendments on Hg transport and sequestration within contaminated sediments. The results of these experiments provide insight into the suitability of the tested amendment materials for Hg stabilization in a co-blended setting.

The addition of agricultural limestone to Hg-contaminated sediment yielded no substantial change in Hg transport or production of MeHg. Some studies have observed limited nanoparticle transport in the presence of carbonate minerals, primarily through ionic strength manipulations and nanoparticle attachment to the limestone grains (Laumann et al., 2013). Under the experimental conditions in this study, the SRW input water was saturated with respect to calcite and dolomite (Appendix A), limiting dissolution of the agricultural limestone amendment. This factor may have prevented an increase in pore water ionic strength and as such mitigated the deposition and immobilization of aggregate Hg-S nanoparticles. The use of limestone specifically as a remediation tool may be best suited to regions where soils and sediments are carbonate-depleted. This could allow for sufficient dissolution of the limestone amendment and provide a greater impact on porewater ionic strength conditions.

Mercury transport was greatly enhanced by the addition of attapulgite clay to contaminated sediment. Despite published success in heavy metal remediation, co-blending Hg-

contaminated sediment with attapulgite clay resulted in a 161 % increase in effluent THg when compared to the Control. This increase in Hg mobilization was likely a result of the destabilization of Hg bound to sediment in the presence of attapulgite clay coupled with clay-facilitated Hg transport. Effluent MeHg concentrations were also increased in the presence of attapulgite clay and may be a due to the increase in dissolved, bioavailable Hg induced by the clay amendment.

The use of unmodified biochar and HNO_3-modified biochar as amendments for Hg stabilization did not yield improved Hg sequestration when compared to the Control. Although the transport of particulate Hg was moderately reduced in the presence of biochar and HNO_3-biochar, little to no effect was observed on filter-passing Hg. In particular, oxidation of biochar to enhance metal chelating functional groups resulted in no appreciable increase in Hg sequestration compared to the unmodified material. A more robust oxidation method using more concentrated HNO_3 at a higher temperature, as in Shim et al. (2001) or Strelko & Malik (2002), may be necessary to promote increased Hg interaction and binding.

The use of a CaS_x solution to impart S functional groups to the surface of reactive amendments yielded vastly improved results in the reduction of Hg transport compared to the unmodified materials. Utilizing CaS_x-modified attapulgite clay as a reactive amendment greatly reduced the transport of Hg through contaminated sediment. The distinction between the unmodified attapulgite clay and the CaS_x-clay was dramatic, with a 92 % reduction in leached 0.45-Hg observed in the effluent from the CaS_x-clay column when compared to the Clay column. Similar immobilization of Hg was observed when biochar treated with CaS_x was blended with Hg-contaminated sediment. Compared to the Control, concentrations of effluent 0.45-Hg were

reduced by 71 % when a 2 % amendment of CaS_x-biochar was incorporated into contaminated sediment. Mercury transport was further reduced by 83 % when the amendment dosage of CaS_x-biochar was increased to 5 %. These results suggest that the utilization of an inexpensive, commercially available solution of CaS_x to modify sorbent materials can greatly limit Hg transport in contaminated sediments. The addition of reduced S groups to the surface of biochar and clay was likely the key factor in the increased Hg-binding capacity of the CaS_x-modified sorbents.

Further research should be carried out to establish the long-term effects of CaS_x-modified sorbent amendments on the environment. While numerous studies have examined the ecotoxicity of biochar in natural settings (Lehmann et al., 2011; Beckingham et al., 2013; Hale et al., 2013), additional information is required to understand the toxicity effects CaS_x may have on the surrounding ecosystem. The oxidation of reduced S imparted to the amendment material should be investigated, as this occurrence has implications for the continued efficacy of the material as a treatment strategy. A long-term leaching experiment may be beneficial to fully investigate the implications of additional S on methylating bacteria over extended periods of time.

References

Álvarez-Ayuso, E., & García-Sánchez, A. (2003). Palygorskite as a feasible amendment to stabilize heavy metal polluted soils. *Environmental Pollution*, *125*(3), 337–344. http://doi.org/10.1016/S0269-7491(03)00121-0

Amos, H. M., Jacob, D. J., Streets, D. G., & Sunderland, E. M. (2013). Legacy impacts of all-time anthropogenic emissions on the global mercury cycle. *Global Biogeochemical Cycles*, *27*(2), 410–421. http://doi.org/10.1002/gbc.20040

Anschutz, P., Sundby, B., Lefrançois, L., III Luther, G. W., & Mucci, A. (2000). Interactions between metal oxides and species of nitrogen and iodine in bioturbated marine sediments. *Geochimica et Cosmochimica Acta*, *64*(16), 2751–2763. http://doi.org/10.1016/S0016-7037(00)00400-2

Asasian, N., & Kaghazchi, T. (2015). Sulfurized activated carbons and their mercury adsorption/desorption behavior in aqueous phase. *International Journal of Environmental Science and Technology*, *12*(8), 2511–2522. http://doi.org/10.1007/s13762-015-0818-x

Babiarz, C., Hoffmann, S., Wieben, A., Hurley, J., Andren, A., Shafer, M., & Armstrong, D. (2012). Watershed and discharge influences on the phase distribution and tributary loading of total mercury and methylmercury into Lake Superior. *Environmental Pollution*, *161*, 299–310. http://doi.org/10.1016/j.envpol.2011.09.026

Babiarz, C. L., Hurley, J. P., Hoffmann, S. R., Andren, A. W., Shafer, M. M., & Armstrong, D. E. (2001). Partitioning of Total Mercury and Methylmercury to the Colloidal Phase in Freshwaters. *Environmental Science & Technology*, *35*, 4773–4782.

Balogh, S. J., Meyer, M. L., & Johnson, D. K. (1998). Transport of mercury in three contrasting river basins. *Environmental Science and Technology*, *32*(4), 456–462. http://doi.org/10.1021/es970506q

Bartlett, R., Mortimer, R. J. G., & Morris, K. (2008). Anoxic nitrification: Evidence from Humber Estuary sediments (UK). *Chemical Geology*, *250*(1-4), 29–39. http://doi.org/10.1016/j.chemgeo.2008.02.001

Basta, N. T., & McGowen, S. L. (2004). Evaluation of chemical immobilization treatments for reducing heavy metal transport in a smelter-contaminated soil. *Environmental Pollution*, *127*(1), 73–82. http://doi.org/10.1016/S0269-7491(03)00250-1

Beckingham, B., Buys, D., Vandewalker, H., & Ghosh, U. (2013). Observations of limited secondary effects to benthic invertebrates and macrophytes with activated carbon amendment in river sediments. *Environmental Toxicology and Chemistry*, *32*(7), 1504–1515. http://doi.org/10.1002/etc.2231

Beesley, L., Moreno-Jiménez, E., & Gomez-Eyles, J. L. (2010). Effects of biochar and greenwaste compost amendments on mobility, bioavailability and toxicity of inorganic and organic contaminants in a multi-element polluted soil. *Environmental Pollution*, *158*, 2282–2287. http://doi.org/10.1016/j.envpol.2010.02.003

Beesley, L., Moreno-Jiménez, E., Gomez-Eyles, J. L., Harris, E., Robinson, B., & Sizmur, T. (2011). A review of biochars' potential role in the remediation, revegetation and restoration of contaminated soils. *Environmental Pollution*, *159*(12), 3269–3282. http://doi.org/10.1016/j.envpol.2011.07.023

Bhattacharyya, K. G., & Gupta, S. Sen. (2008). Adsorption of a few heavy metals on natural and modified kaolinite and montmorillonite: A review. *Advances in Colloid and Interface Science*, *140*(2), 114–131. http://doi.org/10.1016/j.cis.2007.12.008

Bloom, N. S., Preus, E., Katon, J., & Hiltner, M. (2003). Selective extractions to assess the biogeochemically relevant fractionation of inorganic mercury in sediments and soils. *Analytica Chimica Acta*, *479*(2), 233–248. http://doi.org/10.1016/S0003-2670(02)01550-7

Blowes, D. W., Ptacek, C. J., Benner, S. G., McRae, C. W. ., Bennett, T. a, & Puls, R. W. (2000). Treatment of inorganic contaminants using permeable reactive barriers. *Journal of Contaminant Hydrology*, *45*, 123–137. http://doi.org/10.1016/S0043-1354(98)00315-7

Blue, L. Y., Jana, P., & Atwood, D. A. (2010). Aqueous mercury precipitation with the synthetic dithiolate, BDTH2. *Fuel*, *89*(6), 1326–1330. http://doi.org/10.1016/j.fuel.2009.10.031

California Toxic Substances Control. *Coast Wood Preserving Superfund Site, Ukiah, California, Fourth Five-Year Review*. U.S. Environmental Protection Agency: Washington, DC., 2011.

Campbell, L. S., Chimedtsogzol, A., & Dyer, A. (2006). Species sensitivity of zeolite minerals for uptake of mercury solutes. *Mineralogical Magazine*, *70*(August), 361–371. http://doi.org/10.1180/0026461067040341

Carter, L.J. (1977). Chemical plants leave unexpected legacy for two Virginia rivers. *Science, New Series, 198*(4321), 1015-1020.

Ceccatelli, S., Daré, E., & Moors, M. (2010). Chemico-Biological Interactions Methylmercury-induced neurotoxicity and apoptosis. *Chemico-Biological Interactions*, *188*(2), 301–308. http://doi.org/10.1016/j.cbi.2010.04.007

Chadwick, S. P., Babiarz, C. L., Hurley, J. P., & Armstrong, D. E. (2006). Influences of iron, manganese, and dissolved organic carbon on the hypolimnetic cycling of amended mercury. *Science of the Total Environment*, *368*(1), 177–188. http://doi.org/10.1016/j.scitotenv.2005.09.039

Chaves, M. R. M., Valsaraj, K. T., Delaune, R. D., Gambrell, R. P., & Buchler, P. M. (2011). Mercury uptake by biogenic silica modified with L-cysteine, *32*(14), 1615–1625. http://doi.org/10.1080/09593330.2010.545440

Chen, L., Liu, M., Fan, R., Ma, S., Xu, Z., Ren, M., & He, Q. (2013). Mercury speciation and emission from municipal solid waste incinerators in the Pearl River Delta, South China. *Science of the Total Environment*, *447*, 396–402. http://doi.org/10.1016/j.scitotenv.2013.01.018

Chrysochoou, M., Ferreira, D. R., & Johnston, C. P. (2010). Calcium polysulfide treatment of Cr(VI)-contaminated soil. *Journal of Hazardous Materials*, *179*(1-3), 650–657. http://doi.org/10.1016/j.jhazmat.2010.03.052

Chrysochoou, M., Johnston, C. P., & Dahal, G. (2012). A comparative evaluation of hexavalent chromium treatment in contaminated soil by calcium polysulfide and green-tea nanoscale zero-valent iron. *Journal of Hazardous Materials*, *201-202*, 33–42. http://doi.org/10.1016/j.jhazmat.2011.11.003

Clarkson, T. W., & Magos, L. (2006). The toxicology of mercury and its chemical compounds. *Critical Reviews in Toxicology*, *36*(8), 609–662. http://doi.org/10.1080/10408440600845619

Crockett, M. P., Evans, A. M., Worthington, M. J. H., Albuquerque, I. S., Slattery, A. D., Gibson, C. T., Campbell, J. A., Lewis, D. A., Bernardes, G. J. L., & Chalker, J. M. (2016). Sulfur-Limonene Polysulfide: A Material Synthesized Entirely from Industrial By-Products and Its Use in Removing Toxic Metals from Water and Soil. *Angewandte Chemie - International Edition*, *55*, 1714–1718. http://doi.org/10.1002/anie.201508708

Daugherty, S. (2010). *Performance of Treatment Media for the Stabilization of Mercury under Variable Geochemical Conditions*. University of Waterloo.

DeSantis, T.Z., Hugenholtz, P., Larsen, N., Rojas, M., Brodie, E.L., Keller, K., Huber, T., Dalevi, D., Hu, P, & Andersen, G.L. (2006). Greengenes, a chimera-checked 16S rRNA gene database and workbench compatible with ARB. *Applied and Environmental Microbiology, 72*(7), 5069-5072.

Desrochers, K. (2013). *Geochemical Characterization and Assessment of Stabilization Mechanisms for Mercury-Contaminated Riverbank Sediments from the South River, Virginia (USA)*. University of Waterloo.

Desrochers, K. A. N., Paulson, K. M. A., Ptacek, C. J., Blowes, D. W., & Gould, W. D. (2015). Effect of Electron Donor to Sulfate Ratio on Mercury Methylation in Floodplain Sediments under Saturated Flow Conditions. *Geomicrobiology Journal*, *32*(10), 924–933. http://doi.org/10.1080/01490451.2015.1035818

Dowd ,S.E., Callaway, T.R., Wolcott, R.D., Sun, Y., McKeehan, T., Hagevoort, R.G., & Edrington, T.S. (2008a). Evaluation of the bacterial diversity in the feces of cattle using 16S rDNA bacterial tag-encoded FLX amplicon pyrosequencing (bTEFAP). *BMC Microbiology, 8*, 125.

Dowd, S.E., Sun, Y., Wolcott, R.D., Domingo, A., & Carroll, J.A. (2008b). Bacterial tag-encoded FLX amplicon pyrosequencing (bTEFAP) for microbiome studies; bacterial diversity in the ileum of newly weaned salmonella-infected pigs. *Foodborne Pathogens and Disease, 5*(4), 459-472.

Drexel, R. T., Haitzer, M., Ryan, J. N., Aiken, G. R., & Nagy, K. L. (2002). Mercury(II) sorption to two Florida Everglades peats: Evidence for strong and weak binding and competition by dissolved organic matter released from the peat. *Environmental Science and Technology*, *36*(19), 4058–4064. http://doi.org/10.1021/es0114005

Driscoll, C. T., Mason, R. P., Chan, H. M., Jacob, D. J., & Pirrone, N. (2013). Mercury as a global pollutant: Sources, pathways, and effects. *Environmental Science and Technology*, *47*(10), 4967–4983. http://doi.org/10.1021/es305071v

Eggleston, J. (2009). *Mercury Loads in the South River and Simulation of Mercury Total Maximum Daily Loads (TMDLs) for the South River, South Fork Shenandoah River, and Shenandoah River: Shenandoah Valley, Virginia Scientific Investigations Report 2009 – 5076. Scientific Investigations Report 2009-5076*.

Ekino, S., Susa, M., Ninomiya, T., Imamura, K., & Kitamura, T. (2007). Minamata disease revisited: An update on the acute and chronic manifestations of methyl mercury poisoning. *Journal of the Neurological Sciences*, *262*(1-2), 131–144. http://doi.org/10.1016/j.jns.2007.06.036

Fernandes, S. O., Javanaud, C., Aigle, A., Michotey, V. D., Guasco, S., Deborde, J., Deflandre, B., Anschutz, P., & Bonin, P. C. (2015). Anaerobic nitrification-denitrification mediated by Mn-oxides in meso-tidal sediments: Implications for N2 and N2O production. *Journal of Marine Systems*, *144*(2), 1–8. http://doi.org/10.1016/j.jmarsys.2014.11.011

Fitzgerald, W. F., Engstrom, D. R., Mason, R. P., & Nater, E. A. (1998). The Case for Atmospheric Mercury Contamination in Remote Areas. *Environmental Science & Technology*, *32*(1), 1–7. http://doi.org/10.1021/es970284w

Fitzgerald, W. F., & Lamborg, C. H. (2013). *Geochemistry of Mercury in the Environment*. *Treatise on Geochemistry: Second Edition* (11th ed., Vol. 11). Elsevier Ltd. http://doi.org/10.1016/B978-0-08-095975-7.00904-9

Flanders, J. R., Turner, R. R., Morrison, T., Jensen, R., Pizzuto, J., Skalak, K., & Stahl, R. (2010). Applied Geochemistry Distribution , behavior , and transport of inorganic and methylmercury in a high gradient stream. *Applied Geochemistry*, *25*(11), 1756–1769. http://doi.org/10.1016/j.apgeochem.2010.09.004

Gabriel, M. C., & Williamson, D. G. (2004). Principal biogeochemical factors affecting the speciation and transport of mercury through the terrestrial environment. *Environmental Geochemistry and Health*, *26*, 421–434.

Ghosh, U., Luthy, R. G., Cornelissen, G., Werner, D., & Menzie, C. A. (2011). In-situ Sorbent Amendments : A New Direction in Contaminated Sediment Management. *Environmental Science & Technology*, *45*, 1163–1168.

Gibson, B. D., Ptacek, C. J., Lindsay, M. B. J., & Blowes, D. W. (2011). Examining Mechanisms of Groundwater Hg (II) Treatment by Reactive Materials : An EXAFS Study. *Environmental Science & Technology*, *45*, 10415–10421.

Gidley, P. T., Kwon, S., Yakirevich, A., Magar, V. S., & Ghosh, U. (2012). Advection dominated transport of polycyclic aromatic hydrocarbons in amended sediment caps. *Environmental Science and Technology*, *46*, 5032–5039. http://doi.org/10.1021/es202910c

Gilmour, C. C., & Henry, E. A. (1991). Mercury Methylation in Aquatic Systems Affected by Acid Deposition. *Environmental Pollution*, *71*, 131–169.

Gilmour, C. C., Henry, E. A., & Mitchell, R. (1992). Sulfate Stimulation of Mercury Methylation in Freshwater Sediments. *Environmental Science & Technology*, *26*, 2281–2287.

Gilmour, C. C., Riedel, G. S., Riedel, G., Kwon, S., Landis, R., Brown, S. S., Menzie, C. A., & Ghosh, U. (2013). Activated Carbon Mitigates Mercury and Methylmercury Bioavailability in Contaminated Sediments. *Environmental Science & Technology*, *47*, 13001–13010.

Gilmour, C.C., Podar, M., Bullock, A.L., Graham, A.M., Brown, S.D., Somenahally, A.C., Johs, A., Hurt, R.A., Jr., Bailey, K.L., Elias, D.A. (2013). Mercury Methylation by Novel Microorganisms from New Environments. *Environmental Science & Technology, 47,* 11810-11820.

Gomez-Eyles, J. L., Yupanqui, C., Beckingham, B., Riedel, G., Gilmour, C., & Ghosh, U. (2013). Evaluation of Biochars and Activated Carbons for In Situ Remediation Of Sediments Impacted With Organics, Mercury, And Methylmercury. *Environmental Science & Technology*, *47*, 13721–13729.

Gomez-Serrano, V., Macias-Garcia, A., Espinosa-Mansilla, A., & Valenzuela-Calahorro, C. (1998). Adsorption of Mercury, Cadmium and Lead from Aqueous Solution on Heat-treated and Sulphurized Activated Carbon. *Water Resources*, *32*, 1–4.

Graham, A. M., Aiken, G. R., & Gilmour, C. C. (2012). Dissolved Organic Matter Enhances Microbial Mercury Methylation Under Sulfidic Conditions. *Environmental Science & Technology*, *46*, 2715–2723.

Green-Ruiz, C. (2005). Adsorption of mercury(II) from aqueous solutions by the clay mineral montmorillonite. *Bulletin of Environmental Contamination and Toxicology*, *75*(6), 1137–1142. http://doi.org/10.1007/s00128-005-0867-9

Haden, W. L. J., & Schwint, I. A. (1967). Attapulgite: Its Properties and Applications. *Industrial and Engineering Chemistry*, *59*(9), 58–69.

Hale, S. E., Jensen, J., Jakob, L., Oleszczuk, P., Hartnik, T., Henriksen, T., Okkenhaug, G., Martinsen, V., & Cornelissen, G. (2013). Short-term effect of the soil amendments activated carbon, biochar, and ferric oxyhydroxide on bacteria and invertebrates. *Environmental Science & Technology*, *47*, 8674–8683. http://doi.org/10.1021/es400917g

Hamilton-Taylor, J., Davison, W., & Morfett, K. (1996). The biogeochemical cycling of Zn , Cu , Fe , Mn , and dissolved organic C in a seasonally anoxic lake. *Limnology and Oceanography*, *41*(3), 408–418. http://doi.org/10.4319/lo.1996.41.3.0408

Han, F. X., Su, Y., Monts, D. L., Waggoner, C. A., & Plodinec, M. J. (2006). Binding , distribution , and plant uptake of mercury in a soil from Oak Ridge , Tennessee , USA. *Science of the Total Environment*, *368*, 753–768. http://doi.org/10.1016/j.scitotenv.2006.02.026

Hellal, J., Guédron, S., Huguet, L., Schäfer, J., Laperche, V., Joulian, C., Lanceleur, L., Burnol, A., Ghestem, J., Garrido, F., & Battaglia-brunet, F. (2015). Mercury mobilization and speciation linked to bacterial iron oxide and sulfate reduction : A column study to mimic reactive transfer in an anoxic aquifer. *Journal of Contaminant Hydrology*, *180*, 56–68.

Hines, M. E., Horvat, M., Faganeli, J., Bonzongo, J. J., Barkay, T., Major, E. B., Scott, K. J., Bailey, E. A., Warwick, J. J., & Lyons, W. B. (2000). Mercury Biogeochemistry in the Idrija River , Slovenia , from above the Mine into the Gulf of Trieste. *Environmental Research Section A*, *83*, 129–139. http://doi.org/10.1006/enrs.2000.4052

Hsu-Kim, H., Kucharzyk, K. H., Zhang, T., & Deshusses, M. A. (2013). Mechanisms regulating mercury bioavailability for methylating microorganisms in the aquatic environment: A critical review. *Environmental Science and Technology*, *47*(6), 2441–2456. http://doi.org/10.1021/es304370g

Hulth, S., Aller, R. C., & Gilbert, F. (1999). Coupled anoxic nitrification/manganese reduction in marine sediments. *Geochimica et Cosmochimica Acta*, *63*(1), 49–66. http://doi.org/10.1016/S0016-7037(98)00285-3

Jay, J. A., Murray, K. J., Gilmour, C. C., Mason, R. P., Morel, F. M. M., Roberts, A. L., & Hemond, H. F. (2002). Mercury Methylation by Desulfovibrio desulfuricans ND132 in the Presence of Polysulfides. *Applied and Environmental Microbiology*, *68*(11), 5741–5745. http://doi.org/10.1128/AEM.68.11.5741

Jiang, J., Xu, R., Jiang, T., & Li, Z. (2012). Immobilization of Cu (II), Pb (II) and Cd (II) by the addition of rice straw derived biochar to a simulated polluted Ultisol. *Journal of Hazardous Materials*, *229-230*, 145–150. http://doi.org/10.1016/j.jhazmat.2012.05.086

Karagas, M. R., Choi, A. L., Oken, E., Horvat, M., Schoeny, R., Kamai, E., Cowell, W., Grandjean, P., & Korrick, S. (2012). Evidence on the human health effects of low-level methylmercury exposure. *Environmental Health Perspectives*, *120*(6), 799–806. http://doi.org/10.1289/ehp.1104494

Kerin, E. J., Gilmour, C. C., Roden, E., Suzuki, M. T., Coates, J. D., & Mason, R. P. (2006). Mercury methylation by dissimilatory iron-reducing bacteria. *Applied and Environmental Microbiology*, *72*(12), 7919–7921. http://doi.org/10.1128/AEM.01602-06

Kim, E., Seyfferth, A. L., Fendorf, S., & Luthy, R. G. (2011). Immobilization of Hg (II) in water with polysulfide-rubber (PSR) polymer-coated activated carbon. *Water Research*, *45*, 453–460. http://doi.org/10.1016/j.watres.2010.08.045

King, J. K., Kostka, J. E., Frischer, M. E., & Saunders, F. M. (2000). Sulfate-Reducing Bacteria Methylate Mercury at Variable Rates in Pure Culture and in Marine Sediments. *Applied and Environmental Microbiology*, *66*(6), 2430–2437. http://doi.org/10.1128/AEM.66.6.2430-2437.2000.Updated

Kinghorn, A., Solomon, P., & Man Chan, H. (2007). Temporal and spatial trends of mercury in fish collected in the English – Wabigoon river system in Ontario , Canada. *Science of the Total Environment*, *372*, 615–623. http://doi.org/10.1016/j.scitotenv.2006.10.049

Krishnan, K. A., & Anirudhan, T. . S. (2002). Removal of cadmium (II) from aqueous solutions by steam- activated sulphurised carbon prepared from sugar-cane bagasse pith : Kinetics and equilibrium studies. *Journal of Hazardous Materials*, *B92*, 161–183. http://doi.org/10.4314/wsa.v29i2.4849

Kumpiene, J., Lagerkvist, A., & Maurice, C. (2008). Stabilization of As, Cr, Cu, Pb and Zn in soil using amendments - A review. *Waste Management*, *28*, 215–225. http://doi.org/10.1016/j.wasman.2006.12.012

Laumann, S., Mici, V., Lowry, G. V, & Hofmann, T. (2013). Carbonate minerals in porous media decrease mobility of polyacrylic acid modi fi ed zero-valent iron nanoparticles used for groundwater remediation. *Environmental Pollution*, *179*, 53–60. http://doi.org/10.1016/j.envpol.2013.04.004

Lechler, P. J., Miller, J. R., Lacerda, L. D., Vinson, D., Bonzongo, J., Lyons, W. B., & Warwick, J. J. (2000). Elevated mercury concentrations in soils , sediments , water , and fish of the Madeira River basin , Brazilian Amazon : a function of natural enrichments ? *Science of the Total Environment, The*, *260*, 87–96.

Lee, S. H., Lee, J. S., Jeong Choi, Y., & Kim, J. G. (2009). In situ stabilization of cadmium-, lead-, and zinc-contaminated soil using various amendments. *Chemosphere*, *77*(8), 1069–1075. http://doi.org/10.1016/j.chemosphere.2009.08.056

Lehmann, J., Czimczik, C. I., Laird, D., & Sohi, S. P. (2009). Stability of Biochar in the Soil. In J. Lehmann & S. Joseph (Eds.), *Biochar for environmental management: Science and technology* (pp. 183–205). London: Earthscan Publishers. http://doi.org/10.4324/9781849770552

Lehmann, J., & Joseph, S. (2009). Biochar for Environmental Management : An Introduction. In J. Lehmann & S. Joseph (Eds.), *Biochar for Environmental Management* (pp. 1–12). London: Earthscan Publishers. http://doi.org/10.1016/j.forpol.2009.07.001

Lehmann, J., Rillig, M. C., Thies, J., Masiello, C. A., Hockaday, W. C., & Crowley, D. (2011). Biochar effects on soil biota - A review. *Soil Biology and Biochemistry*, *43*, 1812–1836. http://doi.org/10.1016/j.soilbio.2011.04.022

Liang, X., Han, J., Xu, Y., Sun, Y., Wang, L., & Tan, X. (2014). In situ field-scale remediation of Cd polluted paddy soil using sepiolite and palygorskite. *Geoderma*, *235-236*, 9–18. http://doi.org/10.1016/j.geoderma.2014.06.029

Lindqvist, O., Johansson, K., Aastrup, M., Andersson, A., Bringmark, L., Hovsenius, G., Håkanson, L., Iverfeldt, Å., Meili, M., & Timm, B. (1991). Mercury in the Swedish environment - Recent research on causes, consequences and corrective methods. *Water, Air, & Soil Pollution*, *55*(1-2), xi–261. http://doi.org/10.1007/BF00542429

Liu, P., Ptacek, C. J., Blowes, D. W., Berti, W. R., & Landis, R. C. (2015). Aqueous Leaching of Organic Acids and Dissolved Organic Carbon from Various Biochars Prepared at Different Temperatures. *Journal of Environmental Quality*, *44*(2), 684–695. http://doi.org/10.2134/jeq2014.08.0341

Liu, P., Ptacek, C. J., Blowes, D. W., & Landis, R. C. (2016). Mechanisms of mercury removal by biochars produced from different feedstocks determined using X-ray absorption spectroscopy. *Journal of Hazardous Materials*, *308*, 233–242. http://doi.org/10.1016/j.jhazmat.2016.01.007

Liu, W., Vidic, R. D., & Brown, T. D. (2000). Optimization of High Temperature Sulfur Impregnation on Activated Carbon for Permanent Sequestration of Elemental Mercury Vapors Optimization of High Temperature Sulfur Impregnation on Activated Carbon for Permanent Sequestration of Elemental Mercury Vapo. *Environmental Science & Technology*, *34*(3), 483–488. http://doi.org/10.1021/es9813008

Lovley, D. R., & Phillips, E. J. (1988). Novel mode of microbial energy metabolism: organic carbon oxidation coupled to dissimilatory reduction of iron or manganese. *Applied and Environmental Microbiology*, *54*(6), 1472–1480. http://doi.org/10.1103/PhysRevLett.50.1998

Lowry, G. V, Shaw, S., Kim, C. S., Rytuba, J. J., & Brown, G. E. J. (2004). Macroscopic and Microscopic Observations of Particle-Facilitated Mercury Transport from New Idria and Sulphur Bank Mercury Mine Tailings. *Environmental Science & Technology*, *38*, 5101–5111.

Luther III, G. W., Sundby, B., Lewis, B. L., Brendel, P. J., & Silverberg, N. (1997). Interactions of manganese with the nitrogen cycle: Alternative pathways to dinitrogen. *Geochimica et Cosmochimica Acta*, *61*(19), 4043–4052.

Marvin-Dipasquale, M. C., & Oremland, R. S. (1998). Bacterial methylmercury degradation in Florida everglades peat sediment. *Environmental Science and Technology*, *32*(17), 2556–2563. http://doi.org/10.1021/es971099l

Mason, R. P., & Sullivan, K. A. (1998). Mercury and Methylmercury Transport Through an Urban Watershed. *Water Research*, *32*(2), 321–330.

Miller, J. R., Lechler, P. J., & Desilets, M. (1998). The role of geomorphic processes in the transport and fate of mercury in the Carson River basin, west-central Nevada. *Environmental Geology*, *33*(4), 249–262. http://doi.org/10.1007/s002540050244

Myers, C. R., & Nealson, K. H. (1988). Bacterial Manganese Reduction and Growth with Manganese Oxide as the Sole Electron Acceptor. *Science*, *240*(4857), 1319–1321.

O'Day, P. A., & Vlassopoulos, D. (2010). Mineral-Based Amendments for Remediation. *Elements*, *6*, 375–381.

Oak Ridge National Laboratory. (2016). Predicted methylators. Available from: http://www.esd.ornl.gov/programs/rsfa/data/PredictedMethylators/PredictedMethylators_20160420.pdf

Oyekola, O. O., van Hille, R. P., & Harrison, S. T. L. (2009). Study of anaerobic lactate metabolism under biosulfidogenic conditions. *Water Research*, *43*(14), 3345–3354. http://doi.org/10.1016/j.watres.2008.11.044

Paulson, K. (2014). *Methylmercury Production in Riverbank Sediments of the South River, Virginia (USA) and Assessment of Biochar as a Mercury Treatment Option*. University of Waterloo.

Pham, A. L., Morris, A., Zhang, T., Ticknor, J., Levard, C., & Hsu-Kim, H. (2014). Precipitation of nanoscale mercuric sulfides in the presence of natural organic matter : Structural properties , aggregation , and biotransformation. *Geochimica et Cosmochimica Acta*, *133*, 204–215. http://doi.org/10.1016/j.gca.2014.02.027

Pizzuto, J. (2012). Predicting the accumulation of mercury-contaminated sediment on riverbanks — An analytical approach. *Water Resources Research*, *48*, 1–13. http://doi.org/10.1029/2012WR011906

Poulin, B. A., Aiken, G. R., Nagy, K. L., Manceau, A., Krabbenhoft, D. P., & Ryan, J. N. (2016). Mercury transformation and release differs with depth and time in a contaminated riparian soil during simulated flooding. *Geochimica et Cosmochimica Acta*, *176*, 118–138.

Randall, P. M., & Chattopadhyay, S. (2013). Mercury contaminated sediment sites — An evaluation of remedial options. *Environmental Research*, *125*, 131–149.

Ravel, B., & Newville, M. (2005). ATHENA, ARTEMIS, HEPHAESTUS: Data analysis for X-ray absorption spectroscopy using IFEFFIT. In *Journal of Synchrotron Radiation* (Vol. 12, pp. 537–541). http://doi.org/10.1107/S0909049505012719

Reddy, K. R., Kadlec, R. H., Flaig, E., & Gale, P. M. (1999). Phosphorus Retention in Streams and Wetlands: A Review. *Critical Reviews in Environmental Science and Technology*, *29*(July 2015), 83–146. http://doi.org/10.1080/10643389991259182

Ryan, J. N., & Elimelech, M. (1996). Colloid mobilization and transport in groundwater. *Colloids and Surfaces A: Physicochemical and Engineering Aspects*, *107*, 1–56. http://doi.org/10.1016/0927-7757(95)03384-X

Schroeder, W. H., & Munthe, J. (1998). Atmospheric mercury - an overview. *Atmospheric Environment*, *32*(5), 809–822. http://doi.org/10.1016/S1352-2310(97)00293-8

Sellers, P., Kelly, C. A., Rudd, J. W. M., & Machutchon, A. R. (1996). Photodegradation of methylmercury in lakes. *Nature*, *380*(6576), 694–697. http://doi.org/10.1038/380694a0

Serrano, S., Vlassopoulos, D., & O'Day, P. A. (2016). Mechanism of Hg(II) immobilization in sediments by sulfate-cement amendment. *Applied Geochemistry*, *67*, 68–80. http://doi.org/10.1016/j.apgeochem.2016.01.007

Shaw, S. A., Al, T. A., & Macquarrie, K. T. B. (2006). Mercury mobility in unsaturated gold mine tailings , Murray Brook mine , New Brunswick , Canada. *Applied Geochemistry*, *21*, 1986–1998. http://doi.org/10.1016/j.apgeochem.2006.08.009

Shim, J., Park, S., & Ryu, S. (2001). Effect of modification with HNO 3 and NaOH on metal adsorption by pitch-based activated carbon fibers. *Carbon*, *39*, 1635–1642.

Slowey, A. J., Johnson, S. B., Rytuba, J. J., & Brown, G. E. J. (2005). Role of Organic Acids in Promoting Colloidal Transport of Mercury from Mine Tailings. *Environmental Science & Technology*, *39*, 7869–7874.

Stathi, P., Litina, K., Gournis, D., Giannopoulos, T. S., & Deligiannakis, Y. (2007). Physicochemical study of novel organoclays as heavy metal ion adsorbents for environmental remediation. *Journal of Colloid and Interface Science*, *316*(2), 298–309. http://doi.org/10.1016/j.jcis.2007.07.078

Strelko, V., & Malik, D. J. (2002). Characterization and Metal Sorptive Properties of Oxidized Active Carbon. *Journal of Colloid and Interface Science*, *220*, 213–220. http://doi.org/10.1006/jcis.2002.8313

Tadanier, C. J., Schreiber, M. E., & Roller, J. W. (2005). Arsenic mobilization through microbially mediated deflocculation of ferrihydrite. *Environmental Science and Technology*, *39*(9), 3061–3068. http://doi.org/10.1021/es048206d

Tchounwou, P. B., Ayensu, W. K., Ninashvili, N., & Sutton, D. (2003). Environmental exposure to mercury and its toxicopathologic implications for public health. *Environmental Toxicology*, *18*(3), 149–175. http://doi.org/10.1002/tox.10116

Thomas, M. A., Conaway, C. H., Steding, D. J., Marvin-Dipasquale, M., Abu-saba, K. E., & Flegal, A. R. (2002). Mercury contamination from historic mining in water and sediment , Guadalupe River and San Francisco Bay , California. *Geochemistry: Exploration, Environment, Analysis*, *2*, 211–217.

Thompson, A., Chadwick, O. A., Boman, S., & Chorover, J. (2006). Colloid mobilization during soil iron redox oscillations. *Environmental Science and Technology*, *40*(18), 5743–5749. http://doi.org/10.1021/es061203b

Uchimiya, M., Bannon, D. I., & Wartelle, L. H. (2012). Retention of Heavy Metals by Carboxyl Functional Groups of Biochars in Small Arms Range Soil. *Journal of Agricultural and Food Chemistry*, *06*-, 1798–1809.

Uchimiya, M., Chang, S., & Klasson, K. T. (2011). Screening biochars for heavy metal retention in soil : Role of oxygen functional groups. *Journal of Hazardous Materials*, *190*(1-3), 432–441. http://doi.org/10.1016/j.jhazmat.2011.03.063

Ullrich, S. M., Ilyushchenko, M. A., Uskov, G. A., & Tanton, T. W. (2007). Mercury distribution and transport in a contaminated river system in Kazakhstan and associated impacts on aquatic biota. *Applied Geochemistry*, *22*(12), 2706–2734. http://doi.org/10.1016/j.apgeochem.2007.07.005

Ullrich, S. M., Tanton, T. W., & Abdrashitova, S. A. (2001). Mercury in the aquatic environment: a review of factors affecting methylation. *Critical Reviews in Environmental Science and Technology*, *31*(3), 241–293. Retrieved from http://www.tandfonline.com/doi/abs/10.1080/20016491089226

U.S. EPA. Method 1630: Methyl mercury in water by distillation, aqueous ethylation, purge and trap, and CVAFS. EPA-821-R-01-020; U.S. Environmental Protection Agency: Washington, DC, 2001.

U.S. EPA. Method 1631, Revision E: Mercury in water by oxidation, purge and trap, and cold vapor atomic fluorescence spectrometry. EPA-821-R-02-019; U.S. Environmental Protection Agency: Washington, DC, 2002.

U.S EPA. *Reregistration Eligibility Decision for Inorganic Polysulfides*. Prevention, Pesticides and Toxic Substances (7508C); U.S. Environmental Protection Agency: Washington, DC., 2005.

Wang, J., Feng, X., Anderson, C. W. N., Xing, Y., & Shang, L. (2012). Remediation of mercury contaminated sites - A review. *Journal of Hazardous Materials*, *221-222*, 1–18. http://doi.org/10.1016/j.jhazmat.2012.04.035

Waybrant, K. R., Ptacek, C. J., & Blowes, D. W. (2002). Treatment of mine drainage using permeable reactive barriers: Column experiments. *Environmental Science and Technology*, *36*(6), 1349–1356. http://doi.org/10.1021/es010751g

Wayne, D. M., Warwick, J. J., Lechler, P. J., Gill, G. a, & Lyons, W. B. (1996). Mercury contamination in the Carson River, Nevada: A preliminary study of the impact of mining wastes. *Water Air and Soil Pollution*, *92*, 391–408.

Weech, S. A., Scheuhammer, A. M., Elliott, J. E., & Cheng, K. M. (2004). Mercury in fish from the Pinchi Lake Region , British Columbia , Canada. *Environmental Pollution*, *131*, 275–286. http://doi.org/10.1016/j.envpol.2004.02.016

Widdel, F., & Pfennig, N. (1982). Studies on dissimilatory sulfate-reducing bacteria that decompose fatty acids II. Incomplete oxidation of propionate by Desulfobulbus propionicus gen. nov., sp. nov. *Archives of Microbiology*, *131*(4), 360–365. http://doi.org/10.1007/BF00411187

Xiong, Z., He, F., Zhao, D., & Barnett, M. O. (2009). Immobilization of mercury in sediment using stabilized iron sulfide nanoparticles. *Water Research*, *43*(20), 5171–5179. http://doi.org/10.1016/j.watres.2009.08.018

Xu, X., Schierz, A., Xu, N., & Cao, X. (2016). Comparison of the characteristics and mechanisms of Hg(II) sorption by biochars and activated carbon. *Journal of Colloid and Interface Science*, *463*, 55–60. http://doi.org/10.1016/j.jcis.2015.10.003

Yao, K., Habibian, M. T., & O'Melia, C. R. (1971). Water and Waste Water Filtration: Concepts and Applications. *Environmental Science & Technology*, *5*(11), 1105–1112. http://doi.org/10.1021/es60058a005

Yu, R. Q., Flanders, J. R., Mack, E. E., Turner, R., Mirza, M. B., & Barkay, T. (2012). Contribution of coexisting sulfate and iron reducing bacteria to methylmercury production in freshwater river sediments. *Environmental Science and Technology*, *46*(5), 2684–2691. http://doi.org/10.1021/es2033718

Zhu, J., Deng, B., Yang, J., & Gang, D. (2009). Modifying activated carbon with hybrid ligands for enhancing aqueous mercury removal. *Carbon*, *47*(8), 2014–2025. http://doi.org/10.1016/j.carbon.2009.03.047

Zhu, Y., Ma, L. Q., Gao, B., Bonzongo, J. C., Harris, W., & Gu, B. (2012). Transport and interactions of kaolinite and mercury in saturated sand media. *Journal of Hazardous Materials*, *213-214*, 93–99. http://doi.org/10.1016/j.jhazmat.2012.01.061

Appendix A: Supplementary Graphs for Chapter 2

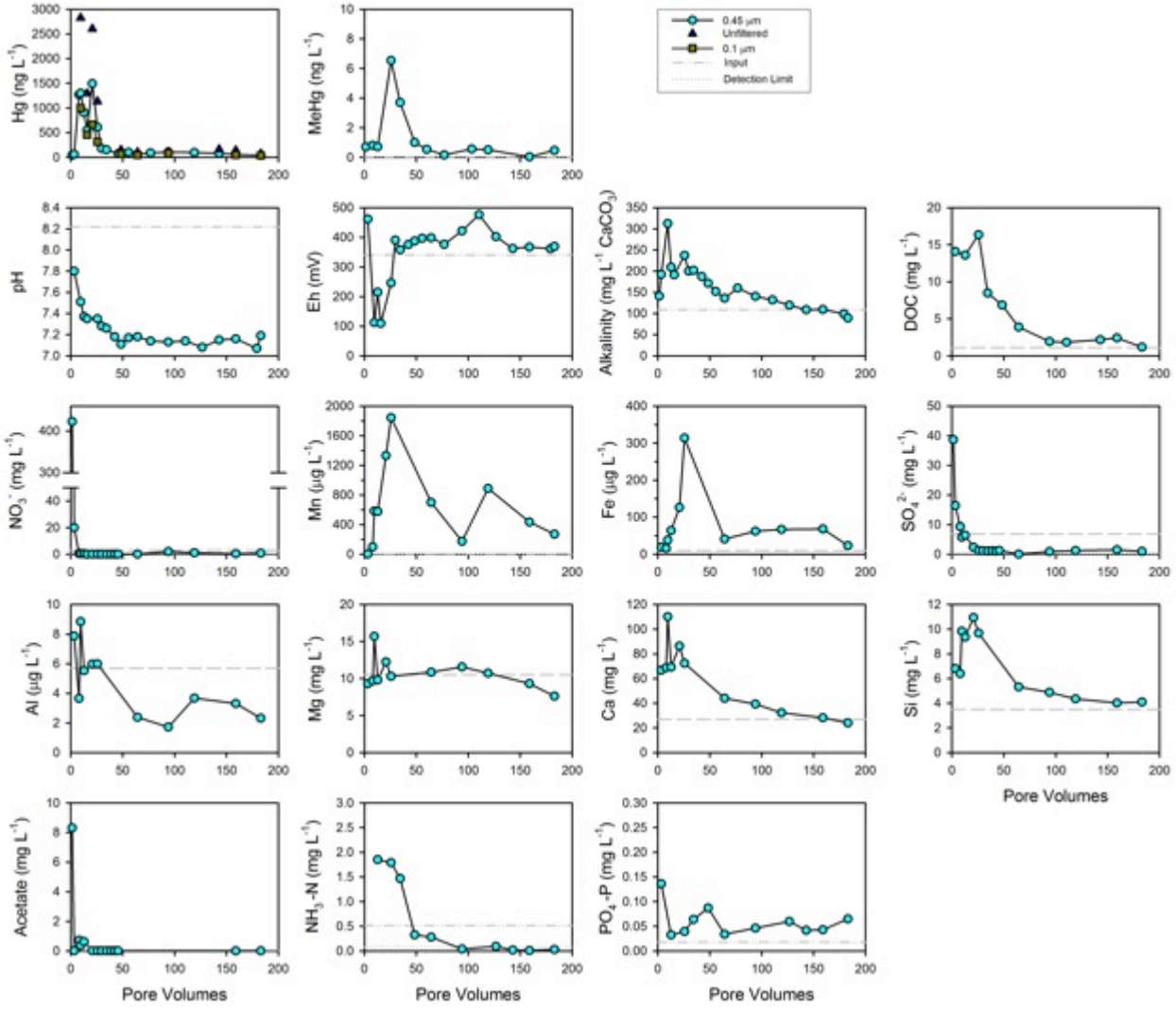

Figure A 1 - Hg, MeHg , redox parameters and geochemistry measured in the Control column effluent.

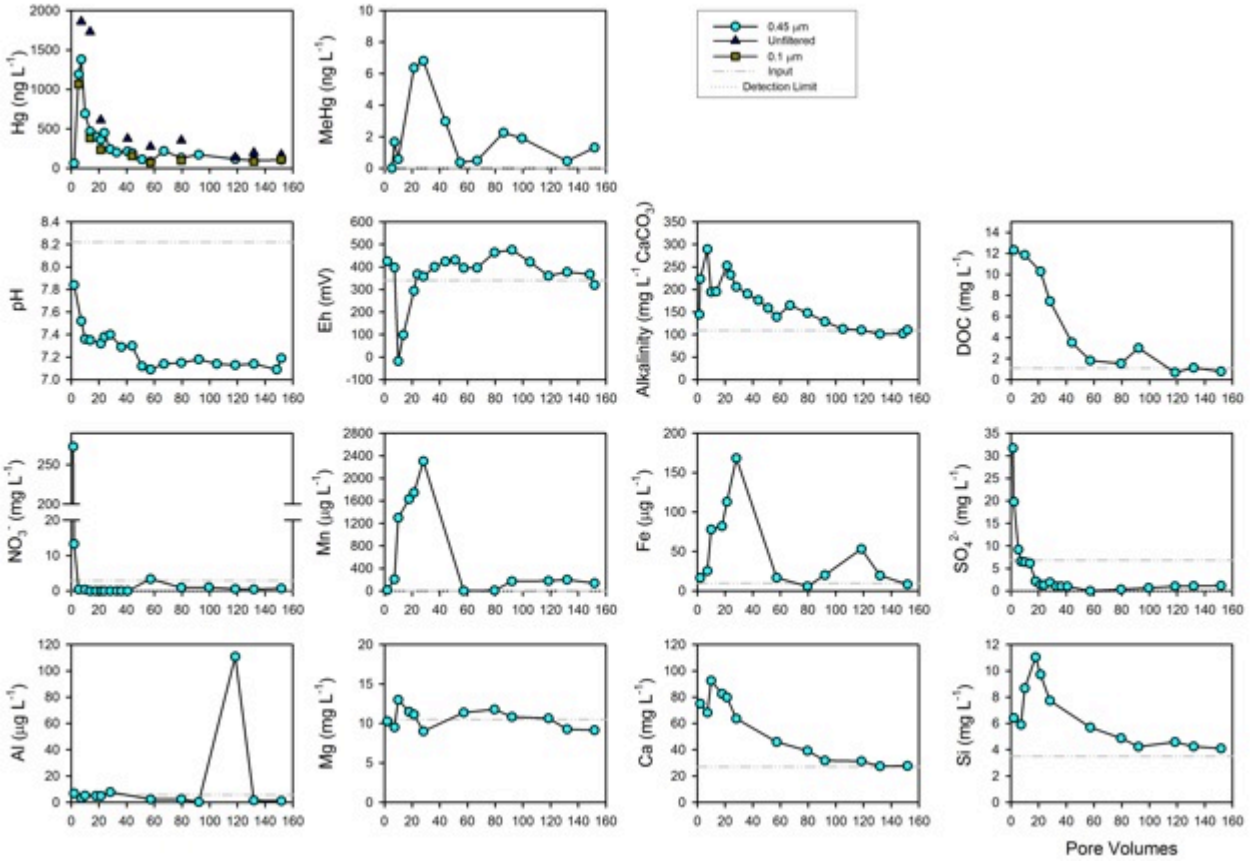

Figure A 2 - Hg, MeHg, redox parameters and geochemistry measured in the Limestone column effluent.

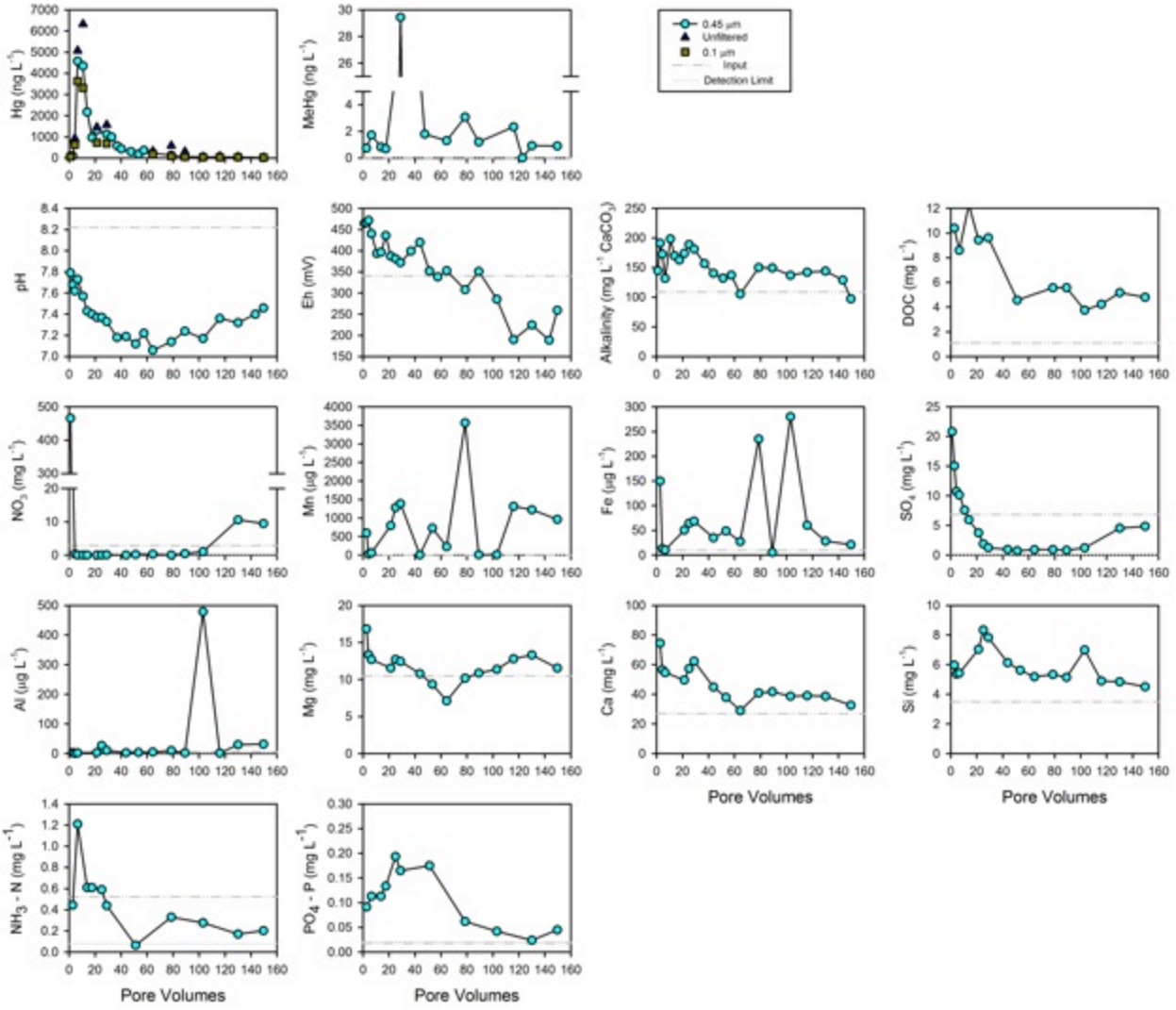

Figure A 3 - Hg, MeHg, redox parameters and geochemistry measured in the effluent of the Clay column.

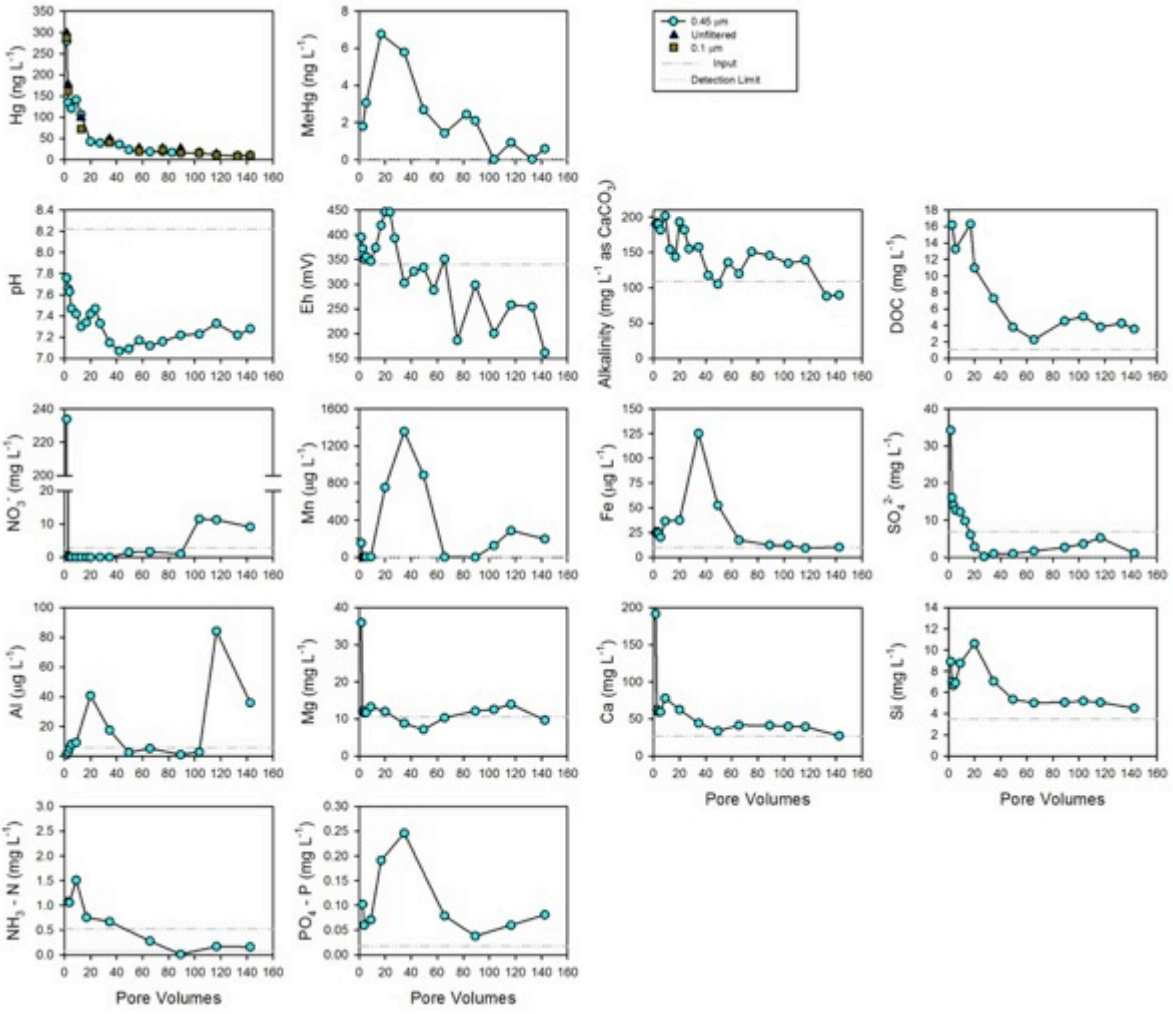

Figure A 4 - Hg, MeHg, redox parameters and geochemistry measured in the effluent of the CaS_x-clay column.

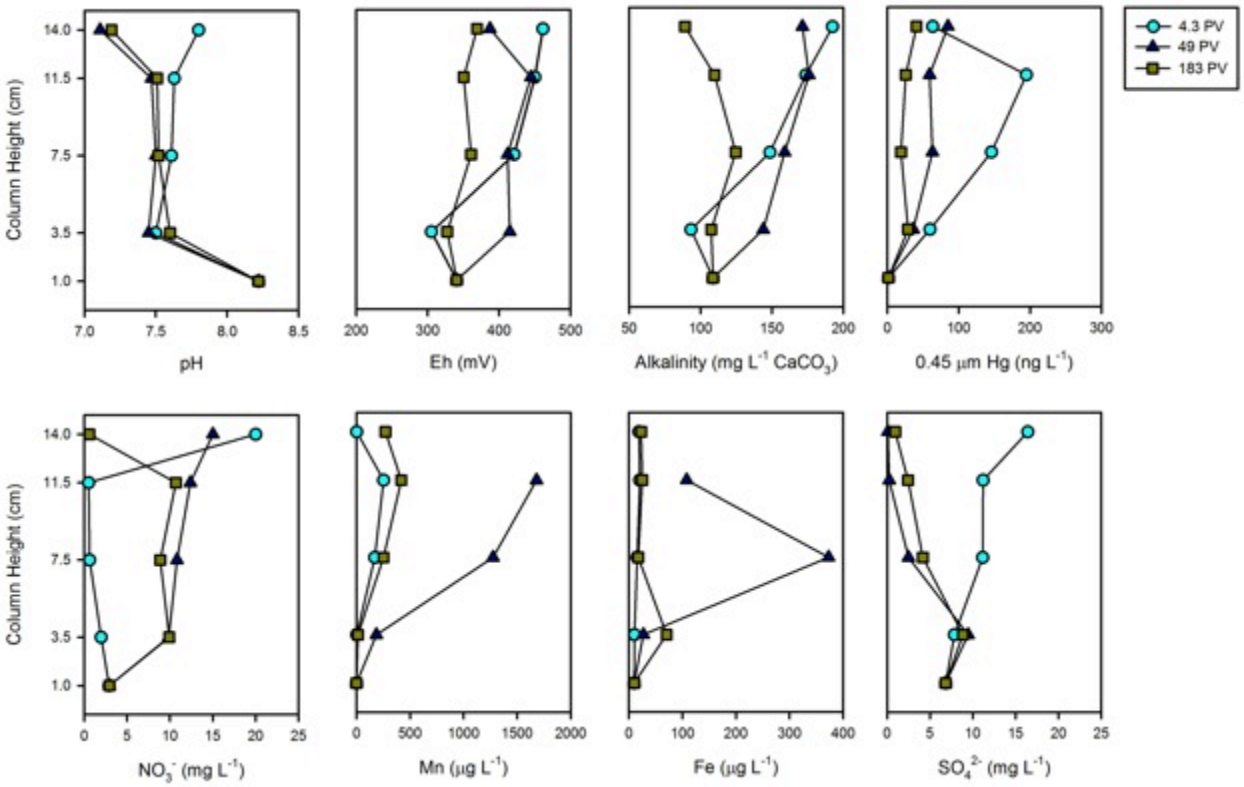

Figure A 5 - Aqueous geochemistry, Hg and redox parameters measured in samples extracted from the ports of the Control column.

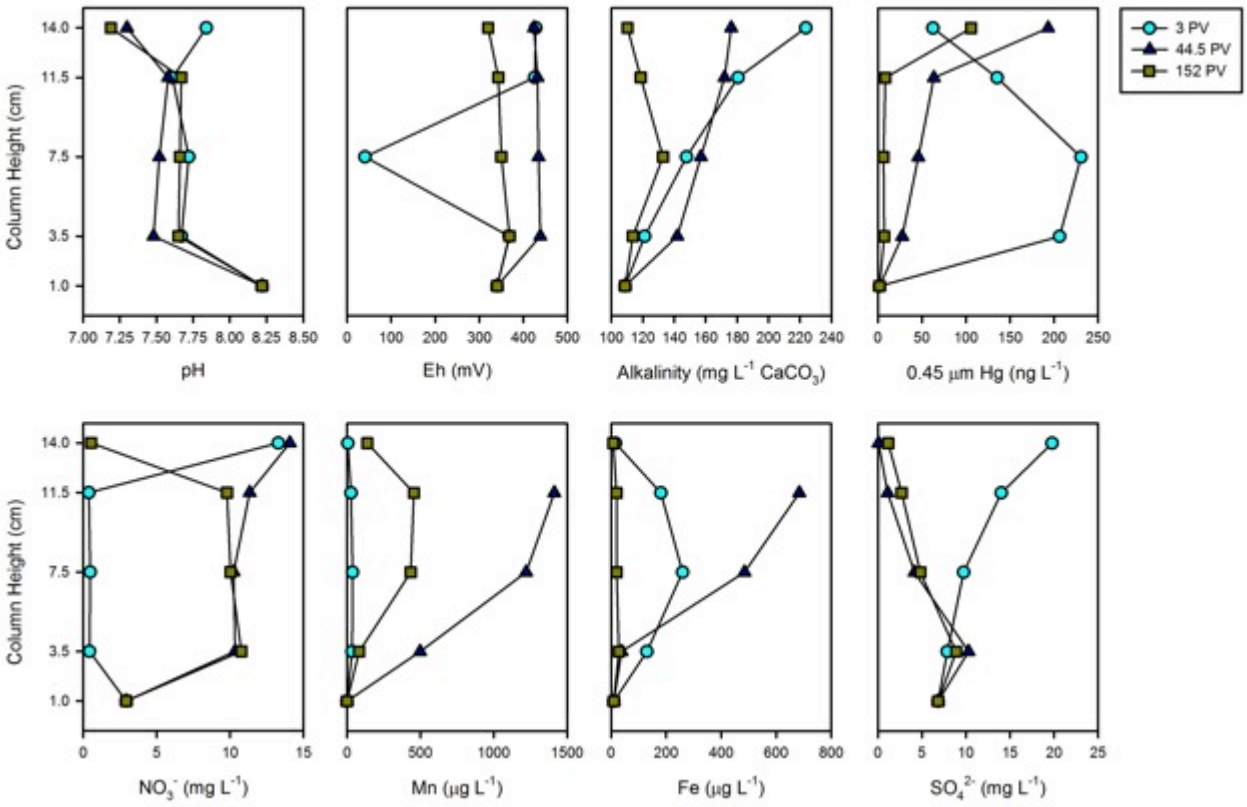

Figure A 6 - Aqueous geochemistry, Hg and redox parameters measured in samples extracted from the ports of the Limestone column.

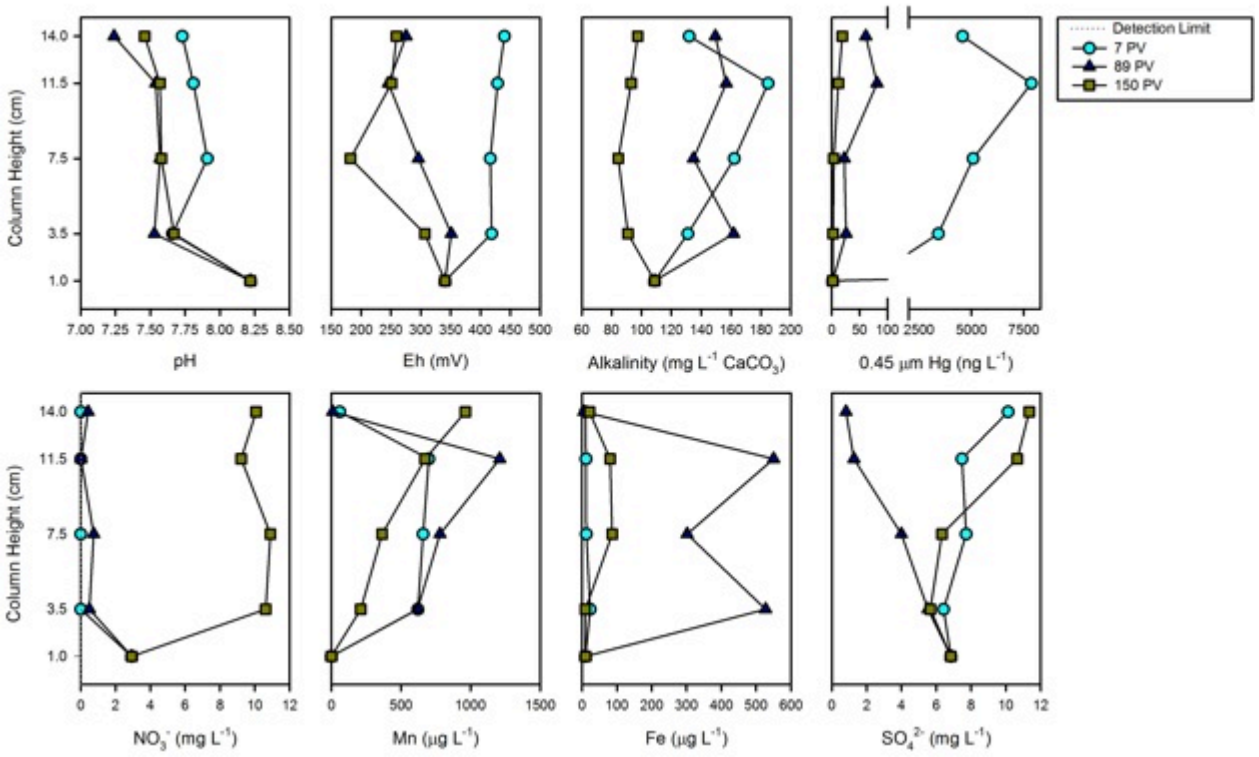

Figure A 7 - Aqueous geochemistry, Hg and redox parameters measured in samples extracted from the ports of the Clay column.

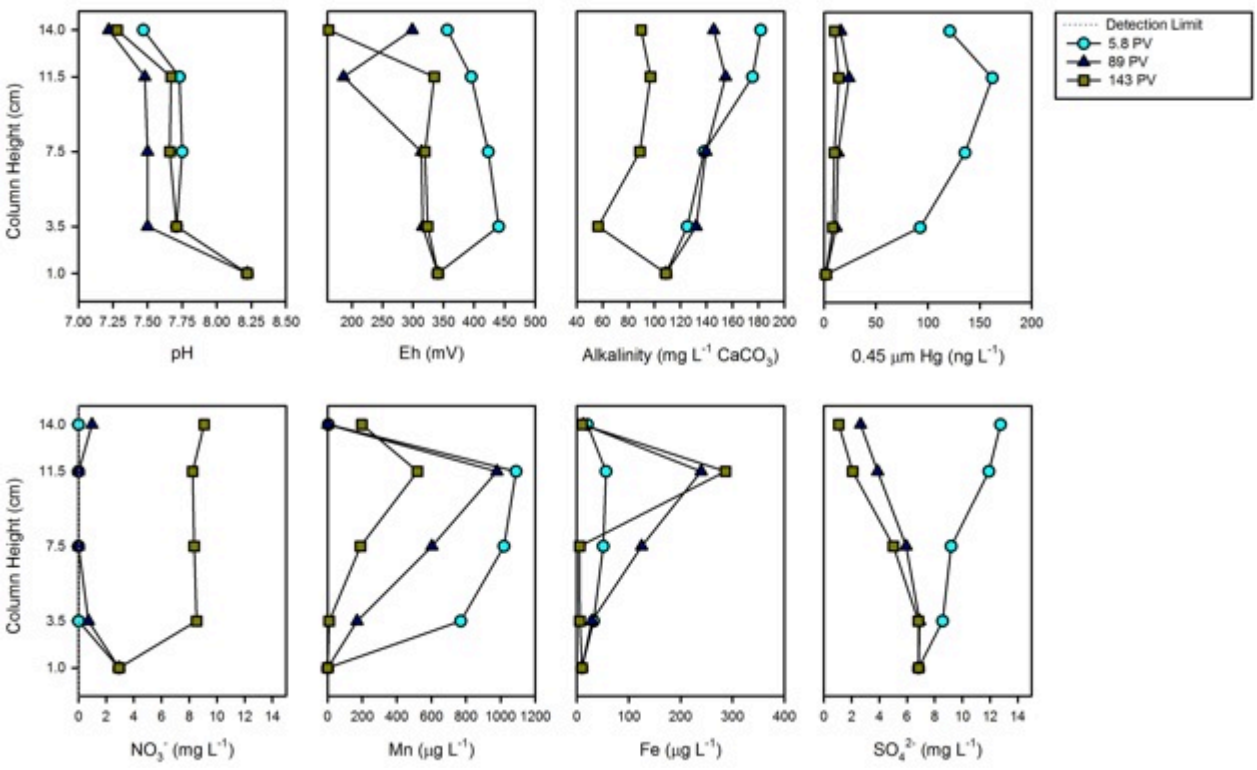

Figure A 8 - Aqueous geochemistry, Hg and redox parameters measured in samples extracted from the ports of the CaS_x-clay column.

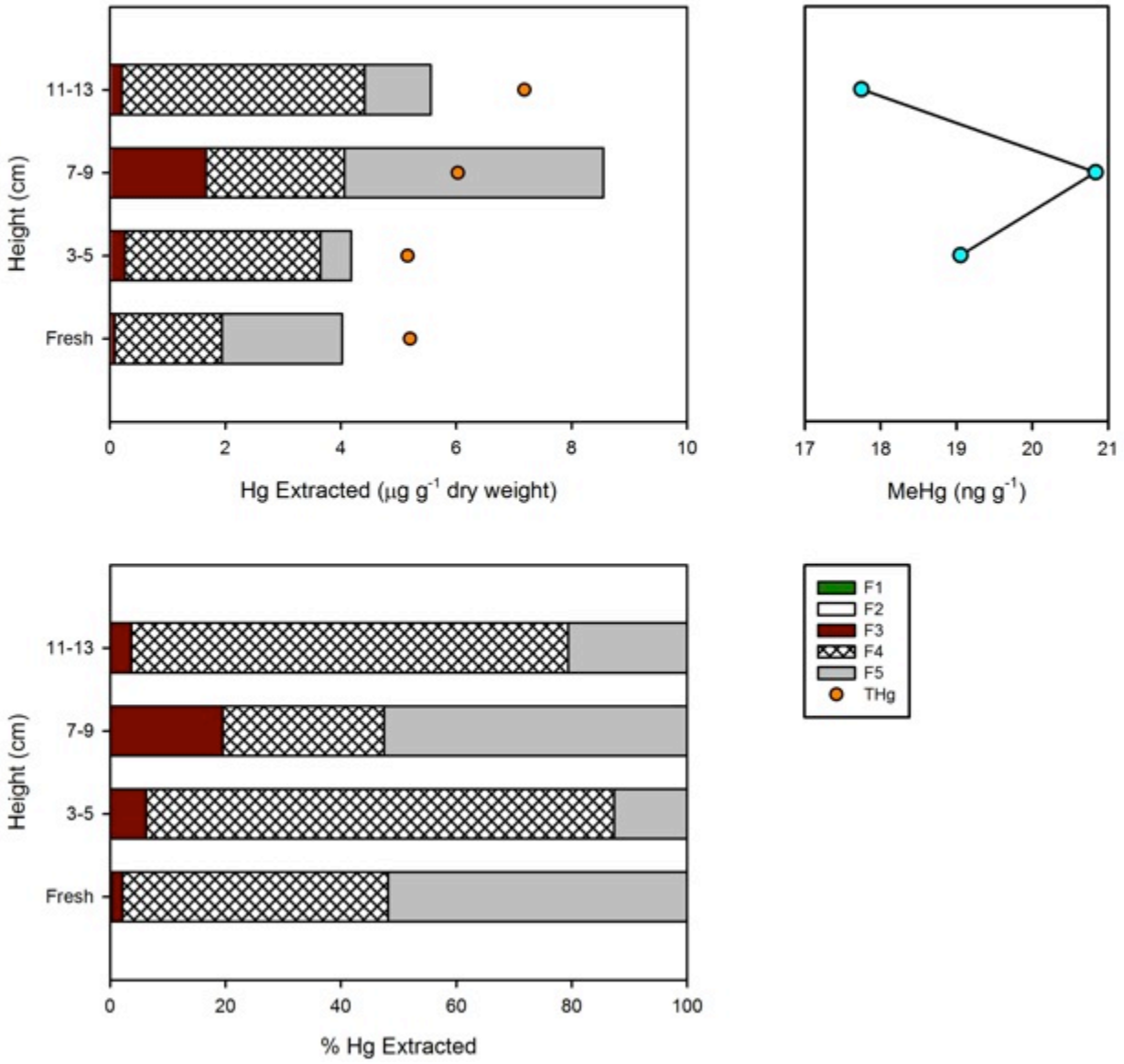

Figure A 9 - Mass and percent Hg from the Control column determined by sequential extraction analysis of column sediment after experiment termination (right). Fraction 1 (F1) targets water soluble Hg, F2 targets weak acid-extractable Hg, F3 organo-complexed Hg, F4 strongly-complexed/elemental Hg and F5 targets Hg sulfides. Fresh sediment concentration is the bulk Hg extracted from sediment used prior to column packing. Solid-phase MeHg (right) analysed after experiment completion.

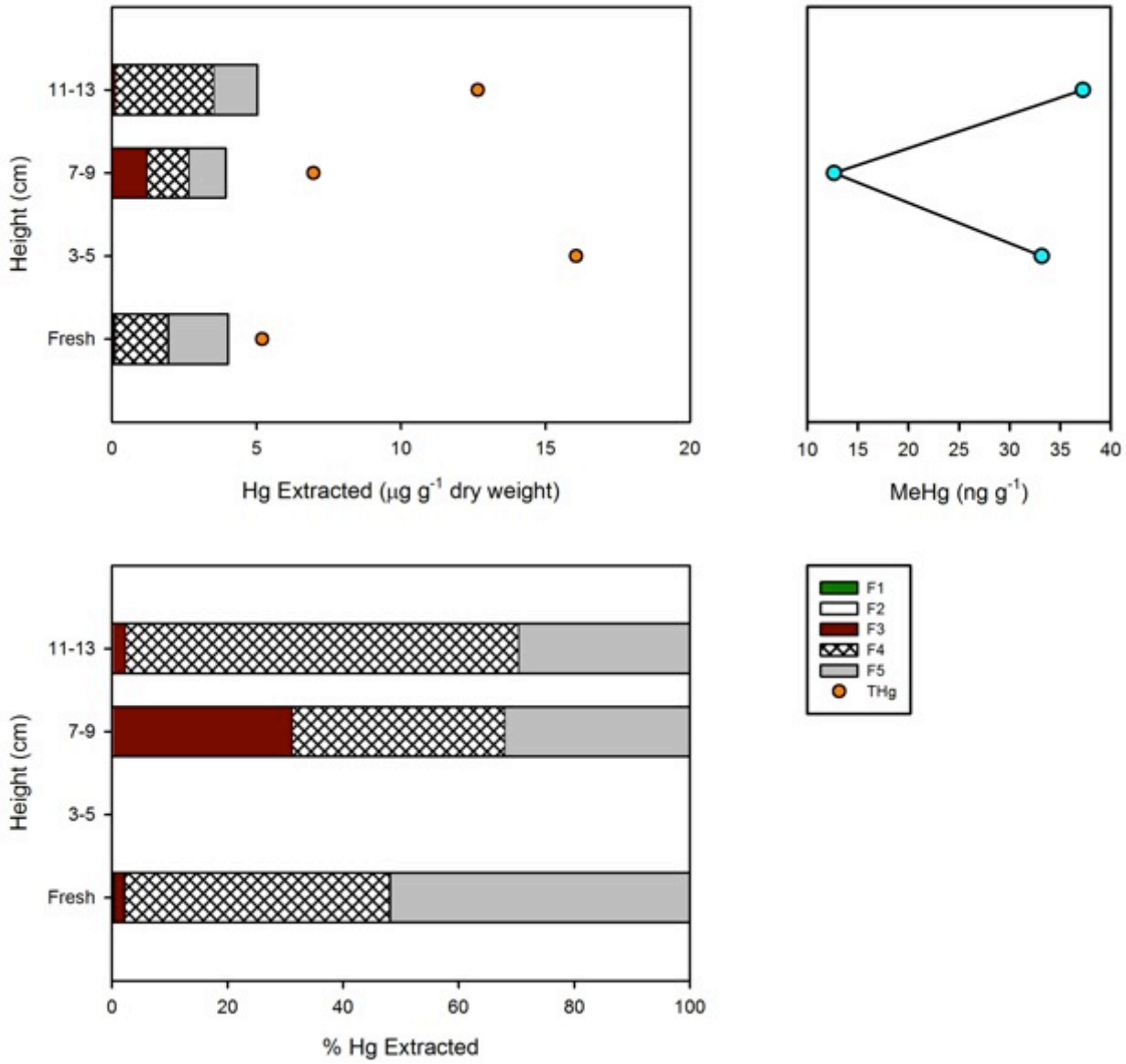

Figure A 10 - Mass and percent Hg in the Limestone column determined by sequential extraction analysis of column sediment after experiment termination (right). Fraction 1 (F1) targets water soluble Hg, F2 targets weak acid-extractable Hg, F3 organo-complexed Hg, F4 strongly-complexed/elemental Hg and F5 targets Hg sulfides. Fresh sediment concentration is the bulk Hg extracted from sediment used prior to amendment and column packing. Solid-phase MeHg (right) analysed after experiment completion. Note: Sequential extraction data is not available for the 3-5 cm transect.

Method for Total Solid-Phase Hg, MeHg and Hg Sequential Extractions

Sequential extractions were performed on thawed sediment samples using the following reagents: Fraction 1 (F1) – deionized water, F2 – 0.1 M CH_3COOH and 0.01 M HCl, F3 – 0.1 M KOH, F4 – 12 M HNO_3 and F5 – aqua regia following the method by Bloom et al. (2003). Sediments in the F1 – F4 fractions were shaken for 24 hours at room temperature prior to centrifugation and filtration while sediment in the F5 fraction was allowed to react in a stationary setting for three days at room temperature. Total Hg digestions were completed independent of the sequential extraction procedure but in an identical manner to the F5 fraction. All digestates were subsequently analysed using the CVAFS technique previously described for aqueous samples. Solid samples for MeHg analysis were prepared with 20 % KCl and 8 M H_2SO_4 before distillation with $CuSO_4$, aqueous ethylation and CVAFS using the same technique described for aqueous MeHg samples.

Table A 1 - Ionic strength, charge balance error and selected mineral saturation indices calculated in effluent samples from the Control column. Parameters were determined using PHREEQC.

Sample ID	Ionic Strength (mol/kg water)	Charge Balance Error (%)	Calcite Saturation Index	Aragonite Saturation Index	Dolomite Saturation Index	Gypsum Saturation Index	Fe(OH)3 Saturation Index
SSRC-2	0.0067	2.4	0.49	0.35	0.44	-2.4	1.3
SSRC-4	0.01	7.1	0.59	0.45	0.66	-2.7	-0.07
SSRC-5	0.0066	3.3	0.13	-0.02	-0.28	-2.8	1.4
SSRC-8	0.007	-0.55	0.17	0.03	-0.19	-3.5	2.3
SSRC-18	0.0047	7.4	-0.41	-0.56	-1.1	N/A	1.5
SSRC-25	0.0047	-0.45	-0.5	-0.64	-1.2	-3.8	1.7
SSRC-37	0.0048	60	-0.92	-1.1	-2.0	-3.5	2.4
SSRC-41	0.0035	6.8	-0.7	-0.84	-1.6	-3.6	1.7
SSRC-47	0.0029	6.6	-0.81	-0.96	-1.8	-3.9	1.3

Table A 2 - Ionic strength, charge balance error and selected mineral saturation indices calculated in effluent samples from the Limestone column. Parameters were determined using PHREEQC.

Sample ID	Ionic Strength (mol/kg water)	Charge Balance Error (%)	Calcite Saturation Index	Aragonite Saturation Index	Dolomite Saturation Index	Gypsum Saturation Index	Fe(OH)3 Saturation Index
SSLS-2	0.0079	-5.2	0.63	0.49	0.71	-2.3	1.3
SSLS-4	0.0074	-11	0.39	0.25	0.25	-2.8	1.4
SSLS-5	0.0079	22	0.19	0.05	-0.15	-2.7	-2.4
SSLS-8	0.0075	0.82	0.21	0.06	-0.13	-3.4	2.0
SSLS-10	0.0061	0.07	0.12	-0.03	-0.3	-3.3	2.2
SSLS-18	0.0049	4.0	-0.48	-0.62	-1.3	-5.9	1.1
SSLS-25	0.0047	-0.93	-0.46	-0.6	-1.1	-4.2	0.65
SSLS-37	0.0037	12	-0.69	-0.83	-1.5	-3.8	1.6
SSLS-41	0.0033	8.3	-0.76	-0.9	-1.7	-3.8	1.2
SSLS-47	0.0033	2.1	-0.67	-0.82	-1.5	-3.8	0.79

Table A 3 - Ionic strength, charge balance error and selected mineral saturation indices calculated in effluent samples from the Clay column. Parameters were determined using PHREEQC.

Sample ID	Ionic Strength (mol/kg water)	Charge Balance Error (%)	Calcite Saturation Index	Aragonite Saturation Index	Dolomite Saturation Index	Gypsum Saturation Index	Fe(OH)3 Saturation Index
SSAP-2	0.0085	-3.1	0.4	0.25	0.47	-2.4	2.2
SSAP-3	0.0062	7.0	0.21	0.06	0.1	-2.6	1.1
SSAP-4	0.0056	17	0.2	0.05	0.07	-2.6	1.0
SSAP-8	0.0054	5.9	-0.08	-0.23	-0.48	-3.1	1.7
SSAP-9	0.0059	7.0	0.01	-0.14	-0.32	-3.3	1.8
SSAP-10	0.006	11	-0.01	-0.16	-0.41	-3.5	1.8
SSAP-14	0.0046	10	-0.38	-0.53	-1.1	-3.7	1.4
SSAP-20	0.0032	2.2	-0.79	-0.94	-1.9	-3.9	1.3
SSAP-24	0.0046	4.6	-0.44	-0.59	-1.2	-3.8	2.2
SSAP-27	0.0046	4.4	-0.33	-0.48	-0.94	-3.8	0.64
SSAP-31	0.0044	10	-0.48	-0.63	-1.2	-3.7	2.2
SSAP-39	0.005	-4.1	-0.31	-0.46	-0.78	-3.1	1.0
SSAP-45	0.0041	4.7	-0.4	-0.55	-0.94	-3.1	1.3

Table A 4 - Ionic strength, charge balance error and selected mineral saturation indices calculated in effluent samples from the CaS_x-Clay column. Parameters were determined using PHREEQC.

Sample ID	Ionic Strength (mol/kg water)	Charge Balance Error (%)	Calcite Saturation Index	Aragonite Saturation Index	Dolomite Saturation Index	Gypsum Saturation Index	Fe(OH)3 Saturation Index
SAPS-1	0.024	-21	0.77	0.62	1.1	-1.8	1.4
SAPS-2	0.0066	5.9	0.33	0.18	0.26	-2.4	1.4
SAPS-3	0.0063	4.5	0.28	0.13	0.16	-2.5	1.4
SAPS-4	0.0062	6.5	0.1	-0.04	-0.19	-2.5	1.3
SAPS-5	0.0074	12	0.2	0.05	-0.06	-2.4	1.5
SAPS-8	0.0062	5.6	0.1	-0.04	-0.2	-3.1	1.5
SAPS-12	0.0047	0.14	-0.38	-0.52	-1.14	-3.7	1.9
SAPS-16	0.0035	4.0	-0.71	-0.85	-1.8	-3.8	1.6
SAPS-20	0.0044	9.4	-0.55	-0.69	-1.4	-3.5	1.1
SAPS-27	0.0048	3.9	-0.37	-0.52	-0.97	-3.3	0.95
SAPS-31	0.005	-4.4	-0.41	-0.56	-1.0	-3.2	0.18
SAPS-35	0.0052	-3.9	-0.31	-0.46	-0.76	-3.0	0.79
SAPS-42	0.0035	-2.6	-0.68	-0.83	-1.5	-3.8	-0.31

Table A 5 - Ionic strength, charge balance error and selected mineral saturation indices calculated in the SRW input. Parameters were determined using PHREEQC.

Sample ID	Ionic Strength (mol/kg water)	Charge Balance Error (%)	Calcite Saturation Index	Aragonite Saturation Index	Dolomite Saturation Index	Gypsum Saturation Index	Fe(OH)3 Saturation Index
SRW	0.0037	-5.0	0.32	0.18	0.54	-3.0	1.0

Appendix B: Supplementary Graphs for Chapter 3

Note: Entries for the control column can be found in Appendix A

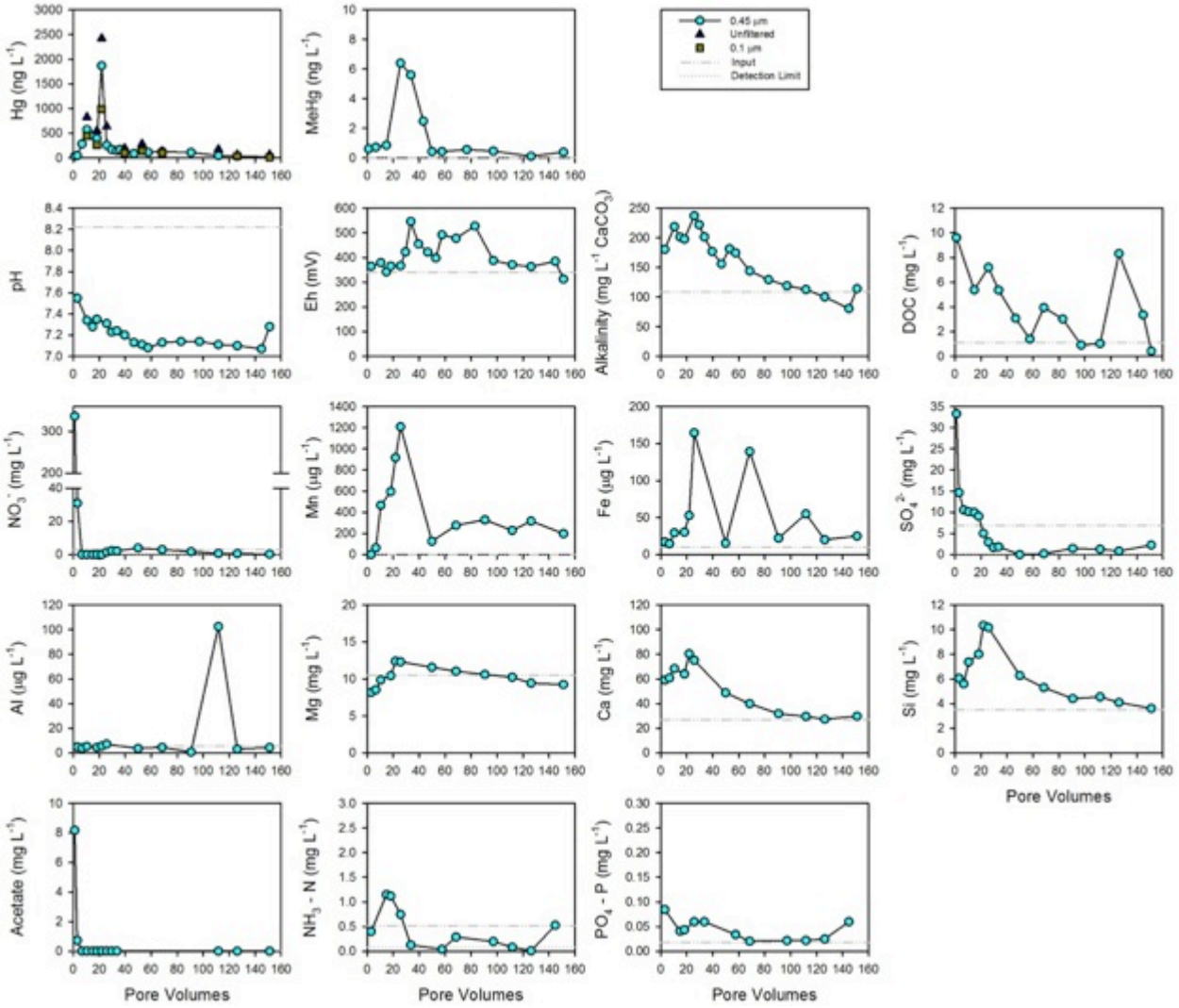

Figure B 1 - Hg, MeHg, redox parameters and geochemistry measured in the effluent of the CC column.

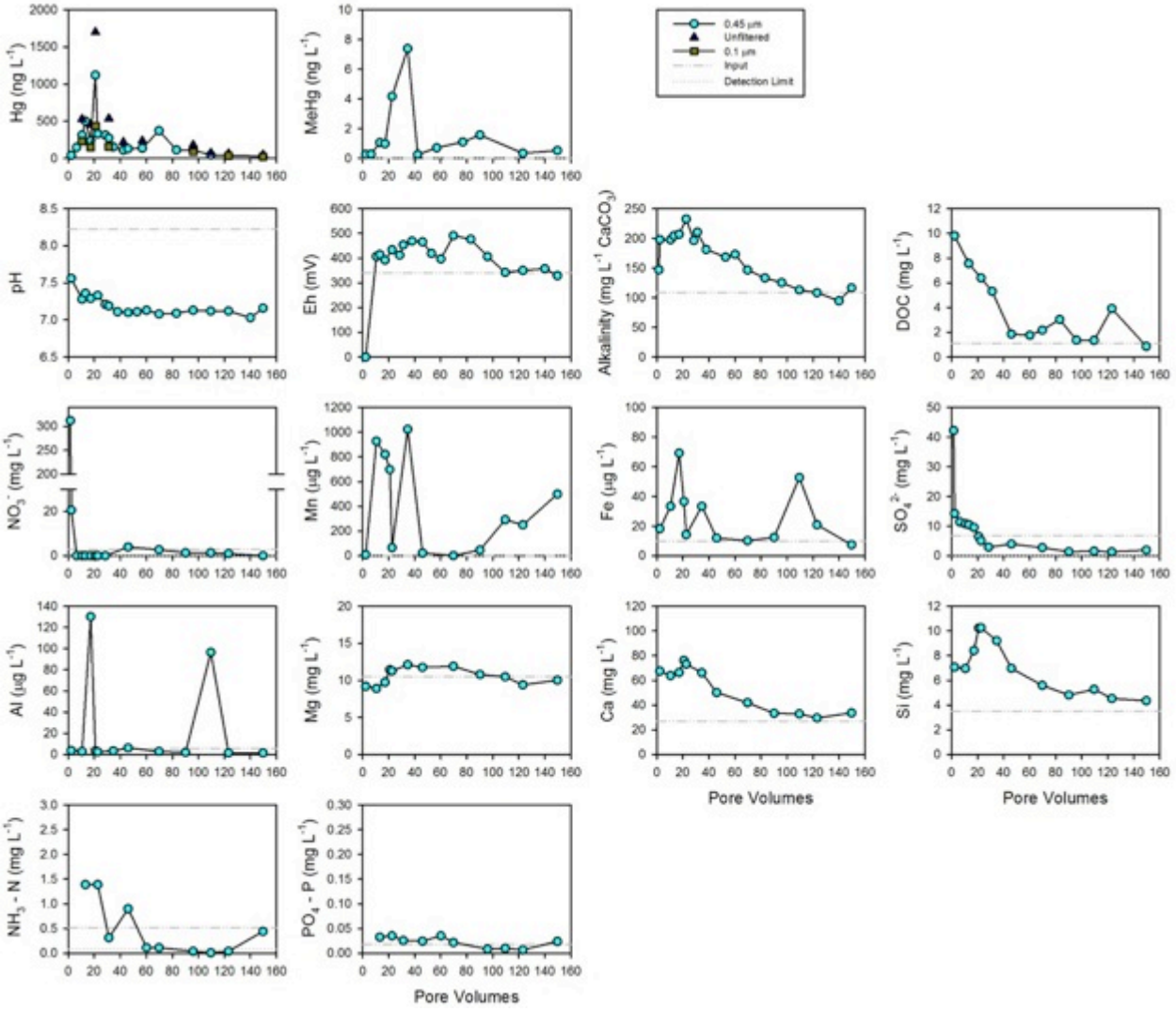

Figure B 2 - Hg, MeHg, redox parameters and geochemistry measured in the effluent of the CC+HNO_3 column.

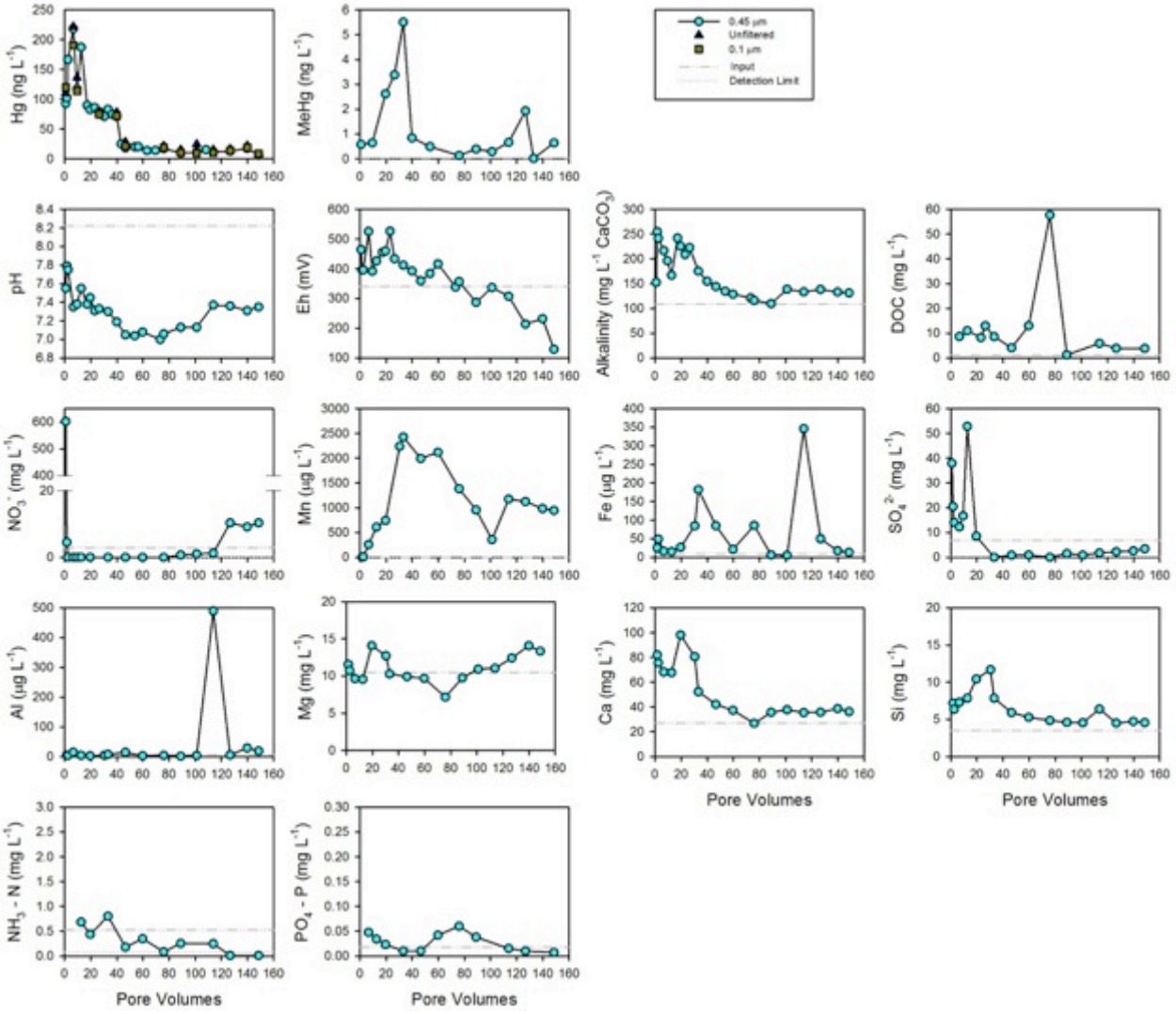

Figure B 3 - Hg, MeHg, redox parameters and geochemistry measured in the effluent of the CC+2%CaS_x column.

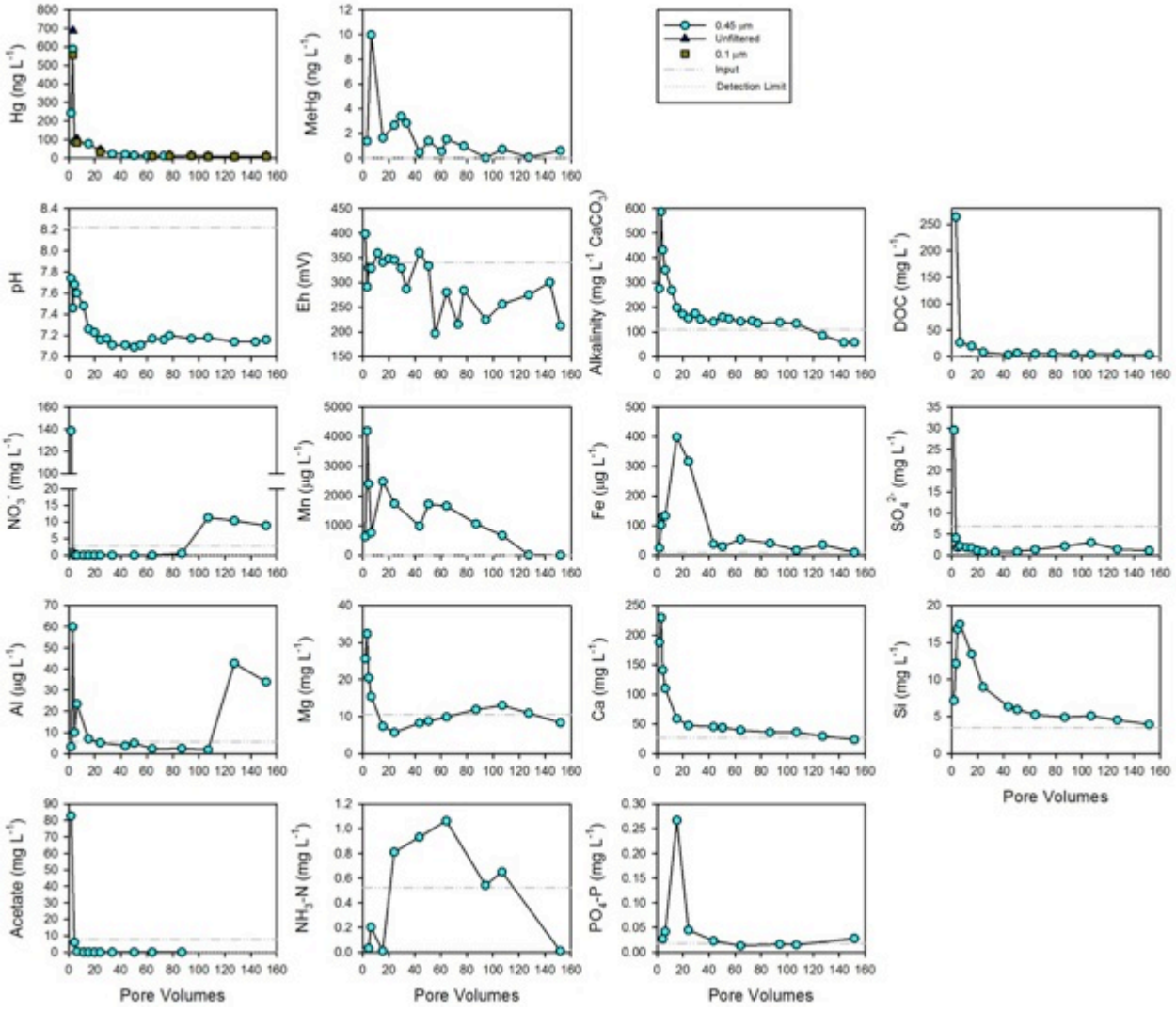

Figure B 4 - Hg, MeHg, redox parameters and geochemistry measured in the effluent of the CC+5%CaS_x column.

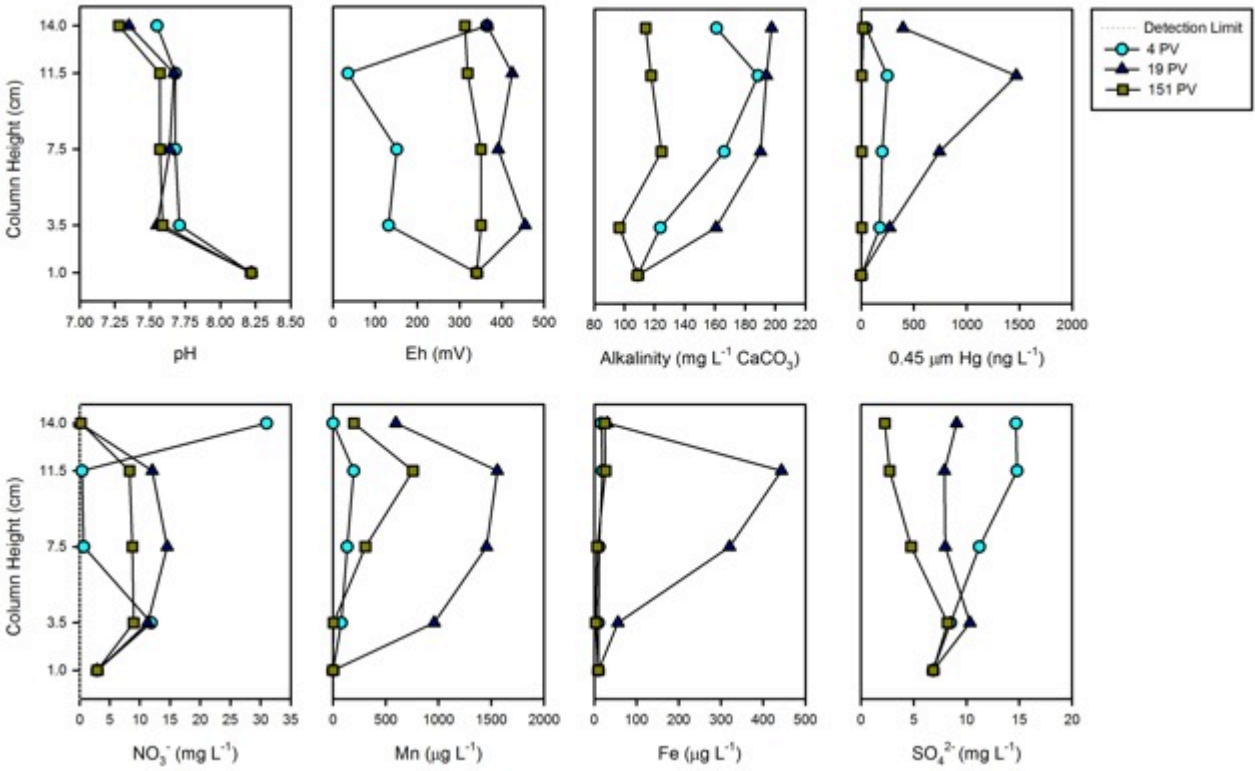

Figure B 5 - Aqueous geochemistry, Hg and redox parameters measured in samples extracted from the ports of the CC column.

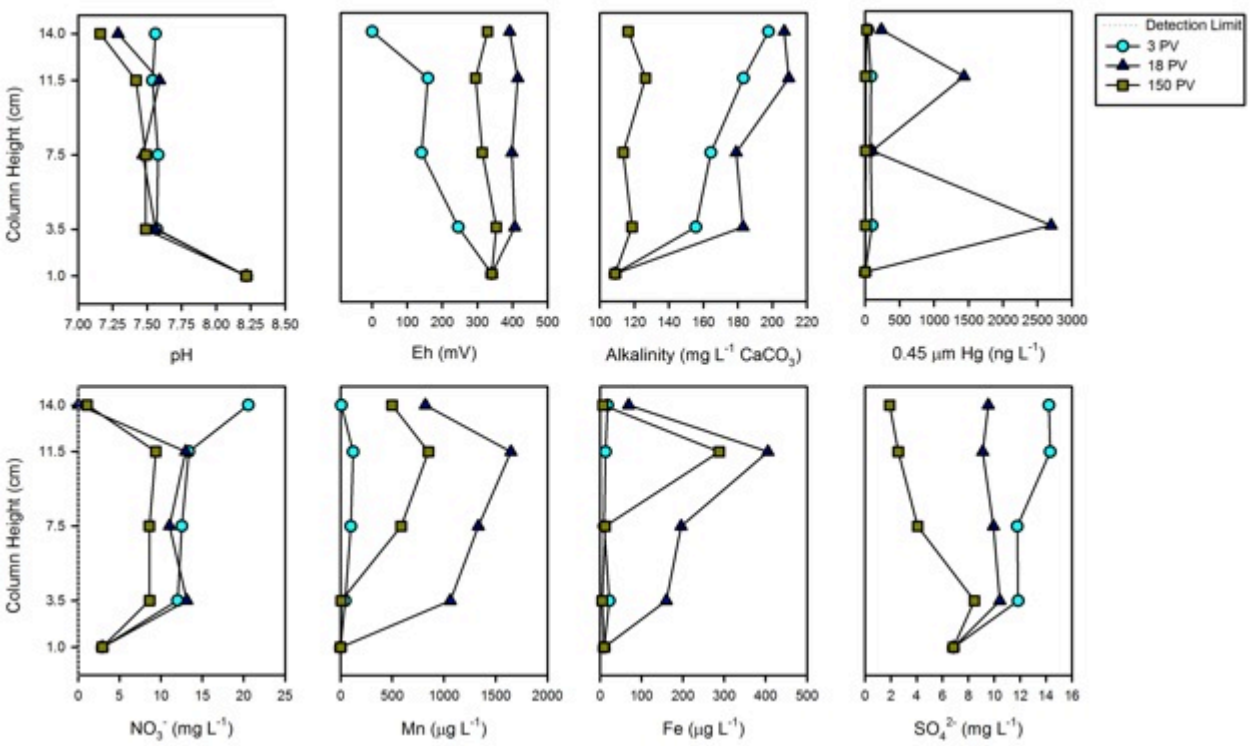

Figure B 6 - Aqueous geochemistry, Hg and redox parameters measured in samples extracted from the ports of the CC+HNO_3 column.

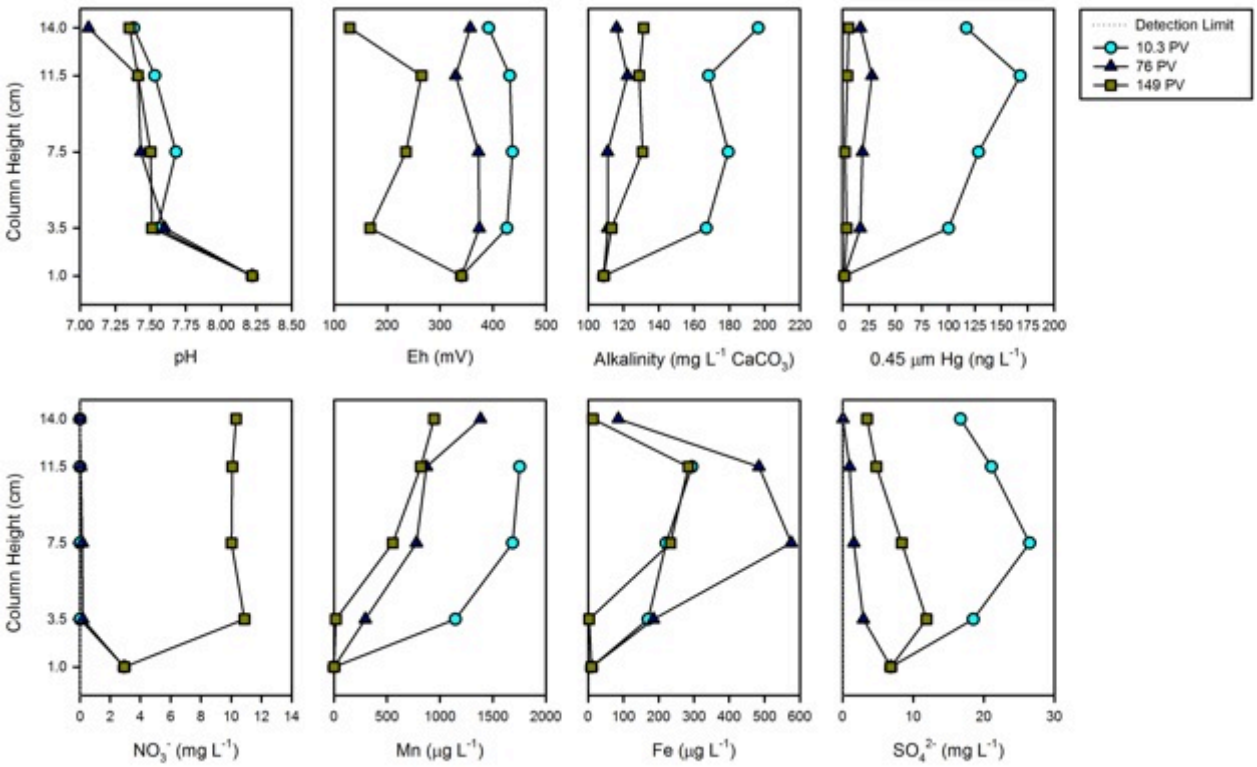

Figure B 7 - Aqueous geochemistry, Hg and redox parameters measured in samples extracted from the ports of the CC+2%CaS_x column.

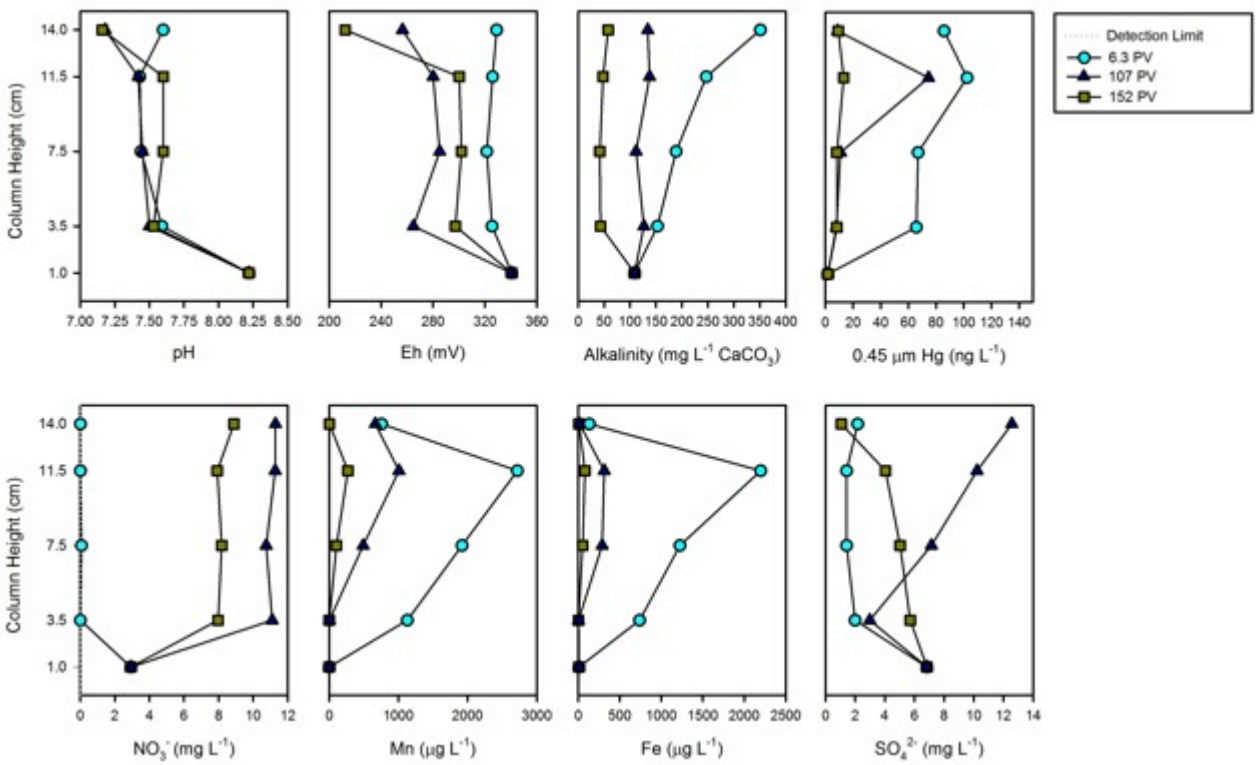

Figure B 8 - Aqueous geochemistry, Hg and redox parameters measured in samples extracted from the ports of the CC+5%CaS_x column.

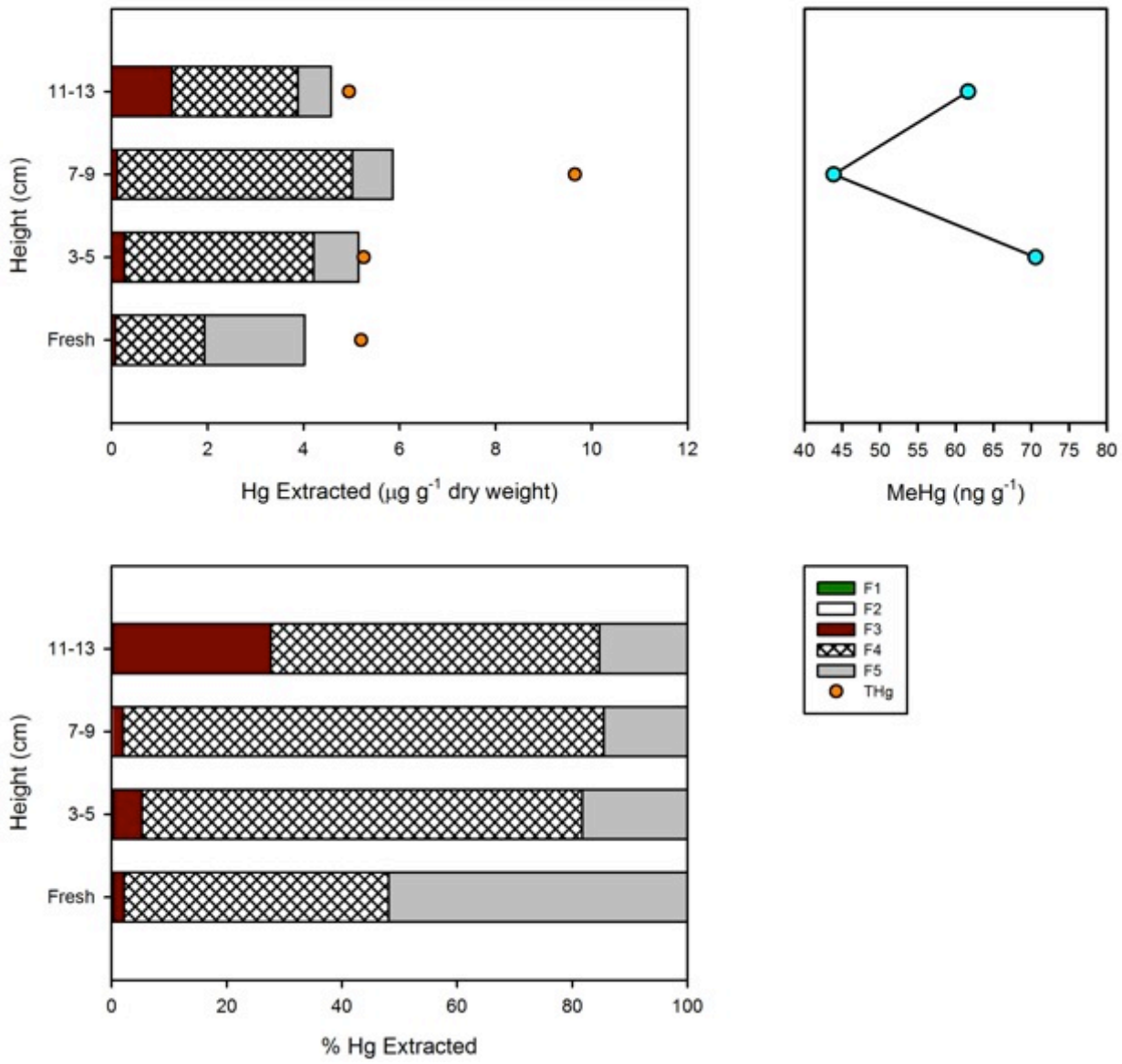

Figure B 9 - Mass and percent Hg in the CC column determined by sequential extraction analysis of column sediment after experiment termination (right). Fraction 1 (F1) targets water soluble Hg, F2 targets weak acid-extractable Hg, F3 organo-complexed Hg, F4 strongly-complexed/elemental Hg and F5 targets Hg sulfides. Fresh sediment concentration is the bulk Hg extracted from sediment used prior to amendment and column packing. Solid-phase MeHg (right) analysed after experiment completion.

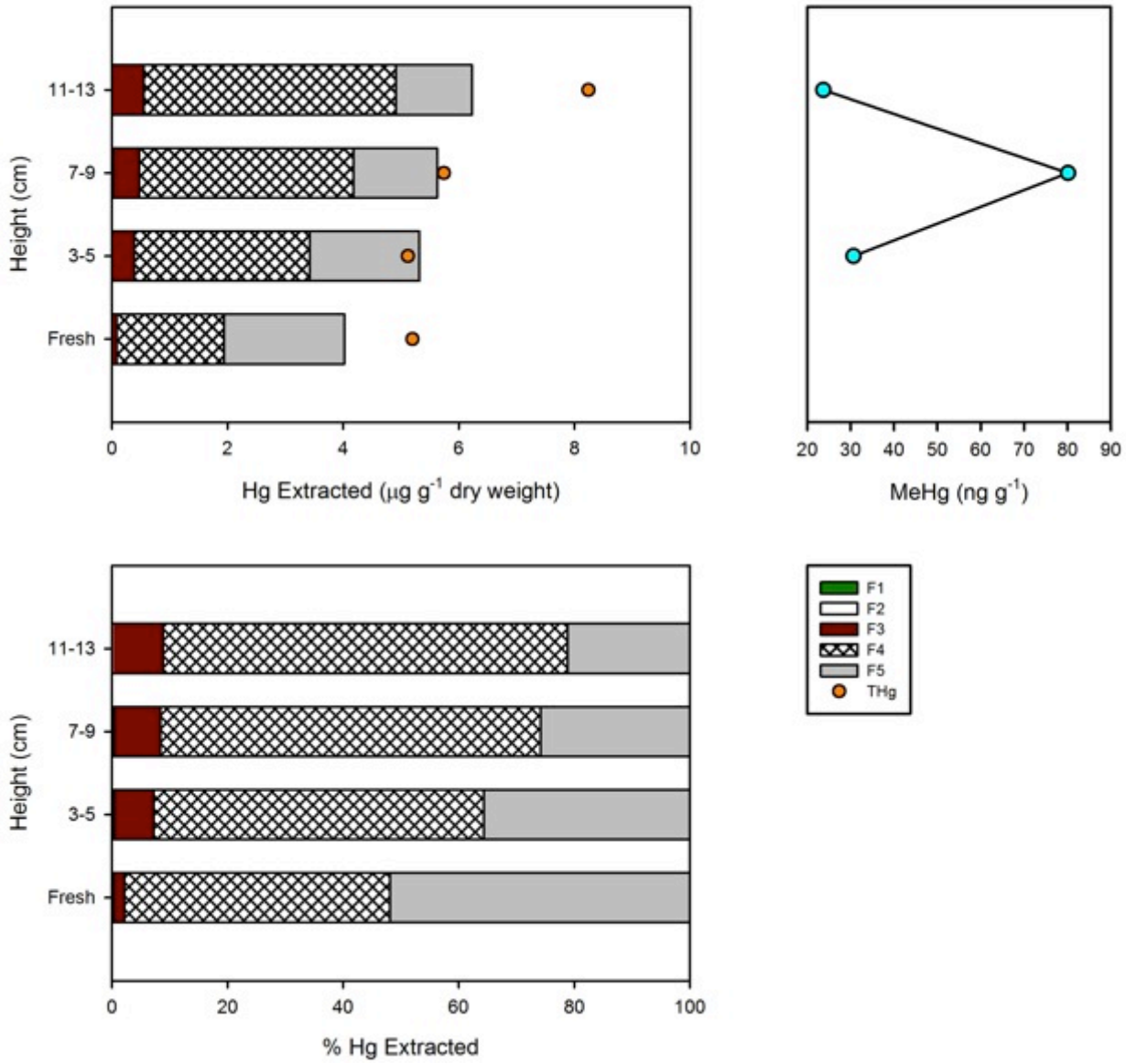

Figure B 10 - Mass and percent Hg in the CC+HNO_3 column determined by sequential extraction analysis of column sediment after experiment termination (right). Fraction 1 (F1) targets water soluble Hg, F2 targets weak acid-extractable Hg, F3 organo-complexed Hg, F4 strongly-complexed/elemental Hg and F5 targets Hg sulfides. Fresh sediment concentration is the bulk Hg extracted from sediment used prior to amendment and column packing. Solid-phase MeHg (right) analysed after experiment completion.

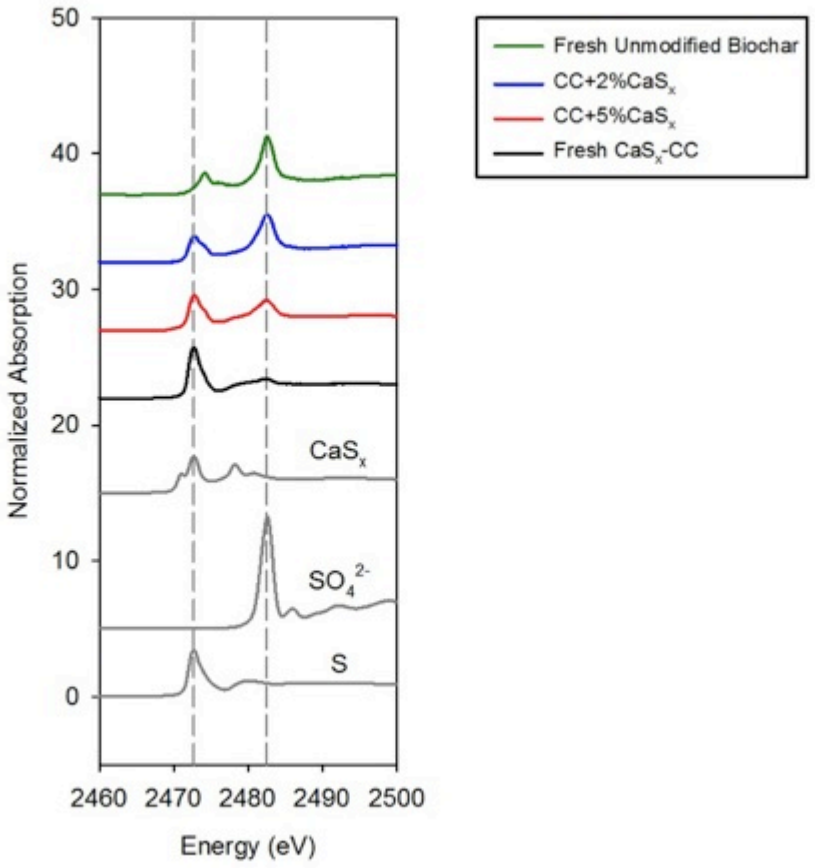

Figure B 11 – Comparison of S K-edge XANES for fresh unmodified biochar, fresh CaS_x-modified biochar, biochar from the CC+2%CaS_x column and biochar from the CC+5%CaS_x column to three reference S standards – polysulfide (CaS_s), oxidized S (SO_4^{2-}) and reduced S (S^0).

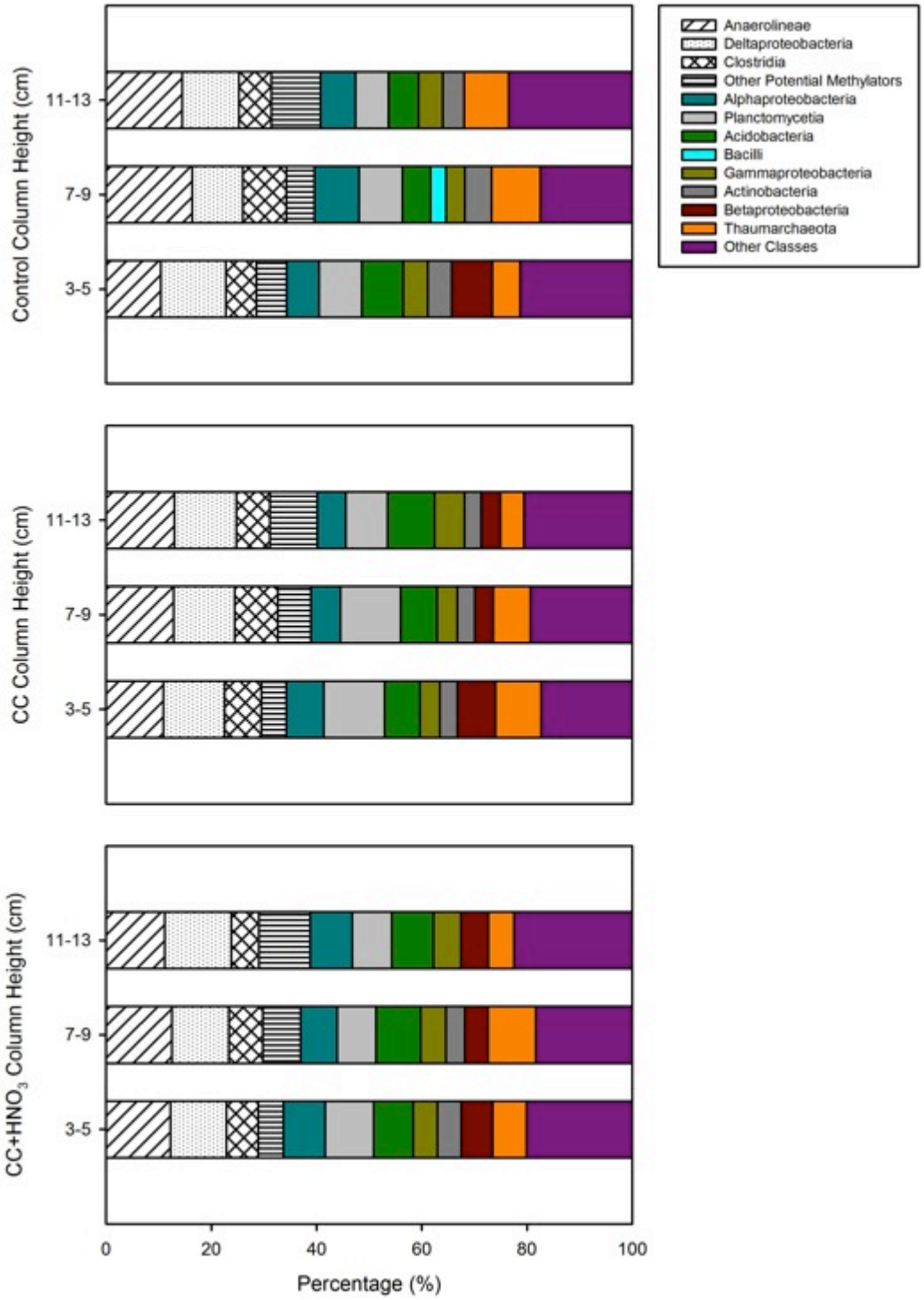

Figure B 12 - Classes of bacteria identified from PCR analysis performed on sediment extracted from the Control (top), CC (middle) and CC+HNO3 (bottom) columns at the time of column decommission. Hatched bars represent classes that contain know methylating bacteria.

Table B 1 - Ionic strength, charge balance error and selected mineral saturation indices calculated in effluent samples from the CC column. Parameters were determined using PHREEQC.

Sample ID	Ionic Strength (mol/kg water)	Charge Balance Error (%)	Calcite Saturation Index	Aragonite Saturation Index	Dolomite Saturation Index	Gypsum Saturation Index	Fe(OH)3 Saturation Index
SSCC-2	0.0069	-13	0.12	-0.03	-0.31	-2.5	1.2
SSCC-4	0.0068	1.6	0.11	-0.04	-0.32	-2.6	1.4
SSCC-6	0.0063	2.1	0.05	-0.09	-0.37	-2.6	1.4
SSCC-8	0.0073	0.82	0.15	0	-0.18	-3.1	2.2
SSCC-22	0.0045	-2.3	-0.48	-0.63	-2.1	-4.4	2.0
SSCC-34	0.0036	7.7	-0.72	-0.86	-2.6	-3.7	1.6
SSCC-38	0.0033	9.3	-0.8	-0.95	-1.8	-3.9	1.2
SSCC-45	0.0035	3.6	-0.54	-0.68	-1.3	-3.5	1.3

Table B 2 - Ionic strength, charge balance error and selected mineral saturation indices calculated in effluent samples from the CC+HNO_3 column. Parameters were determined using PHREEQC.

Sample ID	Ionic Strength (mol/kg water)	Charge Balance Error (%)	Calcite Saturation Index	Aragonite Saturation Index	Dolomite Saturation Index	Gypsum Saturation Index	Fe(OH)3 Saturation Index
SSAC-2	0.0068	-14	0.27	0.12	-3.0	-2.4	-2.1
SSAC-4	0.0062	1.5	-0.02	-0.17	-0.58	-2.6	1.5
SSAC-6	0.0064	0.72	0.02	-0.12	-0.48	-2.6	1.8
SSAC-8	0.007	0.16	0.15	0	-0.2	-2.8	1.1
SSAC-21	0.0049	-1	-0.5	-0.65	-1.2	-3.7	0.86
SSAC-33	0.0038	10	-0.67	-0.81	-1.5	-3.6	1.6
SSAC-37	0.0035	7.4	-0.72	-0.87	-1.6	-3.7	1.2
SSAC-45	0.0038	6.9	-0.6	-0.75	-1.4	-3.5	0.73

Table B 3 - Ionic strength, charge balance error and selected mineral saturation indices calculated in effluent samples from the CC+2%CaS_x column. Parameters were determined using PHREEQC.

Sample ID	Ionic Strength (mol/kg water)	Charge Balance Error (%)	Calcite Saturation Index	Aragonite Saturation Index	Dolomite Saturation Index	Gypsum Saturation Index	Fe(OH)3 Saturation Index
SSCS-2	0.0084	-0.68	0.67	0.52	0.8	-2.2	
SSCS-3	0.0076	1.9	0.58	0.44	0.63	-2.4	1.7
SSCS-4	0.0069	1.0	0.11	-0.04	-0.32	-2.5	1.2
SSCS-6	0.0076	-14	0.24	0.09	-0.07	-1.9	1.2
SSCS-8	0.0086	14	0.36	0.22	0.19	-2.5	1.4
SSCS-12	0.0055	0.27	-0.12	-0.27	-0.64	-5.9	2.2
SSCS-16	0.0046	8.3	-0.53	-0.68	-1.4	-3.8	1.8
SSCS-20	0.0041	8.7	-0.6	-0.74	-1.5	-3.8	1.2
SSCS-25	0.0032	-2.7	-0.79	-0.93	-1.8	-5.2	1.8
SSCS-29	0.0038	13	-0.63	-0.78	-1.5	-3.6	0.54
SSCS-33	0.0043	4.9	-0.51	-0.66	-1.3	-3.8	0.61
SSCS-37	0.0043	8.4	-0.33	-0.48	-0.86	-3.5	2.5
SSCS-41	0.0047	-4.9	-0.32	-0.46	-0.78	-3.4	1.3
SSCS-45	0.005	3.4	-0.35	-0.5	-0.83	-3.3	0.89
SSCS-48	0.0048	-0.82	-0.34	-0.49	-0.81	-3.2	-0.56

Table B 4 - Ionic strength, charge balance error and selected mineral saturation indices calculated in effluent samples from the CC+5%CaS_x column. Parameters were determined using PHREEQC.

Sample ID	Ionic Strength (mol/kg water)	Charge Balance Error (%)	Calcite Saturation Index	Aragonite Saturation Index	Dolomite Saturation Index	Gypsum Saturation Index	Fe(OH)3 Saturation Index
SSCS-5%-1	0.02	-11	0.92	0.77	1.3	-1.9	1.4
SSCS-5%-2	0.019	12	1.0	0.9	1.6	-2.7	2.0
SSCS-5%-3	0.013	2.2	0.97	0.83	1.4	-3.2	2.1
SSCS-5%-4	0.01	-0.42	0.73	0.58	0.92	-3.2	2.1
SSCS-5%-6	0.0057	-0.12	-0.06	-0.21	-0.71	-3.4	2.5
SSCS-5%-8	0.0046	1.6	-0.34	-0.49	-1.3	-3.8	2.4
SSCS-5%-14	0.0048	0.5	-0.43	-0.58	-1.3	-3.8	1.3
SSCS-5%-17	0.0045	3.5	-0.44	-0.59	-1.2	-3.6	1.5
SSCS-5%-27	0.0049	-5.4	-0.5	-0.65	-1.1	-3.3	0.85
SSCS-5%-31	0.0038	2.2	-0.81	-0.95	-1.7	-3.7	1.3
SSCS-5%-36	0.0029	5.6	-1.0	-1.2	-2.2	-3.9	0.13

Appendix C: Quality Assurance and Quality Control for Chapters 2 and 3

Table C 1 - THg QA/QC for the Control Column.

Sample ID	Date Collected	Date Analysed	THg (ng L^{-1})	Repeat THg (ng L^{-1})	Internal Check (ng L^{-1})	Relative Standard Deviation (%)	Matrix Spike Recovery (%)
SSRC-2	July 28, 2014	Sept. 10, 2014	64	61		3.3	
SSRC-4-0.1	Aug. 13, 2014	Sept. 19, 2014	999				121
SSRC-7-0.1	Sept. 2, 2014	Aug. 25, 2015	665	652		1.4	
SSRC-8	Sept. 9, 2014	Sept. 30, 2014	610	614		0.5	
SSRC-8-0.1	Sept. 9, 2014	Nov. 5, 2014	313			3.5	
		Nov. 6, 2014		329			
SSRC-18	Nov. 17, 2014	Dec. 16, 2014	63				86
SSRC-25	Jan. 5, 2015	Feb. 18, 2015	107.7			12	
		May 1, 2015			90.7		

Table C 2 - THg QA/QC for the Limestone Column.

Sample ID	Date Collected	Date Analysed	THg (ng L^{-1})	Repeat THg (ng L^{-1})	Internal Check (ng L^{-1})	Relative Standard Deviation (%)	Matrix Spike Recovery (%)
SSLS-3-0.1	Aug. 6, 2014	Sept. 18, 2014	1067			14	
		Sept. 19, 2014		879			
SSLS-4-UNF	Aug. 14, 2014	Sept. 10, 2014	1860	1955		4	
SSLS-7	Sept. 3, 2014	Sept. 30, 2014	403				99
SSLS-8-0.1	Sept. 11, 2014	Nov. 5, 2015	242	255		4	
SSLS-8	Sept. 11, 2014	Sept. 30, 2014	361			7	
		Oct. 1, 2014		398			
SSLS-18-0.1	Nov. 18, 2014	Dec. 16, 2014	73	73		0.1	
SSLS-25	Jan. 5, 2015	Feb. 18, 2015	133			0	
		May 1, 2015			133		
SSLS-T-1	July 30, 2014	Jan, 14, 2015	135	129		4	
SSLS-M-3	Oct. 22, 2014	Mar. 2, 2016	46				82

Table C 3 - THg QA/QC for the Biochar Column.

Sample ID	Date Collected	Date Analysed	THg (ng L^{-1})	Repeat THg (ng L^{-1})	Internal Check (ng L^{-1})	Relative Standard Deviation (%)	Matrix Spike Recovery (%)
SSCC-3	Aug. 25, 2014	Sept. 10, 2014	282	283		0.2	
SSCC-4-0.1	Sept. 2, 2014	Sept. 18, 2014	449				107
SSCC-6	Sept. 15, 2014	Sept. 30, 2014	397			0.1	
		Oct. 1, 2014		398			
SSCC-12-UNF	Oct. 27, 2014	Nov. 5, 2014	194			5	
		Nov. 6, 2014		209			
SSCC-14	Nov. 10, 2014	Dec. 16, 2014	88				98
SSCC-22	Jan. 5, 2015	Feb. 18, 2015	125.5			7	
		May 1, 2015			114.2		
SSCC-45	June 14, 2015	July 21, 2015	20	22		5	
SSCC-B-2	Sept. 17, 2014	Mar. 2, 2016	271	267		1.2	

Table C 4 - THg QA/QC for the HNO_3-modified Biochar Column.

Sample ID	Date Collected	Date Analysed	THg (ng L^{-1})	Repeat THg (ng L^{-1})	Internal Check (ng L^{-1})	Relative Standard Deviation (%)	Matrix Spike Recovery (%)
SSAC-3	Sept. 3, 2014	Sept. 10, 2014	148	144		2	
SSAC-4-UNF	Sept. 11, 2014	Sept. 18, 2014	528			0.8	
		Sept. 19, 2014		534			
SSAC-6	Sept. 23, 2014	Sept. 30, 2014	237				109
SSAC-6-UNF	Sept. 23, 2014	Sept. 30, 2014	450			4	
		Oct. 1, 2014		474			
SSAC-7-0.1	Oct. 1, 2014	Nov. 5, 2014	435	462		4	
SSAC-13	Nov. 11, 2014	Dec. 16, 2014	109	117		5	
SSAC-21	Jan. 5, 2015	372					116
SSAC-45	June 22, 2015	July 21, 2015	27	27		0.5	

Table C 5 - THg QA/QC for the CC+2%CaS_x Column.

Sample ID	Date Collected	Date Analysed	THg (ng L^{-1})	Repeat THg (ng L^{-1})	Internal Check (ng L^{-1})	Duplicate (ng L^{-1})	Relative Standard Deviation (%)	Matrix Spike Recovery (%)
SSCS-4	Dec. 30, 2014	Jan. 14, 2015	219					100
SSCS-4-UNF	Dec. 30, 2014	Mar. 1, 2016	222	227			1.8	
SSCS-5	Jan. 5, 2015	Jan. 14, 2015	117	118			0.3	
SSCS-8	Jan. 26, 2015	Feb. 18, 2015	83	87			4	
SSCS-10-0.1	Feb. 9, 2015	Mar. 10, 2015	75	76			1.3	
SSCS-11	Feb. 17, 2015	Feb. 18, 2015	71.2		77.8		6	
SSCS-14	Mar. 9, 2015	Mar. 10, 2015	71					105
SSCS-23	May 11, 2015	May 13, 2015	14			13	3.2	

Table C 6 - THg QA/QC for the Attapulgite Clay Column.

Sample ID	Date Collected	Date Analysed	THg (ng L^{-1})	Repeat THg (ng L^{-1})	Relative Standard Deviation (%)	Matrix Spike Recovery (%)
SSAP-1-UNF	Jan. 30, 2015	Feb. 18, 2015	78	76	2	
SSAP-3	Feb. 5, 2015	Feb. 18, 2015	745			116
SSAP-7	Mar. 2, 2015	Mar. 10, 2015	970	987	1	
SSAP-12	Apr. 7, 2015	Apr. 15, 2015	578	557	3	
SSAP-17	May 11, 2015	May 13, 2015	184			93
SSAP-20-0.1	June 1, 2015	June 9, 2015	179			108
SSAP-27-0.1	July 20, 2015	July 21, 2015	55	50	6	
SSAP-31	Aug. 17, 2015	Aug. 25, 2015	44			105
SSAP-35	Sept. 14, 2015	Sept. 15, 2015	86	88	2	
SSAP-39	Oct. 13, 2015	Nov. 11, 2015	51	55	5	
SSAP-M-2	July 22, 2015	Aug. 25, 2015	23	23	0.5	

Table C 7 - THg QA/QC for the CaS_x-modified Attapulgite Clay Column.

Sample ID	Date Collected	Date Analysed	THg (ng L^{-1})	Repeat THg (ng L^{-1})	Relative Standard Deviation (%)	Matrix Spike Recovery (%)
SAPS-1-0.1	Mar. 9, 2015	Mar. 1, 2016	287	583		112
SAPS-1	Mar. 9, 2015	Apr. 15, 2015	280	268	3	
SAPS-5	Mar. 23, 2015	April 15, 2015	141			97
SAPS-14	May 25, 2015	June 9, 2015	36	34	4	
SAPS-18-0.1	June 23, 2015	July 21, 2015	20			99

Table C 8 - THg QA/QC for the CC+5%CaS_x Column.

Sample ID	Date Collected	Date Analysed	THg (ng L^{-1})	Repeat THg (ng L^{-1})	Relative Standard Deviation (%)	Matrix Spike Recovery (%)
SSCS-5%-2	May 6, 2015	May 13, 2015	588		2	
SSCS-5%-2-UNF	May 6, 2015	Mar. 1, 2016	688	1312		103
SSCS-5%-3	May 8, 2015	May 13, 2015	86			92
SSCS-5%-12	July 9, 2015	July 21, 2015	20			91
SSCS-5%-14	July 20, 2015	July 21, 2015	15	13	6	

Table C 9 - THg QA/QC for Sequential Extractions of the Control, Limestone, CC and CC+HNO_3 Columns.

		THg (µg g^{-1}) dry weight					
Sample ID	Date Analysed	F1	F2	F3	F4	F5	THg
CC-T	Dec. 1-10, 2015	8	3.7	1254	2613	699	4947
CC-T-DUP		9	3.5	121	3186	1821	4246
Relative Standard Deviation (%)		**14**	**5**	**116**	**25**	**63**	**11**
RC-B	Dec. 1, 2015		2.6				
RC-B-RE			3.3				
Relative Standard Deviation (%)			**17**				
RC-T	Dec, 1, 2015		1.4				
RC-T-RE	Dec. 2, 2015		1.6				
Relative Standard Deviation (%)			**9**				
CC-T	Dec. 2, 2015			1254			
CC-T-RE				1290			
Relative Standard Deviation (%)				**2**			
LS-B	Dec. 8, 2015				638866		
LS-B-RE					584629		
Relative Standard Deviation (%)					**6**		
CC-B	Dec. 9, 2015						5253
CC-B-RE	Dec. 10, 2015						5768
Relative Standard Deviation (%)							**7**

Table C 10 - THg Method Detection Limits Given a 99% Confidence Interval.

Date	Method Detection Limit (ng L^{-1})
Sept. 10, 2014	0.69
Sept. 19, 2014	0.19
Oct 1, 2014	0.19
Nov. 6, 2014	0.13
Dec. 17, 2014	0.09
Jan. 14, 2015	0.1
Mar. 10, 2015	0.13
June 9, 2015	0.28
July 22, 2015	0.09
Nov. 11, 2015	0.09
Mar. 2, 2016	0.06
AVERAGE	0.19